Investigation of the Melt-down Behaviour of Massive Radial Core Enclosures during LWR Accidents

W. Hering, W. Sengpiel, Chr. Messainguiral*

Institut für Reaktorsicherheit

Projekt Nukleare Sicherheitsforschung

* CEA-DRN, Cadarache, Frankreich

Abstract

At the Institute for Reactor Safety (IRS) of the Forschungszentrum Karlsruhe (FZK) accident analyses were performed for the projected European Pressurised Water Reactor (EPR) up to 1999 using the best estimate severe core damage code SCDAP/RELAP5 (S/R5). From various scenarios investigated with S/R5 the loss-of-offsite power (LOOP) and the 46 cm² small break loss of coolant accident (SBLOCA) were selected to be discussed here in some detail.

To simulate the heavy reflector (HR) and core barrel (CB) behaviour beyond the capabilities of S/R5 mod 3.2 a detailed stand alone analytical tool (LOWCOR2) was developed and used to determine the time of HR melting, its axial position, the melting velocity and the melt mass. Furthermore, results of MELCOR calculations performed at Siemens/KWU were used for the SBLOCA scenario. The analyses were extended by a feasibility study to find out whether ICARE2 and the commercial FEM code FIDAP are applicable.

The axial position of HR and CB melt through strongly depends on the scenario an ranges between 1.0m and 2.5m core elevation. The time period to melt down the HR inner edges lasts up to 17 min and a complete melt through of HR and CB is in the order of magnitude of one hour. At melt through time LOWCOR2 calculated a molten steel mass between 10 Mg and 32 Mg and a melt relocation rate of 35 kg/s along the HR inner surface into the core cavity.

Untersuchung des Abschmelzverhaltens massiver Kernumfassungen im Verlauf von LWR Störfällen

Kurzfassung

Am Institut für Reaktorsicherheit (IRS) des Forschungszentrums Karlsruhe (FZK) wurden bis 1999 Unfallanalysen für den projektierten Europäischen Druckwasser Reaktor (EPR) mit dem „best estimate" Kernschmelzcode SCDAP/RELAP5 (S/R5) durchgeführt. Von den verschiedenen mit S/R5 untersuchten Szenarien wurden der „Ausfall der Wechselspannungsnetze" (LOOP) und das kleine Leck (46 cm²) im kalten Strang der Hauptkühlmittelleitung (SBLOCA) für eine ausführlichere Diskussion ausgewählt.

Um das Verhalten des „heavy reflectors" (HR) und des Kernmantels (CB) auch jenseits der Möglichkeiten von S/R5 untersuchen zu können, wurde ein analytisches Programm entwickelt (LOWCOR2) und angewendet um Informationen über den Zeitpunkt des Schmelzebeginns, der zugehörigen axialen Position, der Abschmelzgeschwindigkeit und der dabei erzeugten Schmelzemasse zu erhalten. Neben den S/R5 Daten wurden auch noch Ergebnisse der MELCOR Rechnungen von Siemens/KWU zum SBLOCA herangezogen. Daneben wurde untersucht, in wieweit ICARE2 und das FEM Programm FIDAP zur Lösung der o.g. Probleme herangezogen werden können.

Die axiale Position des Schmelzebeginns ist abhängig vom Szenario und variiert zwischen 1.0 m und 2.5 m Kernhöhe. Der Zeitbereich für das Abschmelzen der inneren HR-Kanten erstreckt sich über maximal 17 min. Das Zeitintervall bis zum lokalen Durchschmelzen des HR und des CB liegt in der Größenordnung von einer Stunde. Bis zum Durchschmelzen werden zwischen 10 und 32 Mg Stahl verflüssigt und mit max. 35 kg/s entlang der HR Innenseite in den Kernbereich verlagert.

TABLE OF CONTENTS

LIST OF FIGURES

LIST OF TABLES

LIST OF ABBREVIATIONS

ACCU	Accumulator
AIC	Absorber rods with an alloy of Silver (Ag), Indium (In), and Cadmium(Cd)
AMM	Accident Management and Mitigation
BDBA	Beyond Design Basis Accident
BOC	Begin of Cycle
CB	Core Barrel
CORA	Out-of-pile severe fuel damage tests performed at FZKA, 1984-1992, http://hikwww4.fzk.de/irs/organisation/IRS1/CORA01.html
CSC	Control rod drive support columns
DBA	Design Basis Accident
ECC	Emergency Core Cooling
EFWS	Emergency Feedwater System
EOC	End of Cycle
EPR	European Pressurized Water Reactor, http://www.siemens.de/kwu/e/foa/n/products/s11.htm
FE	Fuel Element
FIDAP	Fluid Dynamics Analysis Package
FZK	Forschungszentrum Karlsruhe, Technik und Umwelt, http://www.fzk.de/FZK2
HR	Heavy Reflector, EPR
INEEL	Idaho National Engineering and Environmental Laboratory, USA
IRS	Institut für Reaktorsicherheit, http://hikwww4.fzk.de/irs/organisation/IRS1/irs1_home.html
IRWST	In-containment Refuelling Water Storage Tank
KWU	Kraftwerk Union, Erlangen, part of Siemens, Germany, http://www.siemens.de/kwu
LBLOCA	Large Break Loss Of Coolant Accident
LCSP	Lower Core Support Plate

LOCA   Loss Of Coolant Accident

LOFT   Loss Of Fluid Test (Idaho National Engineering Laboratory, USA)

LWR   Light Water Reactor

MAAP   Modular Accident Analysis Program

MSIV   Main Steam Insulation Valve

MSRV   Main Steam Relieve Valve

MSSV   Main Steam Safety Valve

NEPTUN   DBA Reflood test facility at PSI, http://pss100.psi.ch/~aubert/NEPTUN.html

PCT   Peak core temperature

PSF   Projekt nukleare Sicherheitsforschung, FZK, http://psf-nt-server.fzk.de/psfhome.htm

PWR   Pressurized Water Reactor

PZR   Pressurizer

RCP   Reactor Coolant pump

RELAP5   old: Reactor Excursions and Leak Analysis Program, presently: Reactor Leak and Analysis Program, for LWR transients and SBLOCA, http://www.nrc.gov/RES/RELAP5/

RS   Reactor scram

RCSL   Reactor Control, Surveillance and Limitation System

RPV   Reactor Pressure Vessel

SBLOCA   Small break LOCA

SCD   Severe Core Damage

SCDAP   Severe Core Damage Analysis Package, (USNRC code, developed at INEEL), http://relap5.inel.gov/scdap/home.html

SCDAP/RELAP5: Coupled SCDAP and RELAP5 code to simulate reactor conditions up to SFD conditions

SFD   Severe Fuel Damage

SG   Steam Generator

SAMG   Severe accident mitigation guidelines

SIS   Safety Injection System

SR5CAP   SCDAP/RELAP5 Cooperative Assessment Program, http://www.inel.gov/sr5cap/

TMI-2   Three Mile Island Unit 2, Mitigated SFD accident, http://www.libraries.psu.edu/crsweb/tmi/tmi.htm

UH   Upper head

USNRC   United States Nuclear Regulatory Commission, http://www.nrc.gov, USNRC-Codes (Research): http://www.nrc.gov/RES/rescodes.html

USS   Upper support structure or plate

(Remark: URL-Addresses valid April 2000)

1 INTRODUCTION

Reactor safety analyses should provide useful information to the utilities as well as to the operators in which way the course of an accident may develop in case of an initial failure and what may occur if accident management measures are activated. In a first step this can be done using integral code systems such as MELCOR/1/ and MAAP /2/ which are advantageous with respect to run-time and costs compared to detailed mechanistic codes. However, the reliability of these code systems has to be validated by integral experiments and detailed mechanistic codes. If the validation process is finished, parameter studies can be performed to check the sensitivity of user selectable code options.

Detailed mechanistic code systems such as SCDAP/RELAP5 /3/, /4/ and ICARE2 /5/ suffer less by user related influence since their basis is mainly physical modelling of at least first order. In case of new components or systems in a reactor however, relevant models are not available so that assumptions or user options are included to continue calculations. As a consequence the results obtained are now less qualified and more comparable to those derived from integral code systems. Another possible approach is to extract the boundary conditions calculated with the detailed mechanistic code and to use these data as input for more appropriate tools (separate effect codes) which can be developed outside the complex system of the large code.

Presently two challenging tasks were investigated at FZK. Firstly, the influence of delayed core reflood on the hydrogen source term as well as the core degradation process during early core melt stage. These activities are focussed on the QUENCH project which was part of the EU-4th framework programme. Secondly, in case of ongoing core degradation process, the behaviour of the radial as well as the axial core boundary structures has been investigated. Here, reactor specific conditions have to be considered to ensure realistic simulation of melting and melt relocation processes. In advanced reactors (e.g. AP-600 and EPR) massive core enclosures are foreseen to improve the neutron efficiency by reflecting neutrons. The behaviour of such a radial core enclosure, the so called "Heavy reflector" (HR), has been investigated during the late phase of in-vessel core degradation.

Presently, because even detailed mechanistic codes are not sufficient to estimate transient HR failure behaviour, a coupled approach using detailed stand-alone tools was chosen at FZK/IRS. The main goal is to extract values for the failure time, the failure mode, and possibly the failure or leak size and, very important for the in-vessel steam explosion calculations, the position and the size increase due to erosion by molten materials.

The data set necessary to determine the boundary conditions for in-vessel steam explosion requires the knowledge of failure time, leak position and size, thermal characterisation of released melt and melt outflow rate. Currently, we restrict ourselves to the determination of leak position, leak size and size increase due to erosion by metallic melts. The erosion rates by oxidic melts can be neglected here.

2 ANALYTICAL TOOLS

2.1 Problem Definition

The general problem is to estimate the failure mode of the core enclosure due to melting or even attack of liquid corium. The core enclosure is composed of the heavy reflector and the core barrel in radial direction, the upper core plate on top and the lower core support plate at the bottom (Figure 2.1). The first task is to identify which of these components will fail first, except for the upper core plate the melting of which is of minor concern because it does not significantly effect melt release into the lower plenum.

Generally accident analyses using different tools (section 3) demonstrated that the onset of melting is reached firstly at the radial boundary of the core, however, different axial positions were identified by the calculations.
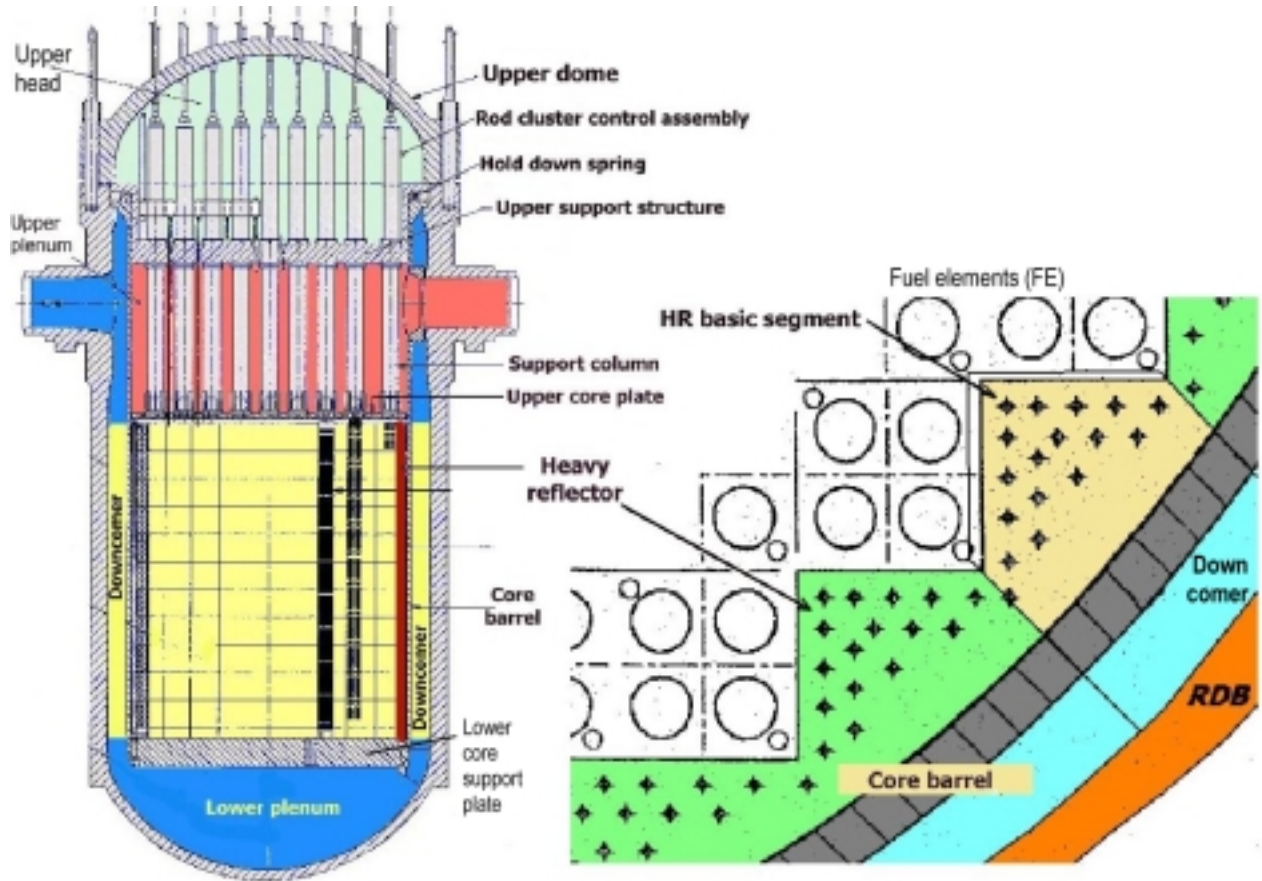
Figure 2.1   Axial (left) and radial (right) shape of the core enclosure composed of heavy reflector (HR) and core barrel (CB).

Therefore, starting conditions derived from different codes and scenarios were used for detailed analyses (section 4). Furthermore, the time scale to melt down the characteristic inner geometry of the HR adjacent to the position of the outermost fuel elements (FE) has to be estimated (Figure 2.1 right). The results are important to determine the time when 2-D (r-z) assumptions are allowed.

In Figure 2.1 the boundaries for the analyses are shown, i.e. at the inner side the core as fuel rod like geometry, porous debris or the crust of a molten pool, and at the outer side the RPV wall, whose outside is kept cold by a sufficient heat transfer to the containment atmosphere.

To investigate the thermal behaviour of the HR and the CB, boundary conditions for the late phase accident sequences are extracted from SCDAP/RELAP5 and MELCOR plant calculations for the small break loss of coolant accident (SBLOCA) and the loss of off-site power (LOOP) scenario described in the next section.

In reactor safety analysis two classes of codes are used for investigations of beyond design basis accidents. In case of advanced reactor concepts, such type of accidents have to be considered as part of the overall safety concept. This leads to the inclusion of core catcher systems as final barriers to keep the molten corium in controllable configuration.

Nevertheless, the conditions which might damage the containment as final barrier for the nuclear source term have to be investigated to demonstrate that no challenging loads may develop up to cool-down of the molten corium in the core catcher.

2.2 SCDAP/RELAP5

The Severe Core Damage Analysis Package SCDAP/RELAP5 (S/R5) is used to investigate in detail the conditions in the reactor pressure vessel (RPV) as well as in the primary circuit during accidents which may be initiated by loss of coolant (LOCA) or by loss of off-site power (LOOP). At FZK/IRS, calculations have been performed with respect to the safety features of advanced reactor concepts for two reasons: (1) to investigate core degradation processes in the French PHEBUS FP test facility and (2) to assist and investigate the FZK QUENCH experiments. Moreover, as part of the CAMP agreement, the thermal hydraulic models were validated and improved with respect to delayed reflood and high surface temperatures.

2.2.1 SCDAP/RELAP5 mod 3.1.F

The version of S/R5 mod 3.1 (S/R5m31) /3/ shows generally reasonable results for early core melt description. However, some shortcomings were detected, which are not yet corrected since the new version S/R5 mod3.2 (S/R5) /4/ had been released in summer 1998. The main deficiencies of S/R5m31 are the lacking hydrogen masses from oxidised absorber and water rods, shortcomings in transition from rod like geometry to pool configuration, and unphysical modelling of heat transfer between the crust of the molten pool and solid enclosures such as HR and CB. The accident analyses have been completed with an upgraded version including improvements concerning FZK out-of-pile facilities (CORA, QUENCH) as well as in-pile components for the French PHEBUS FP test section /7/.

Also reflood calculations have been performed successfully for different initiation temperatures and reflood rates (/8/- /10/) at system pressures above 1 MPa whilst low pressure reflood calculations for the QUENCH facility failed due to rapidly increasing mass errors. The state of thermal hydraulic modelling was still based on RELAP5 mod3.1 /3/, whereas in the CAMP agreement advanced fluid models became available /9/. Due to these difficulties accident analyses were continued beyond the end of 1998 using S/R5m32.

2.2.2 SCDAP/RELAP5 mod 3.2

The first S/R5m32 version released in summer 1998 from INEEL could not be used for FZK/IRS purposes due to several reasons. With a lot of time consuming efforts the most obvious errors have been corrected, and the FZK/IRS code improvements have been adapted to the new code structure and sent to INEEL for implementation into next general code release /11/.

S/R5m32 is coupled to RELAP5 mod3.2.1.2 so that the modified heat transfer packages become available. One remaining disadvantage is that the presence of non-condensable gases (nitrogen from accumulators) in subcooled liquid causes time step collapse. Therefore, in a first calculations the accumulator valves in the surge line were closed to keep the nitrogen outside primary system.

In spite of the problems mentioned above, the version gives more reliable results with respect to the hydrogen source term, one of the main goals of our activities. The transition to late phase configuration had been modified to ensure smoother transition, which is more physically justified than an abrupt change from fuel rod geometry to a debris or a molten pool. Also pool spreading is calculated in a more detailed way, however, the realistic coupling to surroundings by radiation heat transfer is still an open problem.

2.3 ICARE2 V2

ICARE2 /5/, /6/is a severe fuel damage code primarily developed by CEA/IPSN for the interpretation of PHEBUS-SFD loop experiments and presently for the PHEBUS FP series. These experiments represent a narrow fluid channel and imposed fluid (steam or gas) thermohydraulic conditions. The main efforts of the developers aimed to reproduce the fuel and absorber rod behaviour during the transients (oxidation, relocation, fission products release, material interactions, melting).

A major difference between ICARE2 and other mechanistic codes is its flexibility. The typical elements of a loop experiment are defined independently of each other and the code user describes their various relations. For example it is a user assessment to define what kind of heat exchanges affect a given structure (e.g. a fuel rod or an external shroud). This provides the possibility of studying separate effects influences. ICARE2 version V2 extended the code possibilities to the description of debris bed and molten pool environment but without modelling the transition phase from cylindrical fuel rods to debris bed formation. That version has been used for the calculations discussed in the present report. The ICARE2 validation data base comprises following experiments: CORA /12/,/13/ MP /14/, PBF /15/, and PHEBUS FP /16/-/18/.

Extending the application field of ICARE2 from test-loop problems to reactor conditions is possible but only with precautions. In fact the necessary fluid thermohydraulic boundary conditions have to be given and only steam (not water) is considered. Furthermore, the fluid flow redistribution in the core is not accurately modelled in the case of blockages.

As pointed out in a previous work /19/, /20/, as long as convective heat transfer in a multi-channel environment is important in comparison to other heat transfer mechanisms, ICARE2 V2 is not adequate to calculate the temperature evolution in a degraded core. On the other hand,

when conduction and radiation are the major processes of heat exchange in the degraded core, ICARE2 is an interesting tool to investigate the temperature evolution in the core and the surrounding structures.

We found that the HR and CB melting process was one of those problems for which ICARE2 V2 could be used with benefit because:

- it would occur in a badly cooled degrading core with low convective heat extraction,
- melting and relocation of shroud structures can be modelled,
- molten pool and debris bed heat exchanges with HR can be modelled.

For such a detailed analysis, initial and boundary conditions have to be produced by a reliable thermohydraulic model. Thus, the results of a S/R5 LBLOCA calculation have been used as input data as explained in section 5.

2.4 LOWCOR2

LOWCOR2 is a two-dimensional heat conduction program considering phase change by melting or solidification. It has been developed as a stand-alone tool to be applied together with RELAP5 or S/R5 in order to extend the computational capabilities for severe accident analyses towards detailed melt down studies for radial and axial core enclosures, like HR and CB as well as the lower core support plate (LCSP). Degradation of these structures is calculated due to thermal loading by radiation and/or contact with hot materials, and due to ablation caused by momentum transfer of moving melts. The time-dependent boundary conditions (temperatures of degrading fuel rods and of debris regions, e.g.) are adopted from corresponding data of core degradation evaluations with codes like S/R5, MELCOR etc. Thus, LOWCOR2 does not interact directly with the corresponding models for core degradation analyses in codes mentioned above and so does not influence the evolution of the core degradation. However it is planned to merge LOWCOR2 to S/R5 providing a coupling between the core and enclosing structures degradation processes.

LOWCOR2 is based on finite differences schemes of first order to solve heat conduction problems with phase change in cartesian and cylindrical geometries. Phase change processes are approximately taken into account by modification of the effective heat capacities in the nodes undergoing phase changes adding the specific heat of fusion (so-called enthalpy method). The details of the computational and physical models in LOWCOR2 are outlined in /21/. In the following, only three aspects of the LOWCOR2 approach are discussed briefly – the consideration of cavities evolving from local melting and of melt resolidified on colder structural surfaces as well as the consideration of view factors for radiation heat exchange.

2.4.1 Cavities by local melting

The local heat-up and melt process may result in an actual two-dimensional geometry as shown in Figure 2.2. Molten mass flows down to colder regions and a cavity evolves resulting in new boundaries for the residual heat conducting structure. Normally, the evolution of new boundaries and the reduction of the number of unknown temperatures would require to check and eventually reconstruct the system of equations for the $T_{i,j}$ time step after time step – a very computer time

consuming procedure. Instead, we prefer to keep the computational grid fixed (and thus the size of the system of equations), and we change only the effective material properties in the molten area and adjust the new boundary and heat transfer conditions to the modified geometry. Actually, the cavity is considered to consist of a heat conducting gas with high conductivity (i.e. low temperature gradients) which is completely transparent for radiation heat and which is coupled to the solid structure by convective heat transfer conditions. On the left boundary of the cavity, surface temperatures (gas / vapour temperatures) must be defined.
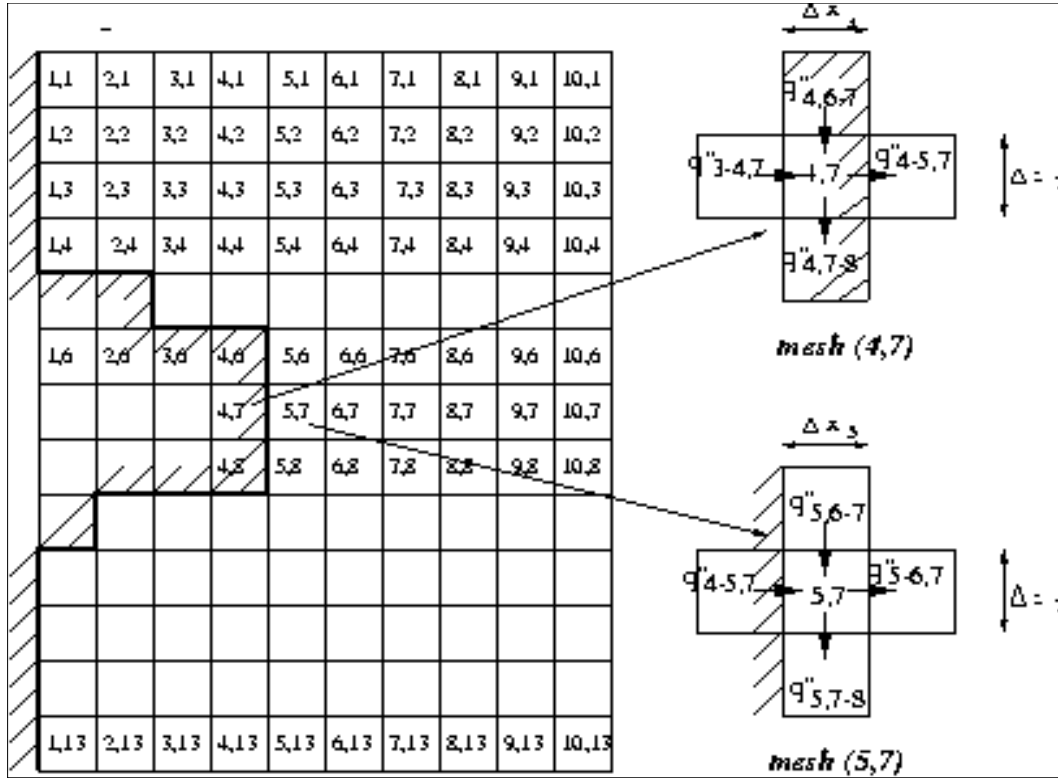
Figure 2.2   Example of the computational grid with evolving cavity due to melting

For the central nodes (5,7) and (4,7) located at the actual boundary on the solid side and the gaseous side, respectively, as indicated in Figure 2.2, we have the balance equations

$$(\rho\, c_p)^{solid}_{eff,5,7} \cdot \partial T_{5,7}/\partial t \,=\, (q''_{4-5,7} - q''_{5-6,7}) \cdot 1/\Delta x_5 + (q''_{5,6-7} - q''_{5,7-8}) \cdot 1/\Delta z_7 + q'''_{5,7} \quad (2.4.1)$$

$$(\rho\, c_p)^{gas}_{eff,4,7} \cdot \partial T_{4,7}/\partial t \,=\, (q''_{3-4,7} - q''_{4-5,7}) \cdot 1/\Delta x_4 + (q''_{4,6-7} - q''_{4,7-8}) \cdot 1/\Delta z_7 + q'''_{4,7} \quad (2.4.2)$$

The terms $q''_{i-,j}$ and $q''_{i,j-}$ are the heat fluxes into the central nodes or out of them, as indicated in Figure 2.2, the $q'''_{i,j}$ are internal heat sources.

The heat flux $q''_{4-5,7}$ at the left surface of node (5,7) is composed of a radiation part and a convective part,

$$q''_{4-5,7} = q''_{rad,4-5,7} + q''_{conv,4-5,7} = \alpha_{rad} \cdot (T^0_{rad} - T_{surf,5-,7}) + \alpha_{conv} \cdot (T_{4,7} - T_{surf,5-,7}) \quad (2.4.3)$$

with

$$T_{surf,5-,7} = (\lambda_{5-}/(\Delta x_5/2) \cdot T_{5,7} + \alpha_{rad} \cdot T^0_{rad} + \alpha_{conv} \cdot T_{4,7}) / (\lambda_{5-}/(\Delta x_5/2) + \alpha_{rad} + \alpha_{conv}) \quad (2.4.4)$$

T^0_{rad} is the temperature of the effective radiation source, α_{rad} and α_{conv} are the radiative and convective heat transfer coefficients , respectively, and λ_{5-} is the heat conductivity at the left boundary of node (5,7).

The heat flux $q''_{4-5,7}$ at the right surface of node (4,7) is due to convection only,

$$q''_{4-5,7} = \alpha_{conv} \cdot (T_{4,7} - T_{surf,4+,7}) \tag{2.4.5}$$

with

$$T_{surf,4+,7} = (\lambda_{5-}/(\Delta x_5/2) \cdot T_{5,7} + \alpha_{conv} \cdot T_{4,7}) / (\lambda_{5-}/(\Delta x_5/2) + \alpha_{conv}) \tag{2.4.6}$$

All other heat fluxes in equations (2.4.1) and (2.4.2) are due to conduction only.

2.4.2 Consideration of resolidifying melt in the computational scheme

Thermal interaction of flowing melt with solid surfaces (heat transfer, ablation) and resolidification on colder surfaces is under development in LOWCOR2. In order to maintain the scheme of the computational grid unchangeable during the degradation process of the structure considered, virtual boundary meshes are taken into account from the beginning which are to receive flowing and resolidifying melt, as shown in Figure 2.3. These boundary meshes represent the gap between HR inner surface and the outermost row of fuel rods and are defined for film type relocation and collection of metallic melt. When these boundary meshes are filled with resolidified material, melt arising from continuing melt down processes will be added to adjacent debris regions as modelled in SCDAP.
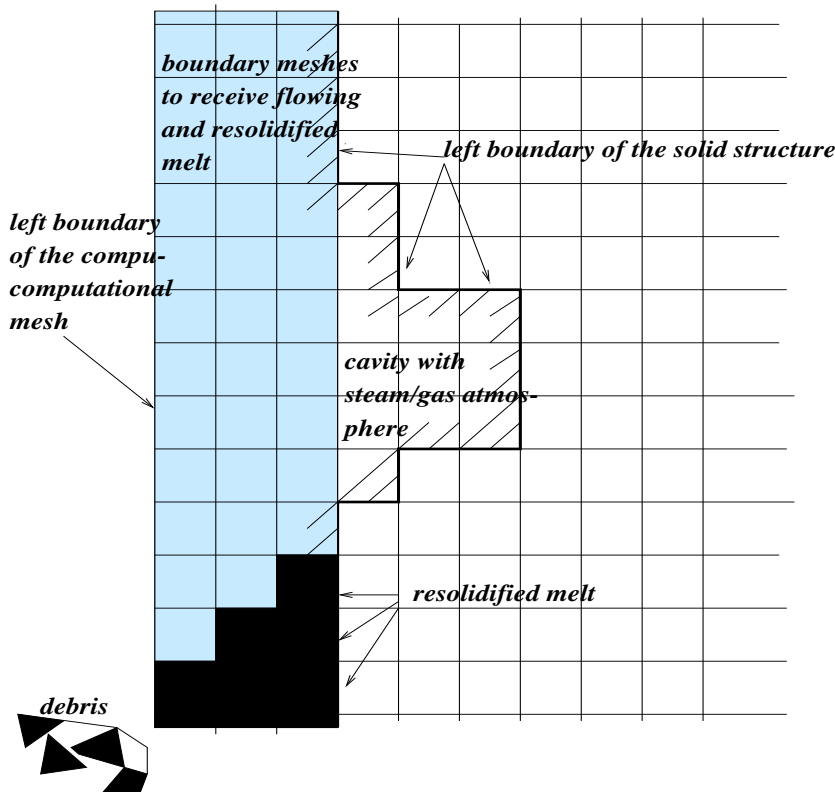
Figure 2.3   Illustration of boundary meshes for reception of flowing and resolidifying melt

2.4.3 *Viewfactors for radiation heat exchange*

The net radiation heat flux from a surface with temperature T_1, surface area A_1 and emission co-efficient ε_1 to a surface with temperature T_2, surface area A_2 and emission coefficient ε_2 is

$$q''_{1 \rightarrow 2} = \varepsilon_{ff} \cdot \sigma \cdot (T^4_1 - T^4_2) \tag{2.4.7}$$

with

$$\varepsilon_{eff} = 1 / (A_2/(A_1 \cdot F_{12}) + A_2 \cdot (1-\varepsilon_1)/(A_1 \cdot \varepsilon_1) + (1-\varepsilon_2)/\varepsilon_2) \tag{2.4.8}$$

where σ is the Boltzmann constant, F_{12} is the geometrical view factor for radiation heat flux from A_1 to A_2 with $A_1 \cdot F_{12} = A_2 \cdot F_{21}$. The view factors from the radiation heat source to the receiving structure like the heavy reflector change in the course of the melting process of the structure and so they must be recalculated after each time step. The calculation is done by the "crossed string" method /4/ . Figure 2.4 shows schematically the geometrical situation for radiation heat exchange between a sub-area A_i as part of the heat source, and a sub-area B_j as part of the developing cavity of the melting structure. The "crossed string" method yields for the view factor from A_i to B_j

$$F_{A_i \rightarrow B_j} = (l_{ad} + l_{bc} - l_{bd} - l_{ac}) / (2 \cdot L_{A_i}) \tag{2.4.9}$$
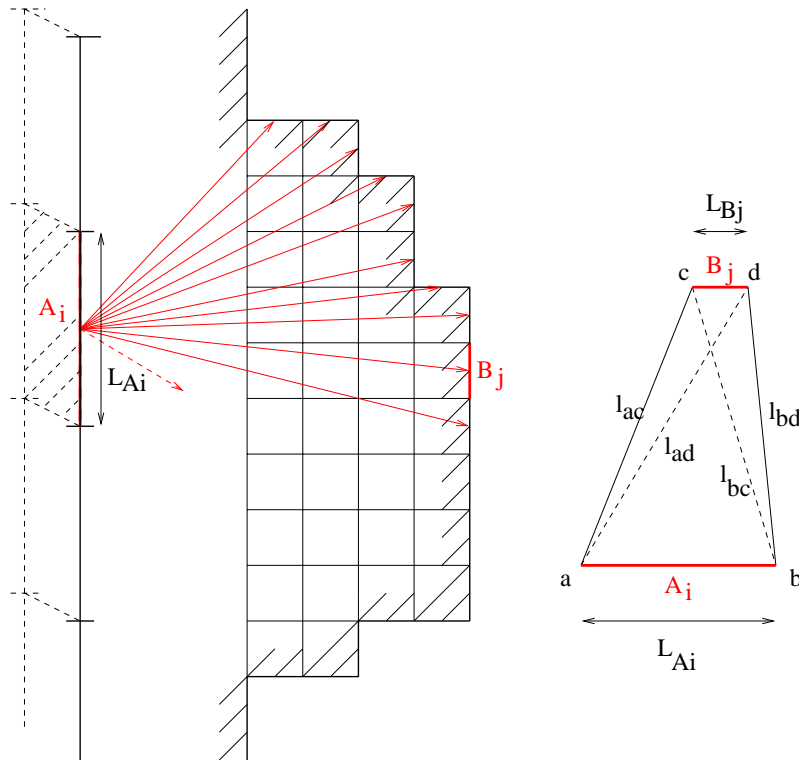
Figure 2.4   Scheme illustrating the calculation of view factors for radiation heat exchange

Moreover, we have the condition:

$$\sum_{j}^{n} F_{A_i \rightarrow B_j} = 1 \tag{2.4.10}$$

The l_{ad}, l_{bc}, l_{bd}, and l_{ac} can be calculated by simple geometrical considerations.

2.5 FIDAP

In severe core damage codes (sections 2.2, 2.3) used to simulate the evolution of in-vessel late phase degradation, the core enclosure structures like HR and CB are modelled as cylindrical components. A cylindrical structure has to use a average HR thickness so that the inner shape along the FE periphery cannot be represented realistically (Figure 2.1). This leads to a constant thickness of app. 0.198 m in the model whereas the maximal thickness is 0.25 m and the minimum 0.102 m.

In order to take into account the possible difference in the melt process resulting from the approximation of the HR thickness, the commercial program: FIDAP/22/, was used. The finite element (FEM) code FIDAP 7.6 (Fluid Dynamics Analysis Package) simulates the behaviour of viscous, compressible, and incompressible fluids by solving the Navier-Sokes-equation, the continuity equation, and the energy equation. The most interesting characteristics are:

- newtonian and non- newtonian fluids,
- laminar and turbulent flows,
- stationary and transient simulation of single and two phase flows,
- flow through porous media (porous body approach),
- heat conduction, radiation, and convective heat transfer,
- rigid, moving, and free surfaces,
- and phase transitions due to melting.

The following boundary conditions for the fluid analysis can be specified: fluid velocity and temperature, turbulent kinetic energy and dissipation, heat flux, surface tension, pressure gradients, and heat transfer by heat conduction, radiation, and convection /23/.

In this study mainly 2-D / 3-D heat conduction including material phase change was considered to simulate precisely the complex lateral shape of HR and CB. First, a 2-D model was developed describing a horizontal slice of the outer core channel, HR, and CB. To take into account axial effects, it has been extended to a 3-D representation. The details of the application of FIDAP are described and discussed in section 6.

3 ACCIDENT SEQUENCE ANALYSES

Three accident scenarios have been studied with S/R5 yielding temperature data of the degrading fuel elements in the outer core ring adjacent to the HR as boundary conditions for the investigation of the HR and CB degradation by means of LOWCORE2, ICARE2, and FIDAP. The first example considered was a LBLOCA (i.e. rupture of pressurizer surge line) selected in order to demonstrate the principal applicability of ICARE2 and FIDAP for the purposes described above. The results of this study are discussed in sections 5 and 6, respectively.

In the following section two scenarios deliver boundary temperatures for detailed analyses with LOWCOR2. First scenario is a small break loss-of-coolant accident (SBLOCA) with a leak in the cold leg of 46 cm² in section 3.2. Second scenario is a loss of off-site power (LOOP) case with complete loss of electrical power systems (section 3.3).

3.1 Plant model

The S/R5 input deck for an adequate plant representation /10/ is based on a RELAP5 input deck from Siemens/KWU. The originally four loop model was reduced to a two loop model, one representative for the damaged loop plus one lumped loop simulating the three unaffected loops. It includes all significant primary circuit components as well as secondary side components necessary to simulate LOCA and LOOP accidents starting from normal operation. Also necessary parts of the reactor control, surveillance and limitation system (RCSL) are realised by RELAP5 trip logic and control variables. All piping are coupled to 1D heat structures to achieve realistic boundary conditions. At the outer surface of the piping walls adiabatic boundary conditions are assumed.

3.1.1 Core model

The reactor core (Figure 2.1 left) is divided axially into 16 zones, with 14 zones representing the active core, each 0.3 m long (Figure 3.1 centre). In radial direction five rings (Figure 3.2) plus a bypass channel simulating the cooling borings in the heavy reflector allow detailed analyses even in the late phase of severe core damage accidents.

In each core channel one representative fuel rod plus one absorber rod is simulated. Radiative heat exchange is modelled between adjacent rings based on the real interface areas of the FE geometry. The fifth ring is surrounded by a SCDAP shroud component simulating the heavy reflector (HR) as well as the core barrel (CB). The cooling borings of the HR are simulated by a material layer with reduced density, heat conduction, and heat capacity values. The outer surface of this shroud component is in contact with the downcomer which is surrounded by another SCDAP shroud component simulating the reactor pressure vessel (RPV) wall, allowing radiative heat transfer across the downcomer.

This is important for radial heat flux calculations in the late phase modelling to investigate the melt down behaviour of HR and CB. The RPV internals above (UCP) and below (LCSP) the core are modelled as RELAP5 heat structure components.
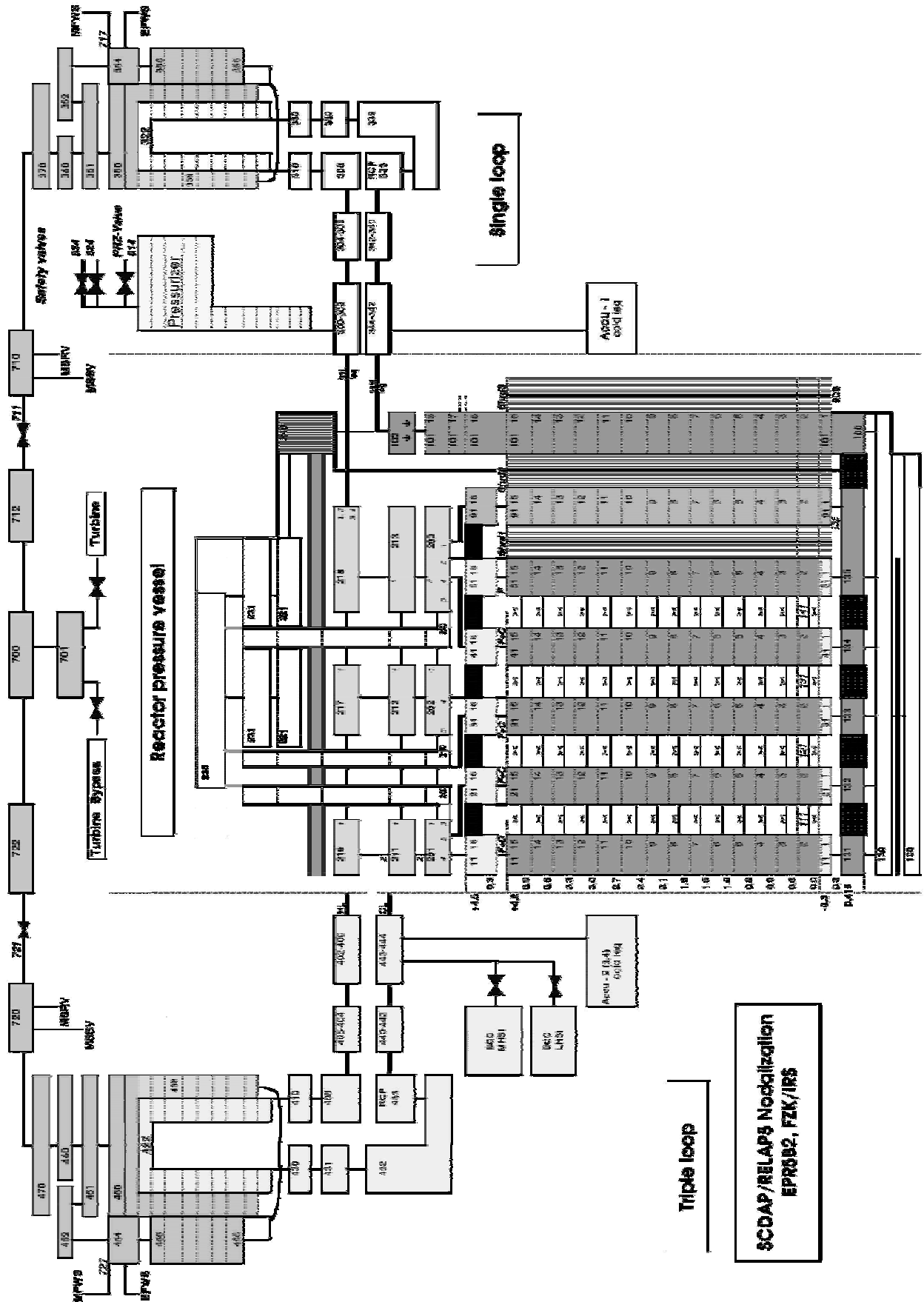
Figure 3.1   Plant nodalisation used for S/R5 analyses. All components shown are re-
quired in the different scenarios except for ECC injection systems
(LHSI, MHSI /10/).
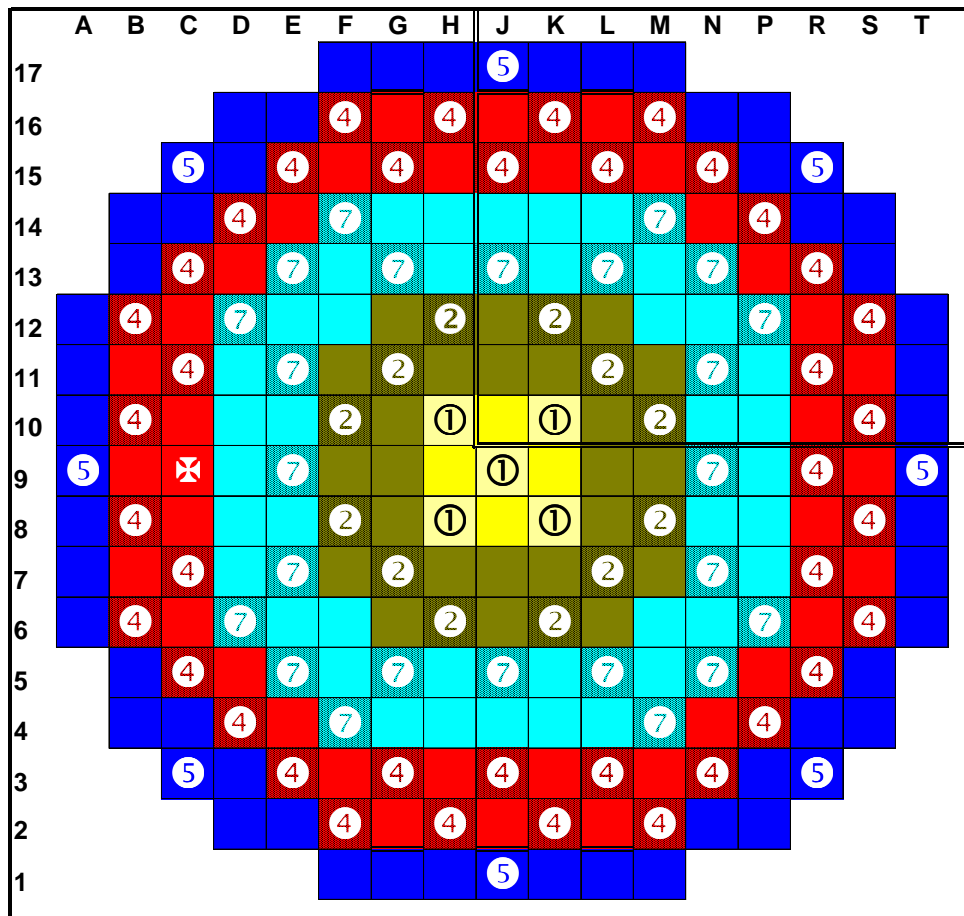
Figure 3.2   Radial core discretization for S/R5 analyses.

3.1.2 Power distribution in the core

The local power in each node of the core is derived from the decay heat and distributed using an axial shape (Figure 3.4) and a radial power profile (Figure 3.5). The decay heat curve derived from the ORIGEN code assuming UO_2 and 50% MOX loading plus an additional safety margin of 5% as shown in Figure 3.3.

The axial power profile was selected as a simplified chopped cosine profile to allow comparison with MAAP and MELCOR results. In this study a begin of cycle (BOC) situation is assumed, since the rather flat radial power profile is most challenging for melting of the HR.

The radial decay power variation shown in Figure 3.4 is rather small (app. 10%) and reflects the optimised BOC core loading state. In axial direction, the decay power varies between 0.34 at the axial ends and 1.435 in core centre.

3.1.3 User parameters of S/R calculations

To simulate severe core damage scenarios, S/R5 required some additional information which are listed here. In case of clad bursting due to fuel rod overpressure a maximum clad strain of 20 % was allowed until clad bursts. The cladding oxide scale failure temperature was set to 2350 K if

less than 60% of the cladding thickness is oxidized, derived from code validation using CORA and PHEBUS tests. The influence of a non-condensable gas layer next to the outer clad surface (N_2, H_2) which may hinder oxidation was taken into account.

Furthermore, the criteria parameter in the S/R5 crust failure model of the molten pool was set to initiate early crust failure, so that at contact between molten pool crust and HR inner surface lateral failure is calculated.
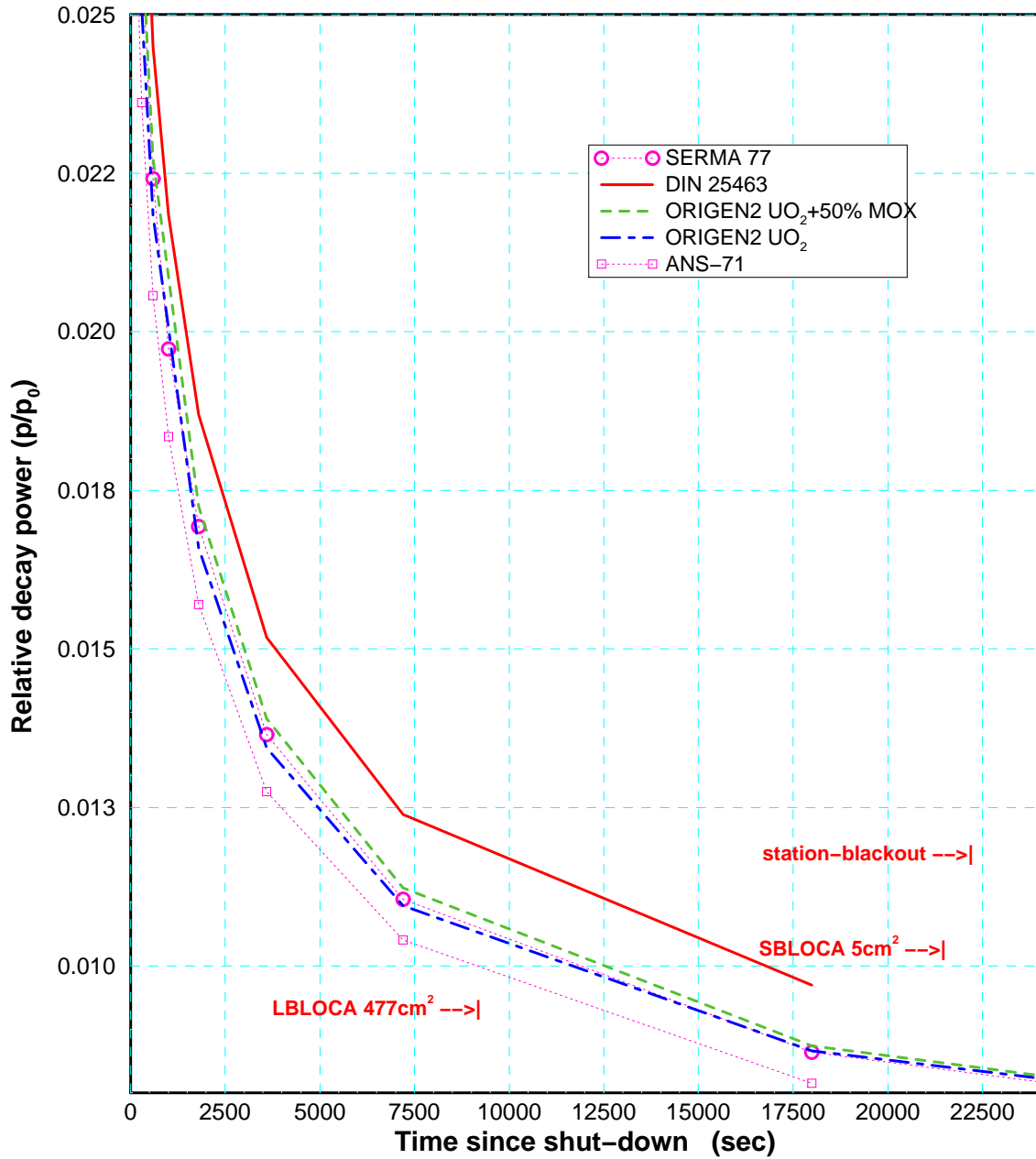
FZK/IRS, W. hering, 10/96

Figure 3.3   Decay heat curve used in the present study: ORIGEN UO_2 + 50%MOX.
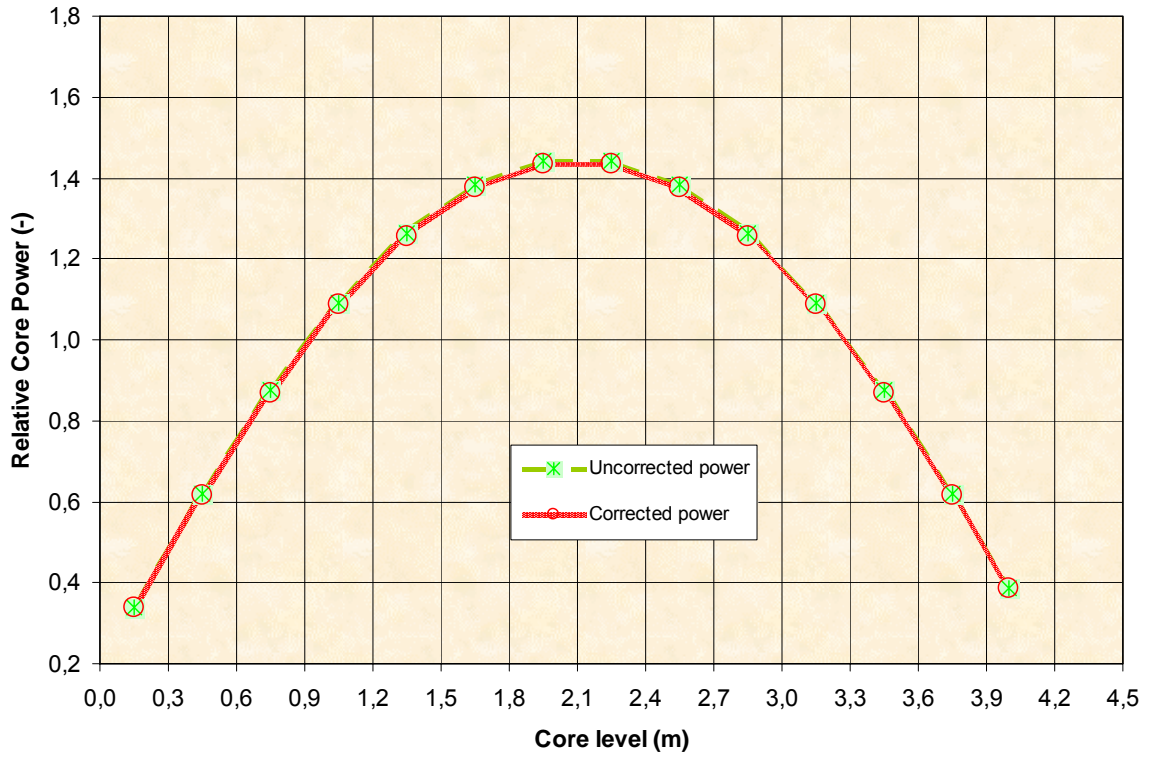
Figure 3.4   Chopped cosine type axial power profile used for accident analyses with S/R5 mod 3.2.
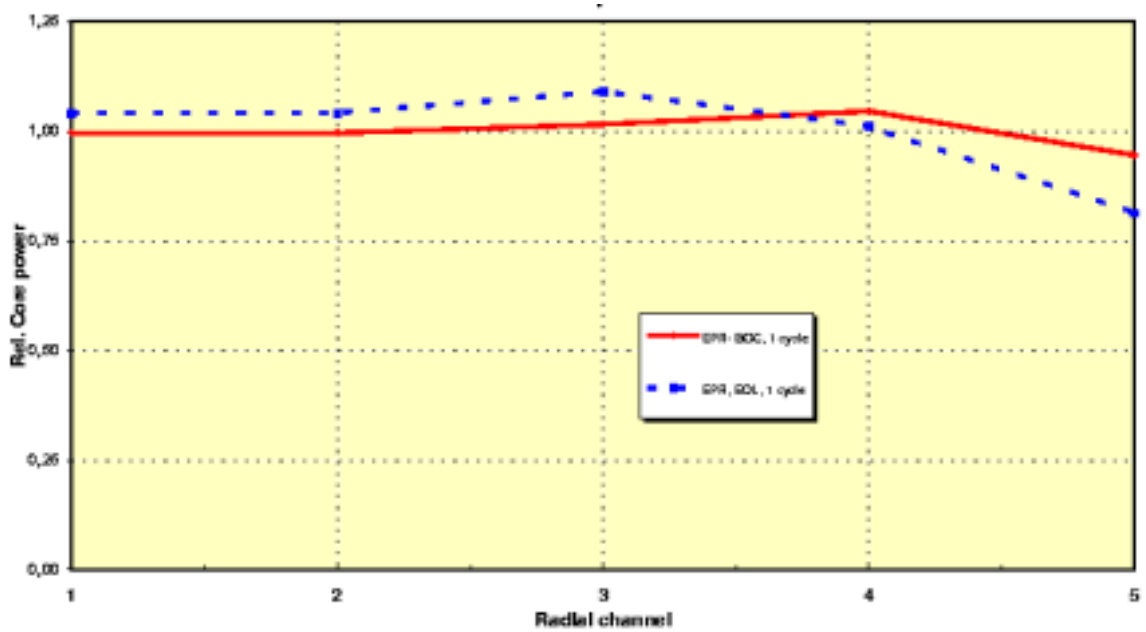
Figure 3.5   Radial power profile for 5 channel discretization used in the S/R5 mod 3.2 analyses

3.2 SBLOCA scenario with S/R5 mod 3.2β

The SBLOCA scenario was selected because of the availability of results calculated during a benchmark exercise by S/R5m31 and S/R5m32 /4/, MELCOR **/1/**, and MAAP /2/. During that benchmark the EPR input deck was adjusted to the actual state of the ongoing development in the basic design optimisation phase represented by the MAAP input deck. So, water inventory was adjusted and the accumulator surge lines were kept open, to allow nitrogen being injected into the saturated liquid of the primary system. The results of S/R5m32β were used as input for the detailed analyses with LOWCOR2 (section 4.2). The effects of the open-loop coupling (missing feed-back) will be discussed hereafter.

To overcome code difficulties arising with non-condensables in sub-cooled liquid the recent code improvements available in RELAP5 mod 3.2.2.β were included in S/R5m32. In S/R5 however, this non-condensables predictor logic causes unexpected results effecting the time scale of reflux condensor mode. For the present study only core temperatures are required as boundary conditions, so that only a short sketch of the course of the SBLOCA accident will be given here. Newer calculations with S/R5 mod 3.2.irs are discussed in /26/.

3.2.1 Thermal-hydraulic phase

After leak detection reactor scram occurs at 37 s due to low primary system pressure signal. Primary system pressure now follows the automatic secondary system pressure (Figure 3.6 b) until 30 min later fast secondary side depressurisation is assumed. The SG water inventory evaporates and at 506 s the collapsed water level in the SG2 falls below 13m, whereas the water level in SG1 is maintained by the EFWS as can be seen in Figure 3.8 b.

Table 3.1   List of events calculated for the SBLOCA scenario with S/R5 mod 3.2β.

Type (General)	Time (min)	Primary System Pressure (MPa)	PCT (K)
Reactor scram (=time of LOOP occurrence)	0.1 sec	15.5	T_{sat}
Fast cool-down of secondary side	32	4.0	T_{sat}
Onset of core heat-up	367	<4.0	T_{sat}
Manually activated primary side depressurisation	----	17.2	T_{sat}
Accumulator injection period	33	4.5	T_{sat}
SG2 secondary side dry-out (LOOP2 w/o EFWS)	75	17.2	T_{sat}
Onset of hydrogen production	424	app. 0.6	1000
Onset of clad failure (ballooning, clad rupture)	425	app. 0.6	1196
Type (Local) Localisation by: R=ring, Z=axial zone	Time (min)	Position in the core R-Z	PCT (K)
Onset of Absorber rod failure	414	R-1, Z-12	
Onset of melt relocation forming localised debris	443	R-1, Z-12	2830
Melting of upper core plate (R1-R5)	459	R-1	
Onset of large debris formation	460	R-1..R-4, Z-9	2830
Onset of pool formation	462	R-1, Z-2.85m	
Debris/Molten pool crust contacts heavy reflector	487	R-5, Z-1.95m	
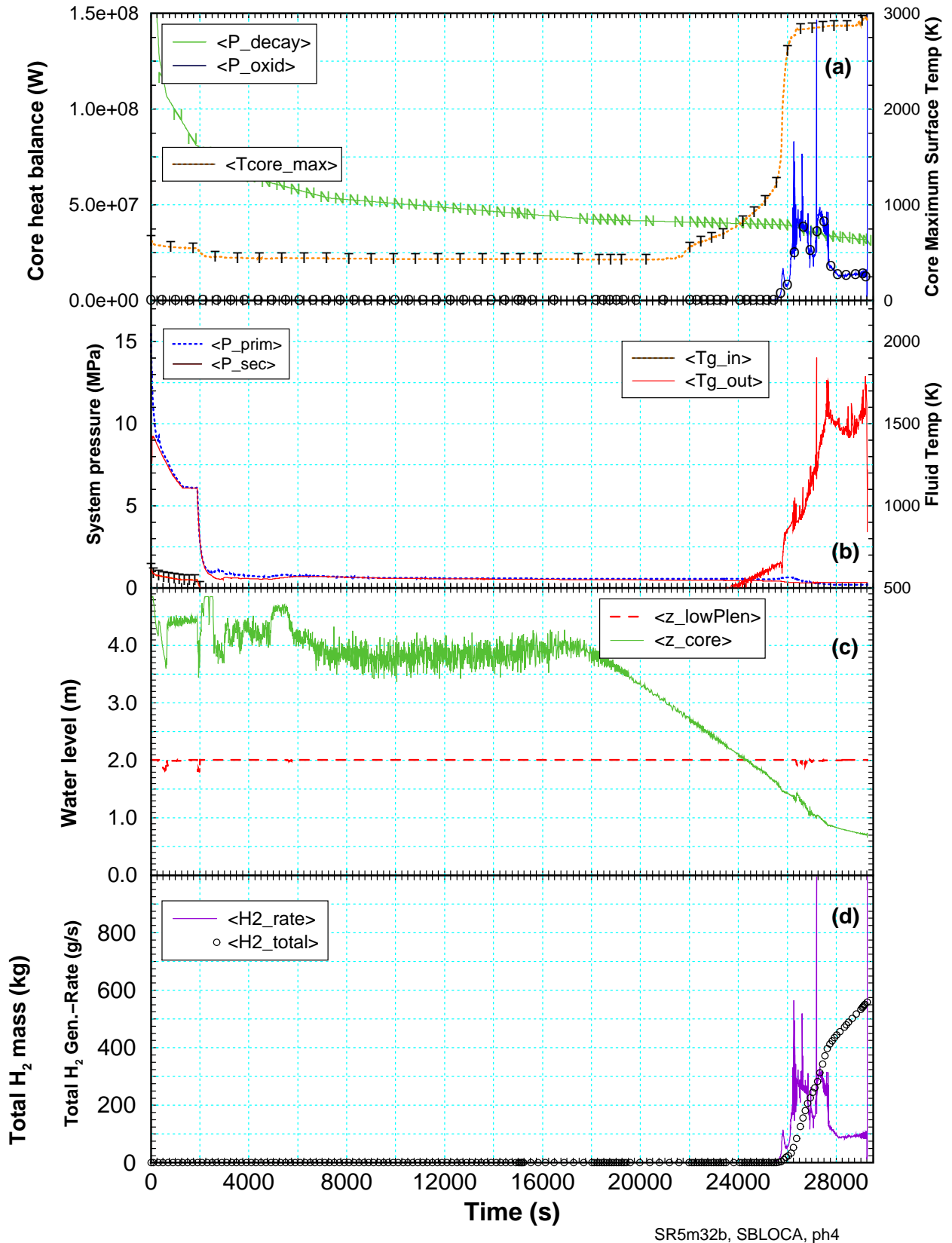
Figure 3.6   Results of SBLOCA with S/R5m32ß: (a) nuclear and chemical power (left side) and PCT (right side), (b) overview of the system pressure (left scale) and core inlet/outlet fluid temperatures (right scale), (c) collapsed water level of core and lower plenum, and (d) hydrogen production rate (left) and total hydrogen mass (right).

At 1911 s the primary system pressure drops below 4.5 MPa so that the accumulators feed in (Figure 3.7 d). Since the accumulator surge lines are not closed, nitrogen enters the primary system just after end of water injection at 2200 s. During the whole thermohydraulic phase (up to 22000 s, 367 min, Table 3.1) in which the PCT is always below 500 K (Figure 3.6 a), the primary system behaviour (Figure 3.7) is dominated by secondary side conditions (Figure 3.8). Between 2300 s and 5100 s the non-condensables influence the hydraulic conditions in the primary circuit keeping the leak outflow unstationary but rather low (Figure 3.7 d). In this period fluid oscillations are calculated for the hot legs of both loops because primary system pressure is higher than secondary system pressure (Figure 3.7 a).

Between 5000 s and 6200 s an increased leak mass flow rate is calculated (Figure 3.7 d), mainly due water-steam mixture fluid at the leak position. This explanation is supported by the high water level in the downcomer and in the core (Figure 3.6 c). Afterwards the hot leg becomes empty so that natural circulation can start. The noise in the core collapsed water level signal between 6000 s and 20000 s is caused by condensed water dripping from hot leg of loop 1. Up to 26000 s a rather stable reflux condensor mode is calculated for the loop 1 with gas velocities of 10-15 m/s (Figure 3.7 c). This velocity is somewhat higher compared to results of recent calculations with S/R5m32 (< 12 m/s) /26/. This can be explained by a reduced momentum exchange between gas and liquid in S/R5m32β. The leak mass flow rate in this period for pure steam is rather low at app. 3.5 kg/s.

The pressure increase at 25500 s (Figure 3.7 a) indicates a massive release of hydrogen which temporarily stops the natural circulation as shown in Figure 3.7 c, no significant heat can be transferred to the secondary side (Figure 3.8 a) so that the oxidation energy and the decay heat remains in the core. App. 1000 s later primary system pressure drops below that of secondary system so that the driving force of the natural convection is lacking. The pressure in the SG1 secondary side remains at app. 0.35 MPa due to pressure losses in SG, valves, and pipes.

In Figure 3.8 c the make-up of the SG by the EFWS is shown. During natural circulation time, the make-up rate of the EFWS is sufficient to maintain enough water. After 26000 s the heat input is vanishing and hence the evaporation rate, so the make-up rate is reduced automatically to avoid overfilling of the SG as shown in Figure 3.8 d. The positive net flow rate after 25000 s leads to a complete fill-up of SG1.

The fluid temperature shown in Figure 3.8 e indicates the different behaviour of both SG. SG2 follows the steam temperature of the primary system. The fluid temperature of SG1 reflects the saturation temperature which is controlled by the SG 1 secondary side pressure.

3.2.2 Core degradation

Core degradation phase starts at app. 22000 s (367 min). Up to 25900 s (432 min) core heat-up is controlled primarily by decay heat (Figure 3.6 a), afterwards chemical energy from the Zry oxidation drives the PCT up to 2800 K. Core degradation process starts with metallic melt relocation at app. 26000 s and within next 1500 s debris is formed in the core leading to formation of a molten pool as shown in Figure 3.10 a+b.
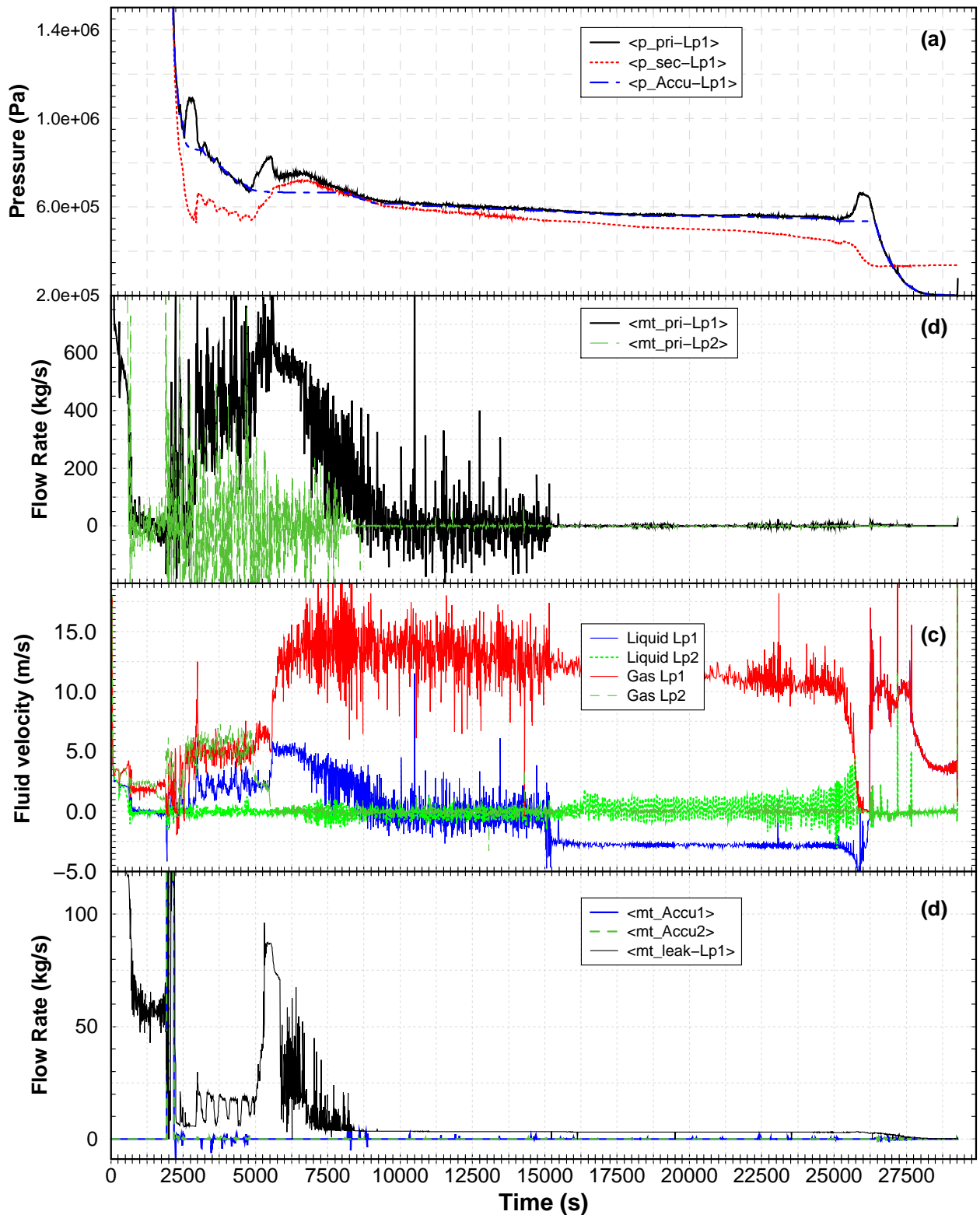
Figure 3.7   Primary system behaviour: (a) primary, secondary and accumulator pressure, (b) mass flow rate in the hot leg of both loops, (c) gas and liquid velocity in the hot leg pipes, and (d) mass flow rates from accumulator and through leak.
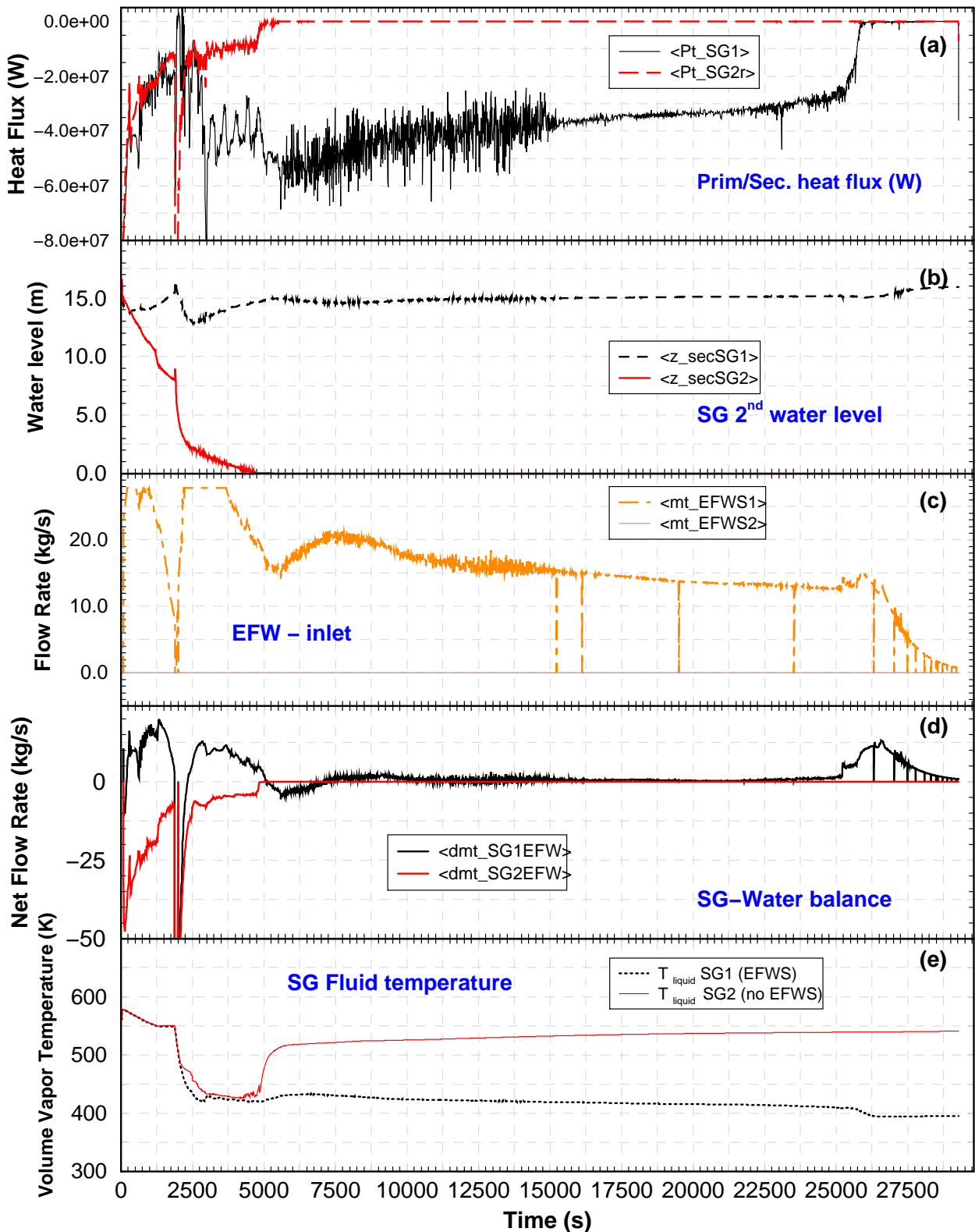
Figure 3.8   Secondary system behaviour: (a) heat transfer from primary side, (b) collapsed water level in SG, (c) emergency feed-water system makeup rate, (d) internal SG circulation, and (e) fluid temperature in both SG.
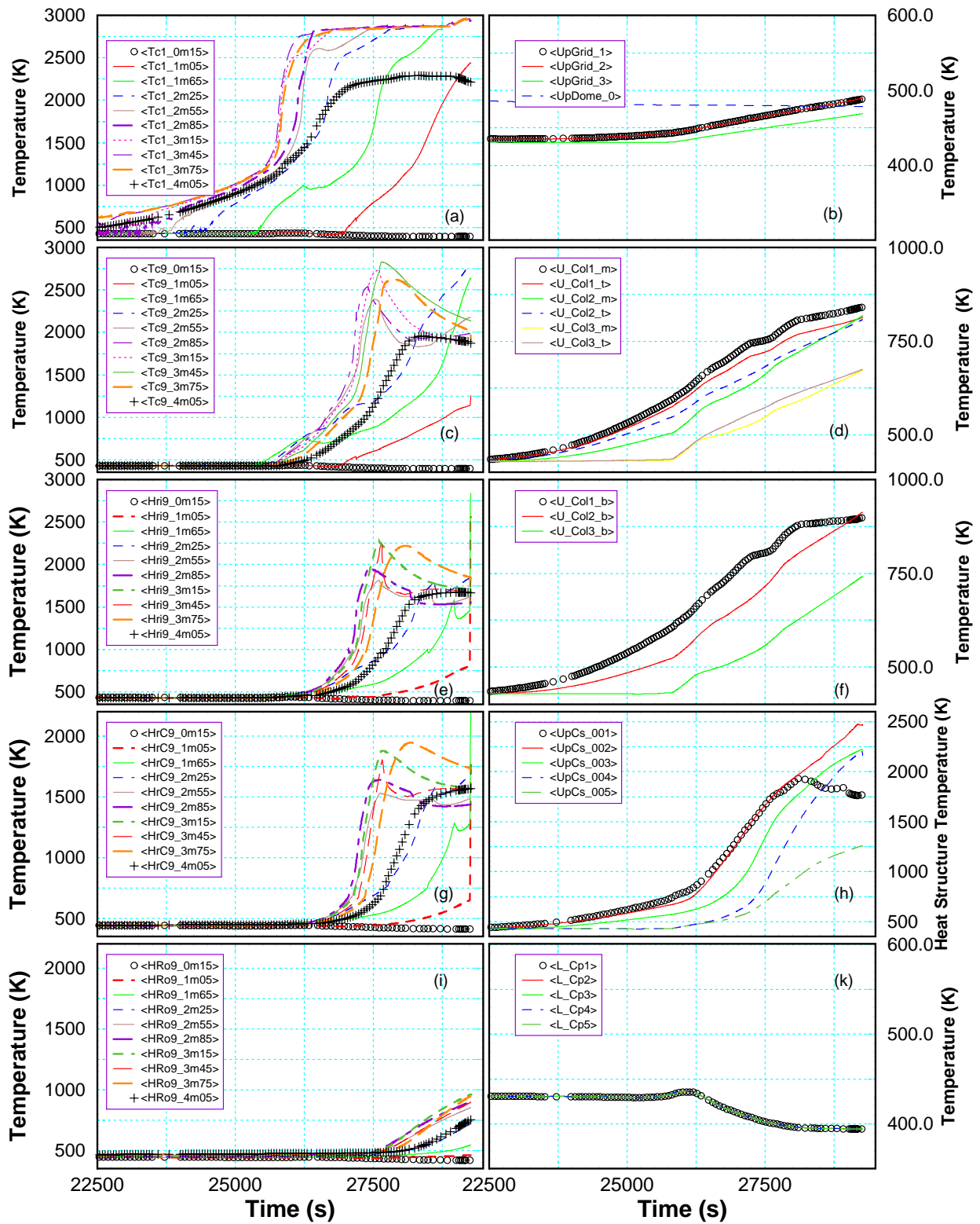
Figure 3.9 Temperature history in the core: (a) centre ring, (d) outermost ring adjacent to the radial core enclosure, (e) HR inner surface, (g) HR–CB interface, (i) CB outer surface, and right column: (b) upper support plate (USS), (d) upper part of support columns, (f) lower part of support columns, (h) upper core plate, and (k) lower core support plate.
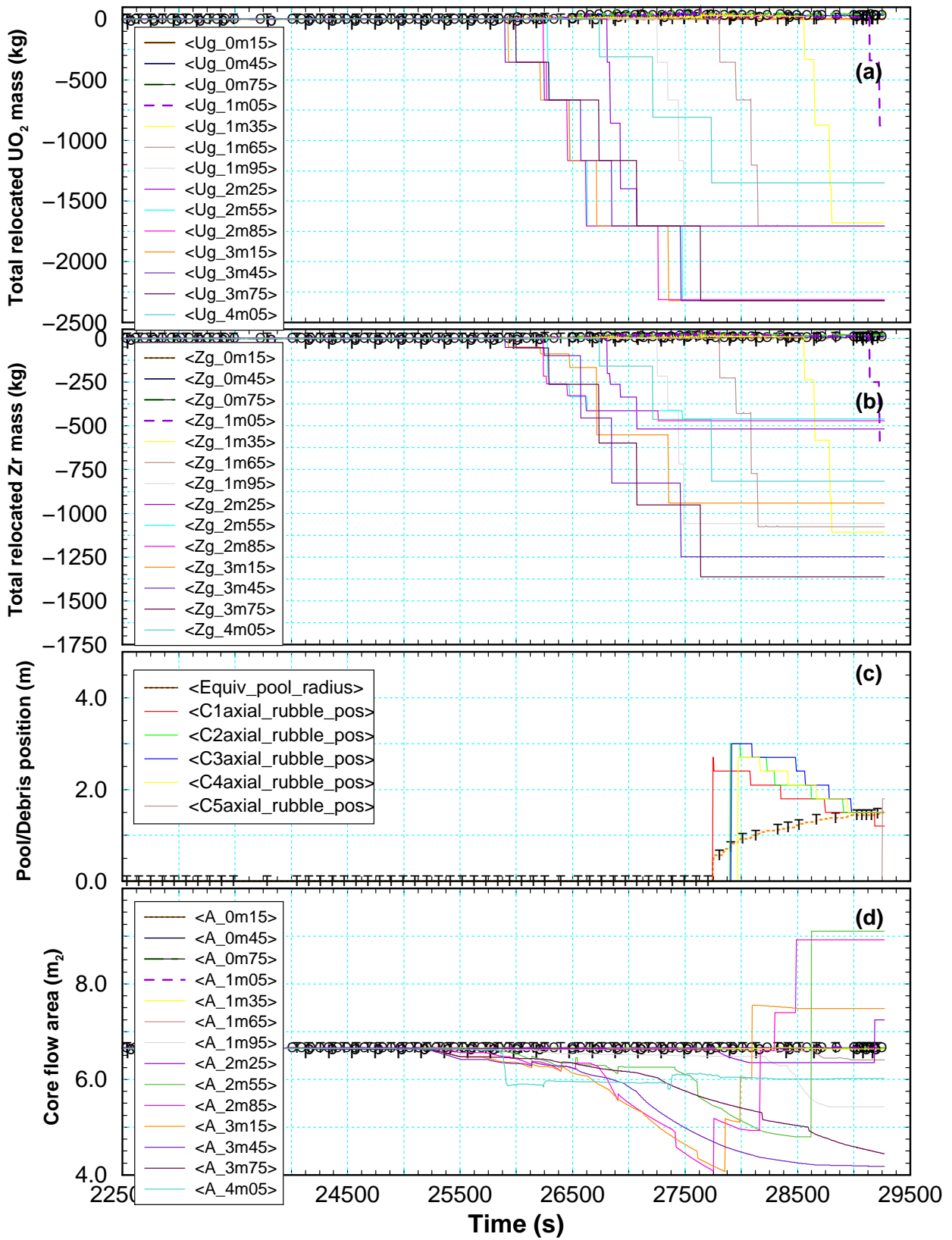
Figure 3.10   Late phase material relocation: (a) relocation of UO$_2$, (b) relocation of Zr, (c) evolution of equivalent pool radius (-T-) and axial position of supporting rubble, and (d) net flow area of the whole core.

The growth of the molten pool is shown in Figure 3.10 (c) as well as its axial position in the core. A better understanding of the in-core molten pool development is given in Figure 3.11. Here the axial and radial position of the lower crust supporting the molten pool is shown at times when the code calculates a change in configuration.

For this study the temperature history adjacent to the HR is important. In Figure 3.9 the core centre as well as the outer ring temperatures are given on the left side together with the temperatures calculated by S/R5m32ß for HR and CB. In this calculation a core wide thermal radiation simulation scheme was used. This promotes a more pronounced radial core damage spreading compared to five individual rings without inter-ring radiative heat exchange. In S/R5 the fluid temperature used to compute the absorbed thermal energy in the fluid is averaged over all channels in one radiation enclosure. This leads to an increased absorption and hence to a higher core outlet temperature. When debris or molten pool formation is calculated S/R5 stops the calculation of the radiative heat transfer for this level and this enclosure.
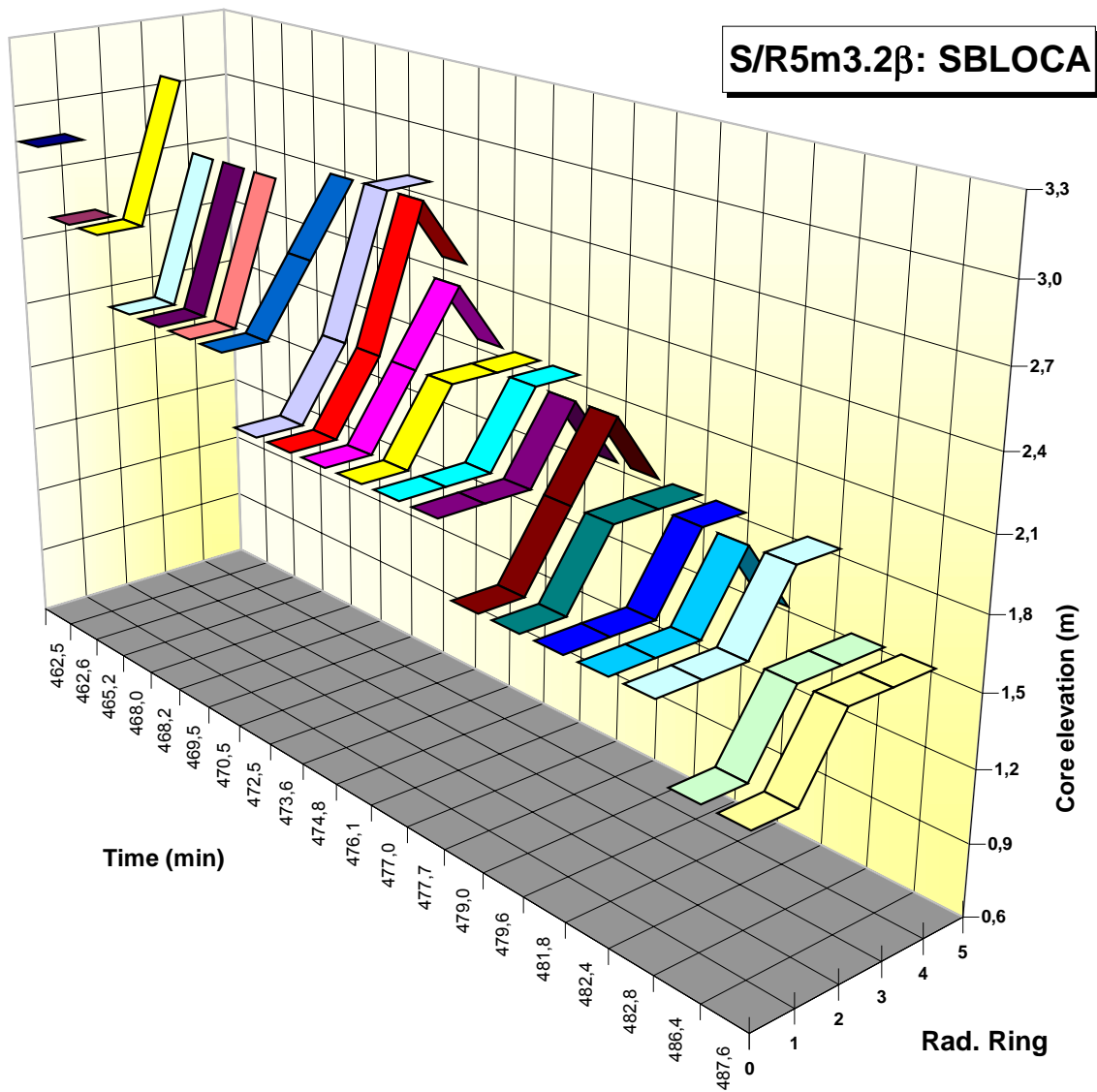
Figure 3.11   Late phase in vessel molten pool spreading indicated by the upper end of the lower crust position for all five rings in the core starting from 27747 s (462 min). The back wall represents the HR.

As a consequence HR heat-up is reduced in the section between 1.2 m and 3.0 m. In case of low pressure steam atmosphere radiative heat transfer contributes significantly to the HR heat-up. Just below molten pool level a radiative heat flux of $6.4*10^{+5}$ W/m^2 is calculated whereas a convective heat transfer coefficient of 105 W/m^2.K, a surface temperature of 1115 K, and a fluid temperature of 1242 K lead to a convective heat flux of $-1.32*10^{+4}$ W/m^2. So the neglect of the radiative heat transfer from the crust to the HR cools down the HR to fluid temperature level.

On the right side of Figure 3.9 temperatures of the upper plenum internals as well as the lower core support plate are given. Collapsed water level in the core remains at 0.7 m as shown in Figure 3.6, so that the lower core support plate is kept cold at saturation temperature. The upper core plate temperatures shown in Figure 3.9 h indicates onset of melting of the innermost two sections at 27500 s (458 min), for section 3 app. 120 s, and for section 4 app. 500s later. The outermost ring remains solid. For this calculation the molten material is kept in place. The support columns are calculated to remain intact, even the lowest axial section. The steep temperature increase in Figure 3.9 e +g is caused by the numerical instability of the shroud failure model when in contact with molten corium.

		h	min	sec			
	At time:	29271	487,85	8,13		HR Shrd	
	1	2	3	4	5		
	1	3	5	7	9	11	FE-head
14 4,05	I	I	I	P	I		
13 3,75	v	v	v	v	I		
12 3,45	v	v	v	v	P		
11 3,15	v	v	v	v	I		
10 2,85	v	v	v	v	P		
9 2,55	v	v	v	v	P		
8 2,25	v	v	v	v	P		
7 1,95	M	M	M	M	M		47,650 Mg UO2
6 1,65	M	M	M	M	P		0,400 Mg Zr
5 1,35	M	P	P	P	I		8,600 Mg ZrO2
4 1,05	P	I	I	I	I		3,400 Liq. Debris
3 0,75	I	I	I	I	I		3,400 Liq. Debris
2 0,45	I	I	I	I	I		60,050 Total
1 0,15	I	I	I	I	I		

FE-feet Support plate

0,370 Mg UO2
0,004 Mg Zr
0,067 Mg ZrO2
0,000 Mg SS
0,000 Mg AgInCd
0,441 Total

Debris app. 0,1 m

Figure 3.12   Final state of SBLOCA with S/R5m32β; code fails just after contact between molten pool and HR.

3.2.3 Final state

In Figure 3.12 a sketch of the final state is given for the last time step of the calculation at 29271 s (488 min). It shows that the molten pool, indicated by (M) contacts the HR inner surface at 1.95m core elevation so that the code fails due to numerical instabilities at that time. A tiny fraction of the molten pool inventory has relocated thought the downcomer (Figure 3.12, right) but has not yet interacted with water in the lower plenum. The upper half of the core is partially voided due to temperatures above melting point of UO_2-ZrO_2.

<u>Mass errors</u>

In the primary system the mass error amounts to 10.6 Mg which has to be compared with the remaining water mass in the primary system of app. 39.7 Mg (app. 26 %). In the secondary system, a mass of 137.1 Mg is maintained in the SG1 and SG 2 so that the mass error of app. 1.050 Mg is negligible.

3.3 LOOP scenario with S/R5 mod 3.2

From different scenarios investigated with S/R5 (section 2.2) the loss of off-site power (LOOP) scenario was selected for the following presentation to be representative for delayed reflood prior to onset of oxidation and core degradation. For this scenario, a total loss of off-site power and additionally a complete loss of on-site emergency power driven by the small and the large diesel generators is assumed. Only battery power is available for the reactor control and safety systems, and to activate valves. For the LOOP "base case" no operator interaction is assumed besides primary depressurisation so that simulation proceeds into core degradation. Formation of a molten pool in the core is calculated after app. 3.9 h (Figure 3.13 d) and a contact between crust of the molten pool and the heavy reflector at app. 4.5 h. For the reflood study, however, it is assumed that electrical power supply for ECC pumps can be re-established before the peak core temperature (PCT) exceeds 2300 K at 3.8 h after reactor scram. In the following section a short overview of the base case is given since some data are required in the next section.

3.3.1 Thermal-hydraulic phase

In Figure 3.13 results of LOOP "base case" calculation are shown, starting 2400 s after loss of off-site power. At loss of power, the absorber rods immediately drop into the core, shutting down the reactor. Primary coolant pumps and main feed water coolant pumps slow down, and after 10 s main coolant pumps stop (Table 3.2).

Table 3.2   List of events calculated for the LOOP scenario.

Type (General)	Time (min)	Primary System Pressure (MPa)	PCT (K)
Reactor scram (=time of LOOP occurrence)	0.1 sec	15.5	T_{sat}
Evaporation of SG secondary side	100	16.9	T_{sat}
Fast cool-down of secondary side	192	4.0	T_{sat}
Onset of core heat-up	198	<4.0	T_{sat}
Manually activated primary side depressurisation	142	17.2	T_{sat}
Accumulator injection period	158	4.5	T_{sat}
SG secondary side dry-out (no injection by EFWS)	104	17.2	T_{sat}
Onset of hydrogen production	228	0.9	1000
Onset of clad failure (ballooning, clad rupture)	229	0.88	1205
Type (Local) Localisation by: R=ring, Z=axial zone	Time (min)	Position in the core R-Z	PCT (K)
Onset of Absorber rod failure	233	R1 - Z11	2240
Onset of melt relocation forming localised debris	235	R1 - Z11	2830
Onset of large debris formation	240	R1 - Z11	2840
Melting of upper core plate (R1-R5)	244	R2: 260 min	2860
Onset of pool formation	252	R1 – Z10	2870
Debris/Molten pool crust contacts heavy reflector	305	R5 – Z7	2890
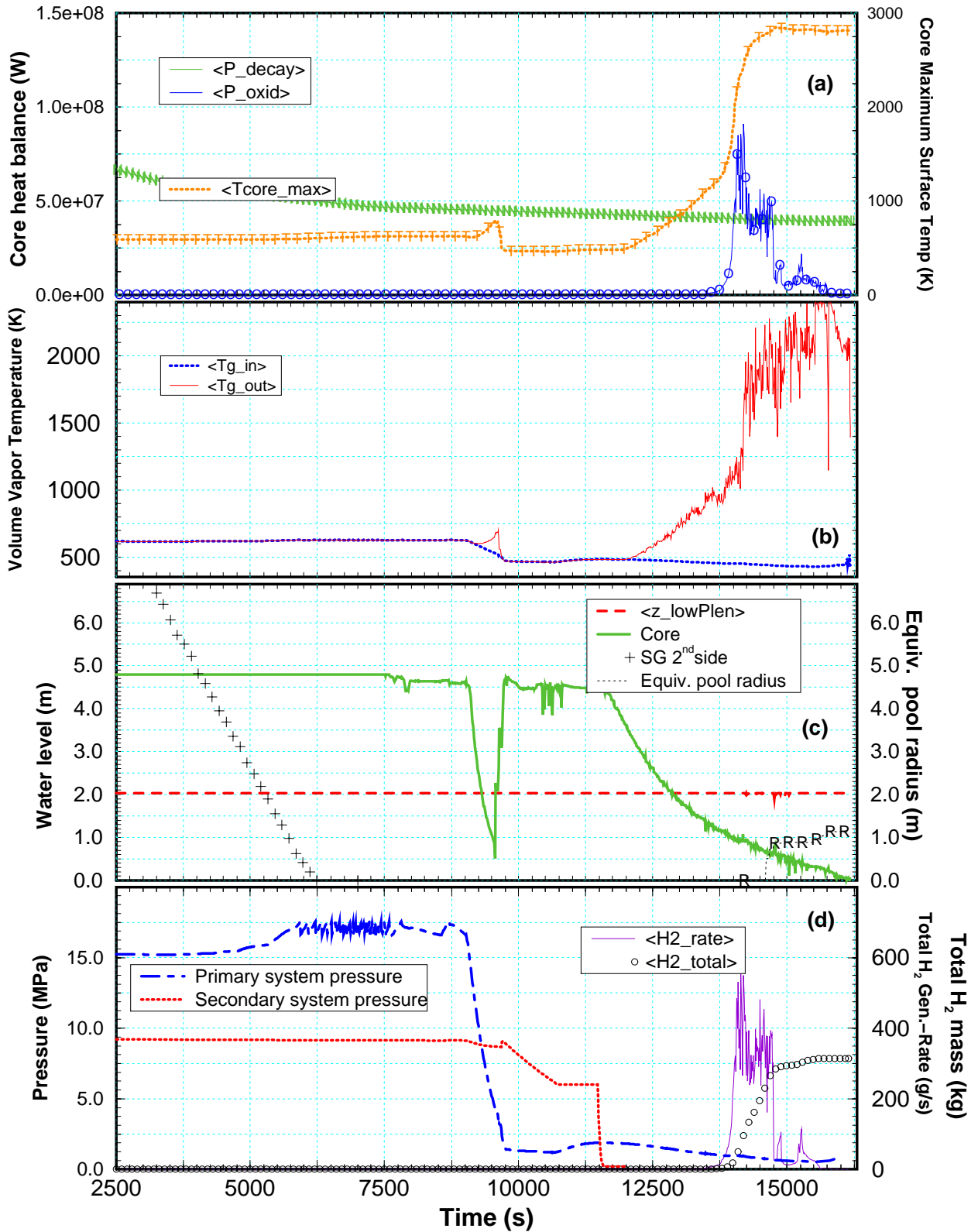
Figure 3.13   Results of LOOP "base case" with S/R5m32: (a) nuclear and chemical power (left scale) and PCT (right scale), (b) core inlet and outlet fluid temperatures, (c) collapsed water level of SG secondary side, core and lower plenum (left), and equivalent radius of molten pool in the core (-R-, right), and (d) pressure history (left) and hydrogen production rate and total hydrogen mass (-o-, right scale).

Several seconds later the turbine valve is closed, turbine bypass valve is assumed to remain closed, so that no heat can be transferred to the steam condenser directly. From that time on heat transported from the core to the SG - now by natural convection - increases secondary system pressure up to the set point of safety valves at about 9.1 MPa (Figure 3.13 d). This relatively safe state of natural circulation is maintained up to SG dry-out (Figure 3.13 c) at about 6000 s (100 min). Afterwards no feasible secondary side measure may affect the primary side effectively.

Up to SG dry-out the primary system temperature remains at saturation level (Figure 3.13 b), then the primary system pressure increases up to the set point of the first safety valve (Figure 3.13 d, valve opens at 17.6 MPa). When the pressure drops below 16.6 MPa the safety valve closes and the cycle starts again, as can be seen in Figure 3.13 d. This cycling lasts up to about 9000 s (150 min) until the core outlet vapour temperature exceeds a defined value so that the primary side depressurisation is initiated by opening the dedicated pressurizer (PZR valves 824 + 834). Then the ECC initiation signal is triggered by the signal "system pressure low" starting secondary side depressurisation, as can be seen in Figure 3.13 d.

About 600 s (10 min) after that primary system depressurisation, the primary system pressure has dropped below 4.5 MPa and the accumulator check valves open. Four minutes later, the accumulators are empty and the core is refilled as can be seen in Figure 3.13 c. In this study fast secondary side depressurisation is simulated 1800 s (30 min) after ECC initiation, however, there is no influence on the primary side, since the SGs are already empty (Figure 3.13 c).

After refill the primary system pressure is sustained at about 1.0 MPa corresponding to the specified containment pressure of 0.2 MPa and the pressure losses along the flow path through hot leg, surge line, PZR, and depressurisation valve.

The boil-down period starts at about 11520 s (192 min) with a collapsed water level of 4.5 m in the core. 11880 s (198 min) into the transient the core heat-up phase starts, the PCT rises with about 0.45 K/s for 1800 s up to 1300 K. In Figure 3.14 the corresponding cladding temperatures of the first ring (a), of the 3rd (c), the 5th ring (e), the heavy reflector inner surface (g) and outer (i) temperatures are given for the time window of reflood calculations for indicated elevations (4m05 = 4.05 m). On the left side the temperatures of vessel structures are given: upper head (b), the upper support plate (d), the absorber rod guide tube in the upper plenum (f), the upper core plate (h), and the lower core plate (k). At 14600 s (243 min) even the upper core plate has not reached melting temperature (Figure 3.14 h).

3.3.2 Component failures

Clad ballooning and failure (breach) is calculated to occur in the four inner rings at 13750s (229 min) and in the outer ring about 300 s later. This delay is mainly due to the HR which acts as an efficient heat sink because of radiative and convective heat transfer since its inner surface temperature is just above saturation temperature. At 14003s (233 min), first absorber rod failure leading to melt relocation is calculated. The cladding of the fuel rod fails with subsequent melt release at 14105 s (235 min) in the 12th axial node of the central ring, and metallic melt relocates as droplets into the 11th axial node. Within the next three seconds the same process is calculated to happen in adjacent rings up to the 4th ring, the fuel rod in the 5th ring follows 10s later.
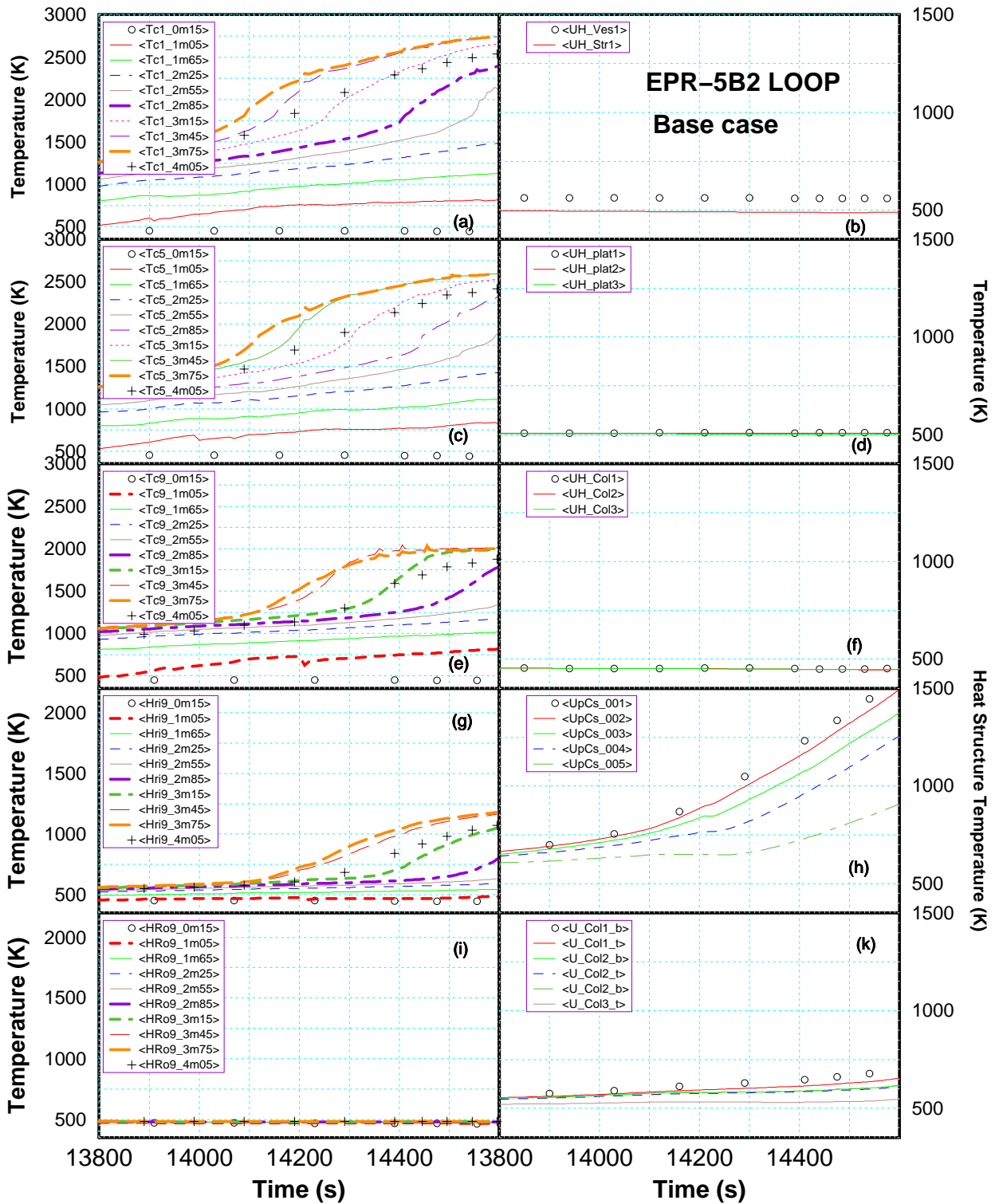
Figure 3.14 Temperature history of the LOOP base case scenario: core temperatures (left) (a) centre, (c) average, and (e) outermost ring, (g) HR inner surface and (i) CB outer surface temperature, RPV internals (right): (b) upper head, (d) USS, (f) upper part of CSC, (h) lowest part of CSC, and (k) LCSP temperature.
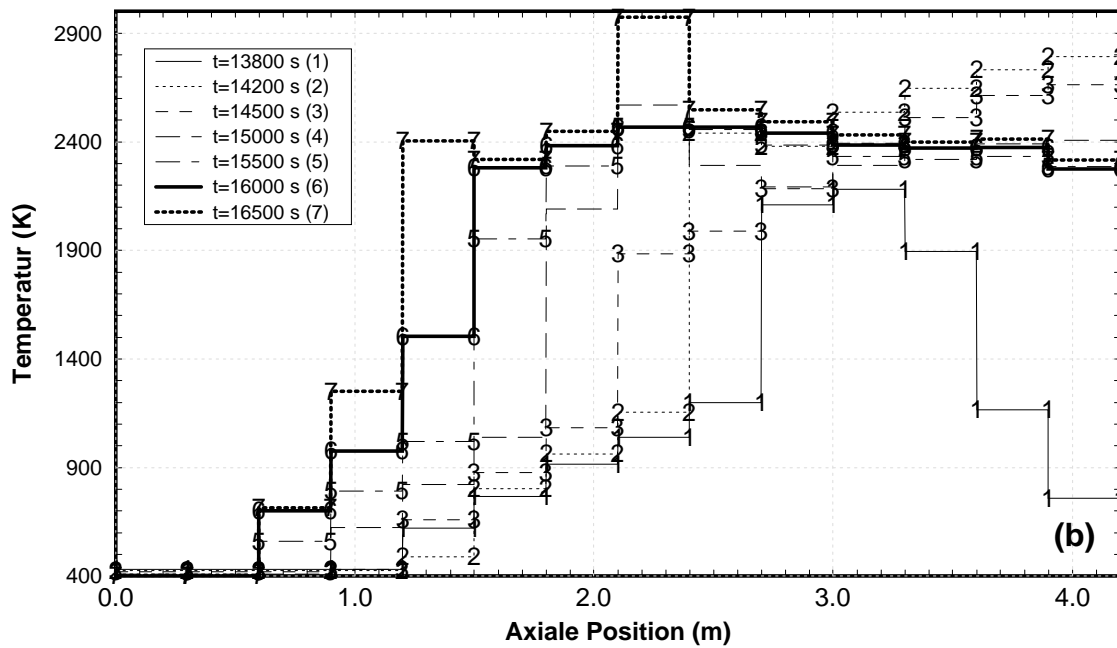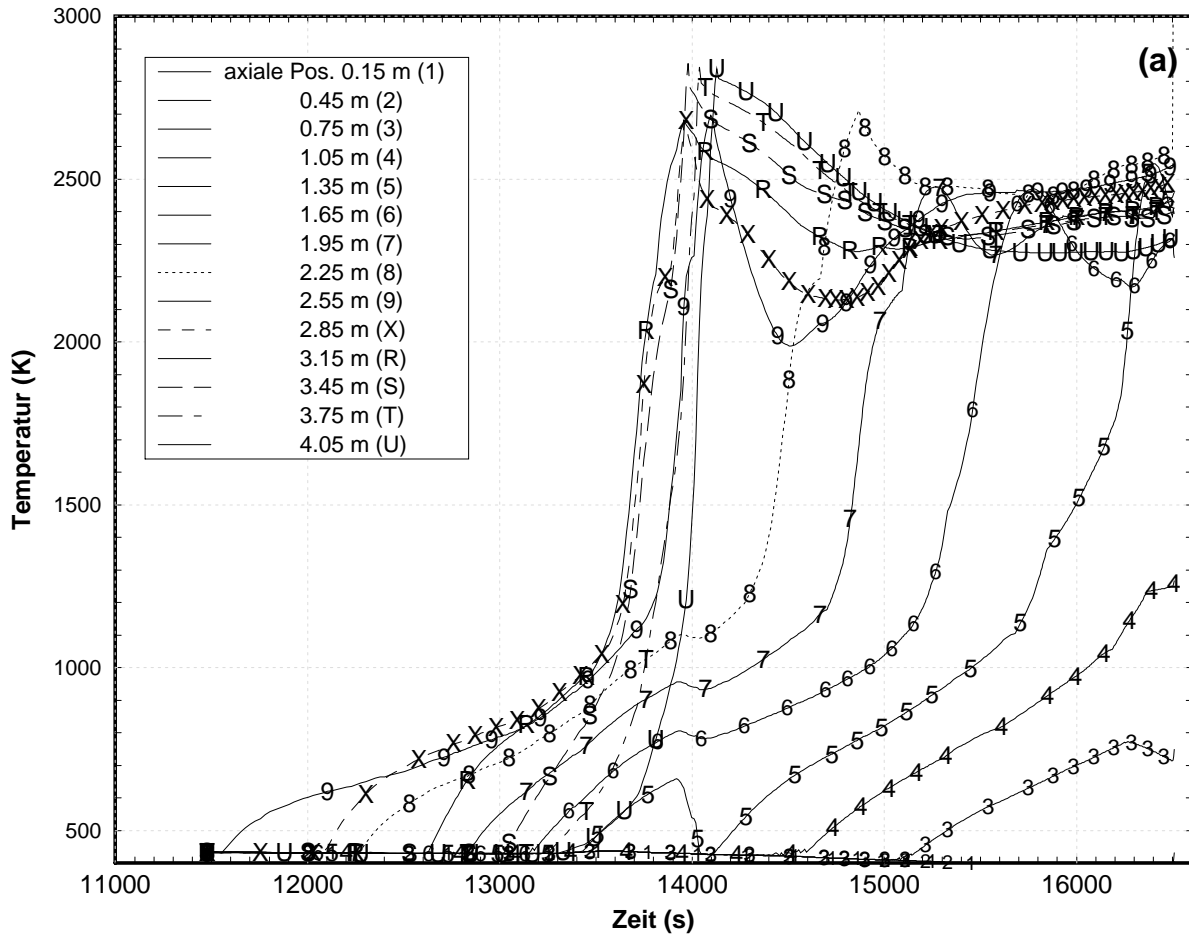
Figure 3.15 Axial boundary conditions for detailed analyses with LOWCOR2: top: time dependant development of fuel rod or debris temperatures in the outer-most ring of the core, and bottom: axial temperature profiles for several times.
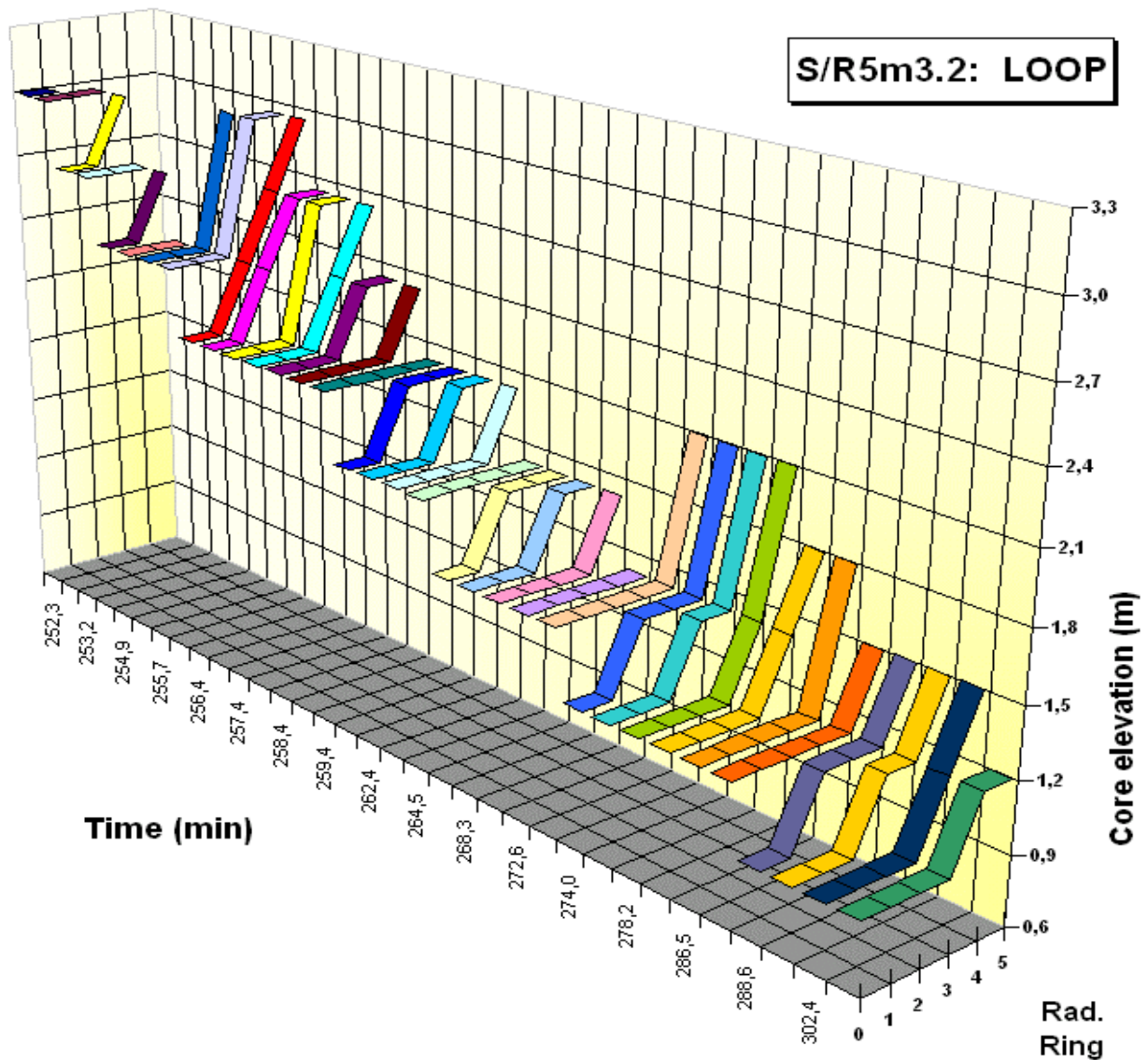
Figure 3.16   Axial and radial position of the lower crust of the molten pool in the LOOP scenario for times at which relocation events were calculated between 15136 s (252 min) and 18234 s (304 min). The crust is situated on top of porous debris one zone below, the back wall represents the HR. .

3.3.3 Core degradation

At around 14195 s (3.9 h) the PCT reaches 2300 K, the core is only slightly damaged, and only limited melt relocations have occurred. After 14950 s a molten pool is formed in the centre channel of the core spreading in radial direction and relocating downwards. The collapsed water in the core still declines, and at about 16200 s (4.5 h), water remains only in the lower core support plate and the lower plenum.

The molten pool is held in place by a crust of solidified melt and residues of fuel rods and guide tubes. The stability of this crust is decisive for the further development of the accident. In the best case, i.e. when the heat removal from the crust exceeds the heat generation inside the pool, the crust thickness increases. At the present time, only speculations are possible about the mechanical stability of the crust because of its largely unknown composition and the way in which

the crust is supported by some fuel rods remaining in place. Prior to direct contact the core internals are heated by thermal radiation to such a temperature level that the steel is molten and relocates downwards.

3.3.4 Final State

As can be depicted from Figure 3.17 the molten pool contacts the HR at app. 1.2 m elevation. In this calculation no interaction between core enclosure (HR) and molten pool was activated. Also no lower plenum model (Couple) was used. Therefore S/R5 only balances the material released through breaches assuming instantaneous failure of the enclosure.
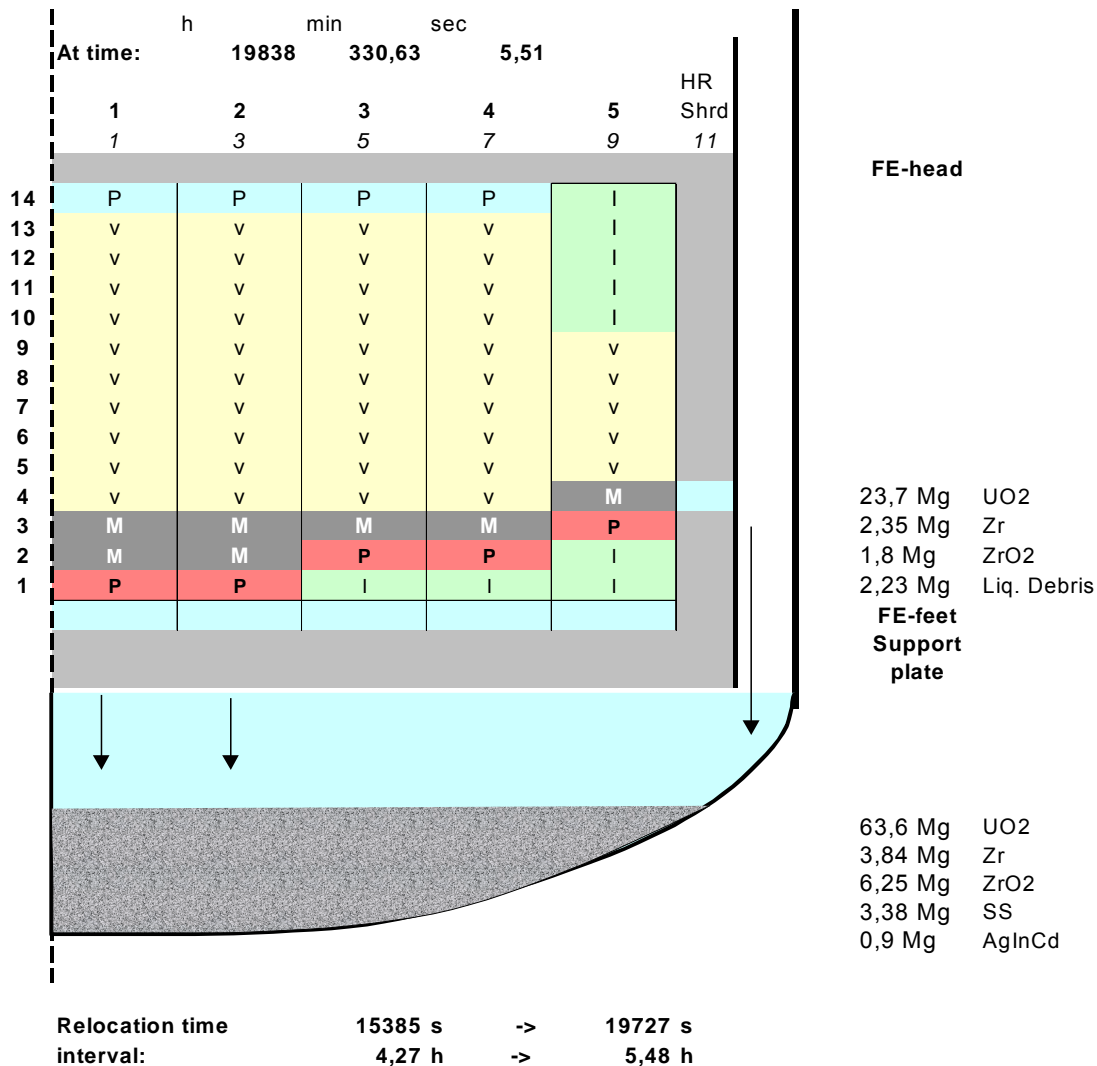
Figure 3.17   Final state of LOOP "base case" calculation including melt slumping into lower plenum assuming failure of core enclosure. No interaction with the water is considered in this calculation by S/R5m32.

Especially for failure analyses for the LCSP, the distribution of molten material in the core and lower plenum indicates, that no further cooling from the bottom could be assumed. This leads to boundary conditions for LOWCOR2 calculations assuming hot surfaces on both sides. In this stage of the accident, however, the risk of a fuel coolant interaction is rather low due to lacking water evaporated by melt dripping through the downcomer app. 0.3 h earlier.

4 ANALYSES WITH LOWCOR2

LOWCOR2 has been applied to investigate the damage propagation in the heavy reflector of the EPR up to local melt-through events both for the 46 cm^2 leak and the LOOP accident sequences. The case of the 46 cm^2 leak has been investigated with S/R5 (section 2.2) and MELCOR /1/, the LOOP case has been studied recently with S/R5 /4/. In the following, LOWCOR2 results concerning the heavy reflector (HR) failure due to thermal loading impressed on the inner side of the HR in the course of the core degradation, will be discussed for the cases of the 46 cm^2 leak and the LOOP.

Two different subjects of interest have been defined. The first concerns the behaviour of the total HR modelled as a hollow cylinder in two-dimensional cylindrical geometry. The second refers to a detail of a cross-section with the inner edges as shown in Figure 2.1. In this model the local melt-down process of the squared inner side of a basic HR element has been studied. The computational models applied are shown in Figure 4.1. The S/R5 calculations for the EPR active core have been performed with an axial subdivision into 14 zones, the MELCOR calculations with an axial subdivision into 10 zones. So, the core degradation analyses provide transient temperatures of the fuel bundles and debris configurations for 14 and 10 axial zones, respectively, in the outer radial positions adjacent to the inner side of the HR. These fuel rod and debris temperatures have been considered as the temperatures of the radiation heat source heating up the heavy reflector from its inner side. The axial subdivision of the heavy reflector has been even refined in the corresponding LOWCOR2 models as shown in Figure 4.1 so that, depending on the code providing the inner side boundary conditions, we have axial subdivisions into 56 or 60 zones totally for analyses with S/R5 and MELCOR boundary conditions, respectively.

The model for the LOWCOR2 analyses using a cross-sectional segment in Cartesian geometry is shown in detail in Figure 4.1. The size of the individual mesh zone is 1.0x1.0 cm^2, and the computational mesh contains 16 coolant channels as indicated in the HR cross-section shown in Figure 2.1.

4.1 Boundary conditions

The boundary conditions reflecting the temperatures of the heat sources for radiation heat transfer to the inner surface of the heavy reflector, as calculated by S/R5m32 and MELCOR for the 46 cm^2 leak accident and by S/R5m32 for the LOOP case, are shown in Figure 4.2 to Figure 4.4. Concerning the boundary conditions on the outer side of the core barrel (CB), we assumed radiation heat transfer to the inner RPV wall having a constant temperature of 450 K. At top and bottom radiation heat transfer to a constant heat sink of 1000 K and 450 K, respectively, have been taken into account. These assumptions correspond approximately to the conditions resulting from the analyses with S/R5m32 and MELCOR. For the radiation emissivities, factors of 0.4 for the inner side and of 0.3 for the residual sides have been used.

Convective and contact heat transfer modes have been considered to be negligible under the thermohydraulic conditions of the scenarios discussed herein.
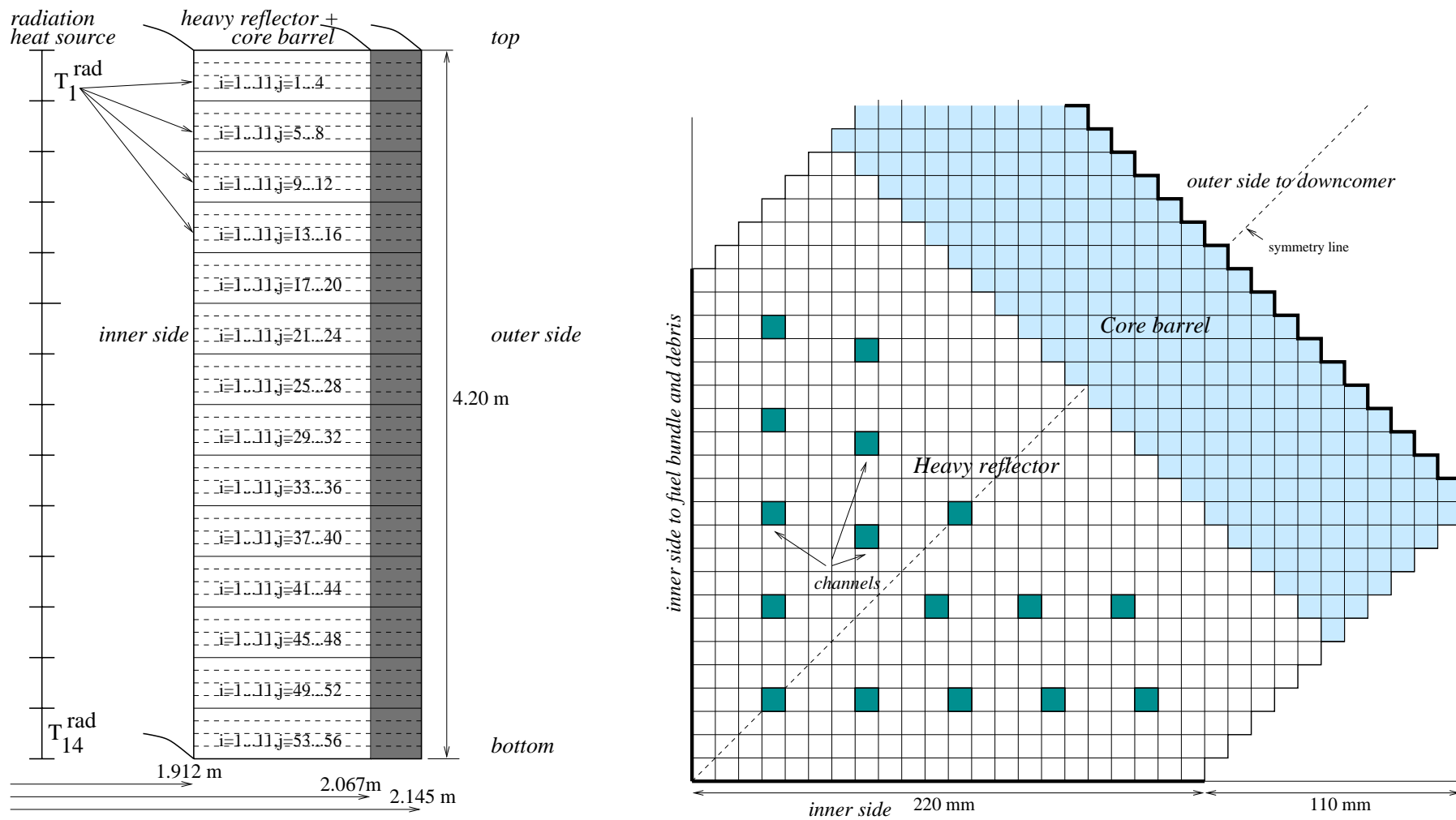
Figure 4.1   Computational models for HR and CB melt-down analyses in cylindrical coordinates (left side, and in cartesian coordinates for a representative cross-sectional element (right side).
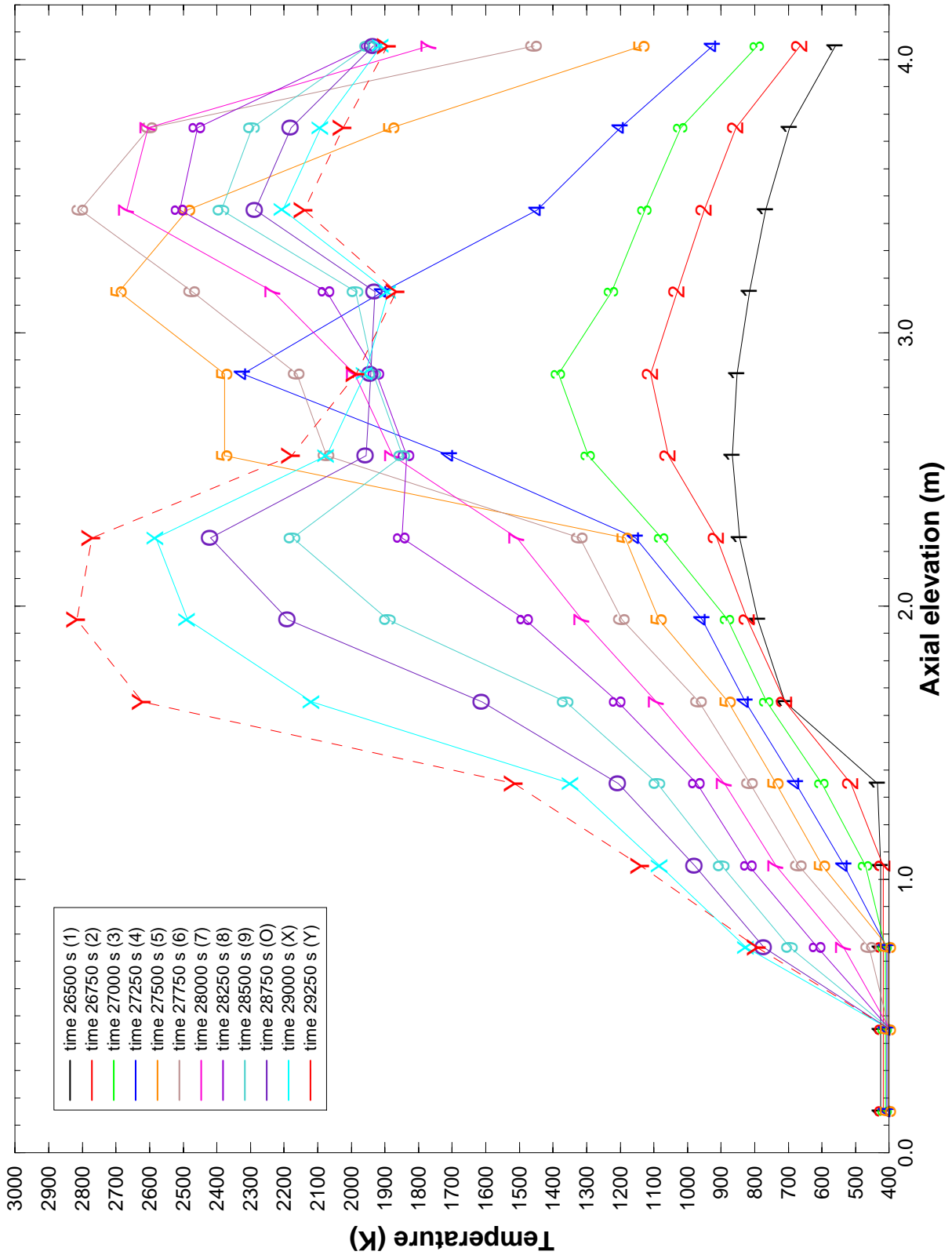
Figure 4.2   Temperatures of fuel rods and fuel debris adjacent to the HR inner surface in fourteen axial zones as calculated with S/R5m32b for the SBLOCA scenario; parameter is the time.
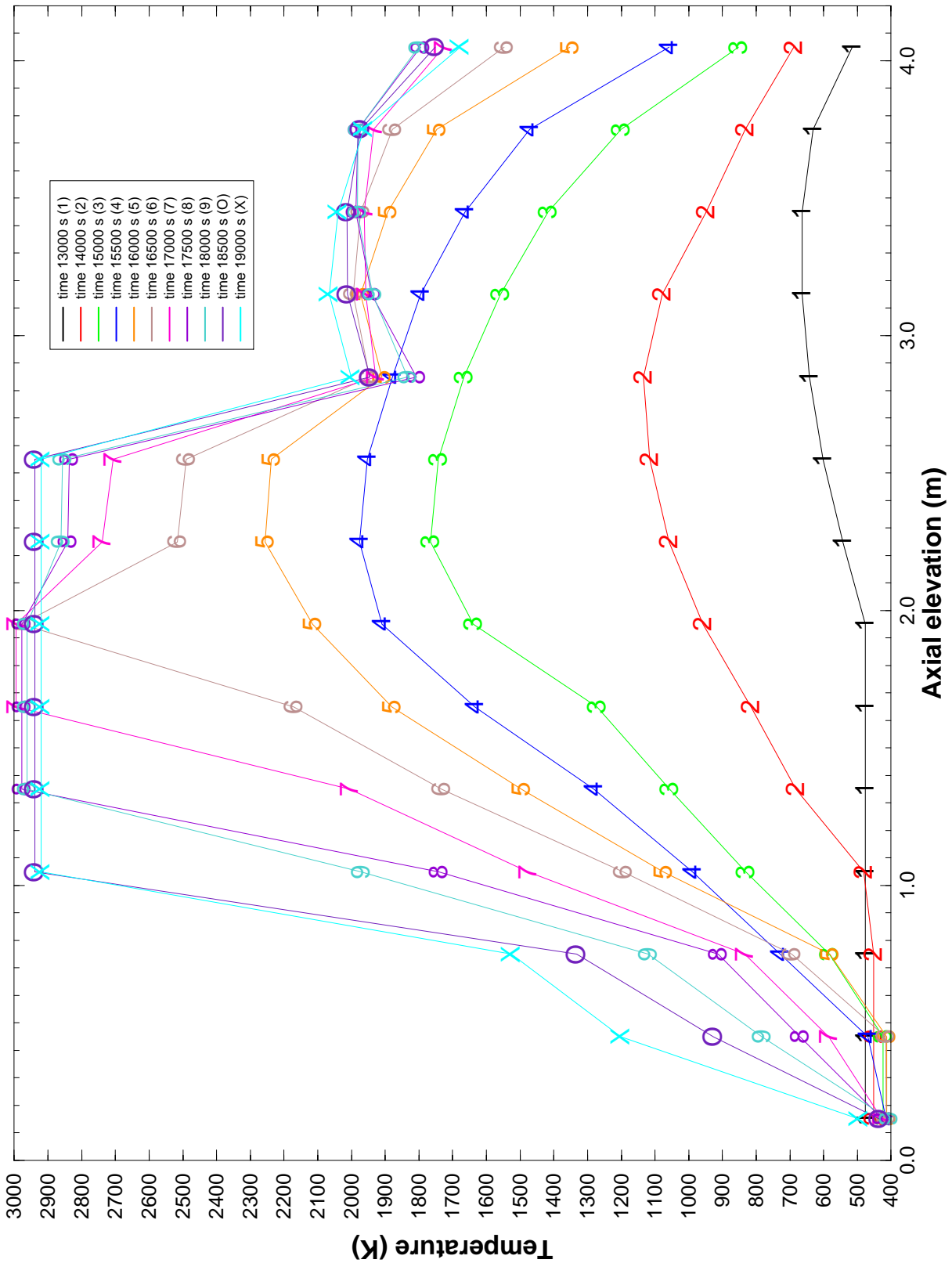
Figure 4.3 Temperatures of fuel rods and fuel debris adjacent to the HR inner surface in fourteen axial zones as calculated with S/R5m32 for the LOOP scenario; parameter is the time.
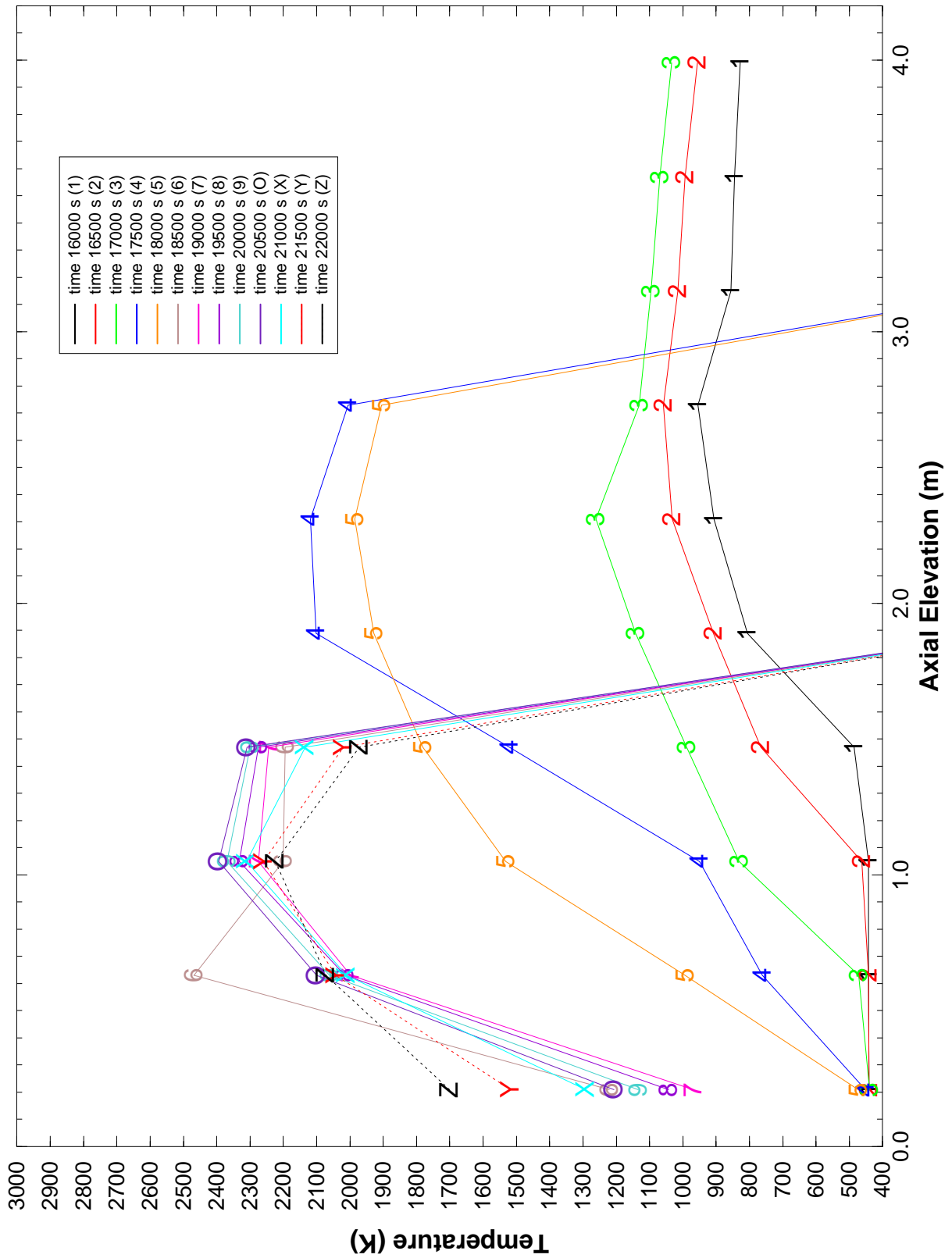
Figure 4.4   Temperatures of fuel rods and fuel debris adjacent to the HR inner surface in ten axial zones as calculated with MELCOR 1.8.3 for the SBLOCA scenario; parameter is time.

4.2 Results using SCDAP/RELAP5 conditions

With the boundary conditions defined above the temperature transient in the HR and CB re-
sulted in a sequence of damage progression as indicated in Figure 4.5. The damage indicator
ICOND refers to maximum temperature levels locally reached during the transient characterising
the onset of degradation by melting. ICOND = 1 means $T_{HR} < T_{sol}$, ICOND = 2 means $T_{sol} \leq T_{HR}$
$< T_{liq}$, and ICOND = 3 means $T_{HR} \geq T_{liq}$; T_{sol} and T_{liq} are the solidus and liquidus temperatures,
respectively.

4.2.1 SBLOCA scenario

Up to the end of the LOWCOR analysis which is due to the limitation of the range of validity of
the inner boundary conditions resulting from the S/R5 calculation, the melt-through process in
the HR has reached about half of the thickness of the HR. As examples illustrating the local
melting process, Figure 4.6 shows that the melting of the inner edges of the HR at an elevation of
3.15 m (Figure 4.5 a to Figure 4.5 d) occurs within about 10 –15 minutes starting at about 27500
s. Melt through occurs app. 10 min later at that elevation.

4.2.2 LOOP scenario

The sequence of the melt through process of the HR exposed to inner thermal loadings in the
course of a LOOP accident as calculated by S/R5m32 is shown in Figure 4.7. Under the condi-
tions assumed (Figure 4.3), it is evident that melt through of the HR occurs within about 1500 s
after begin of local melting at an elevation of about 2 m.

Onset of HR inner edge melt down is calculated to occur at an elevation of 1.95 m at about
16000s, as shown in Figure 4.8. App. 10 min later inner rectangular shape has vanished (Figure
4.9) so that the HR shows a rather cylindrical inner surface.

4.3 Results using MELCOR SBLOCA conditions

A comparison of the SBLOCA results concerning the HR melt through of MELCOR and S/R5
scenarios reveals that:

(a) the begin of local HR melting using MELCOR conditions is about two hours earlier than for
the corresponding case with S/R5 conditions, and

(b) the damage progression under MELCOR conditions is shifted to the lower half of the HR
whereas for S/R5 conditions the HR melting starts to occur in the upper half.
One reason for this behaviour may be the overestimated radiative heat exchange between in-
dividual rings in the core, which may favour more radial core damage spreading than an axial
spreading.

Melt through of the HR and CB at an elevation of 1.05 m occurs within about one hour after be-
gin of local melting, as is illustrated in the sequence of melt progression shown in Figure 4.10.
The onset of melting of the inner HR edges starts at an elevation of 1.05 m at 18500 s (Figure
4.11) and last app. 1000 s (Figure 4.12) until nearly cylindrical inner shape is calculated.
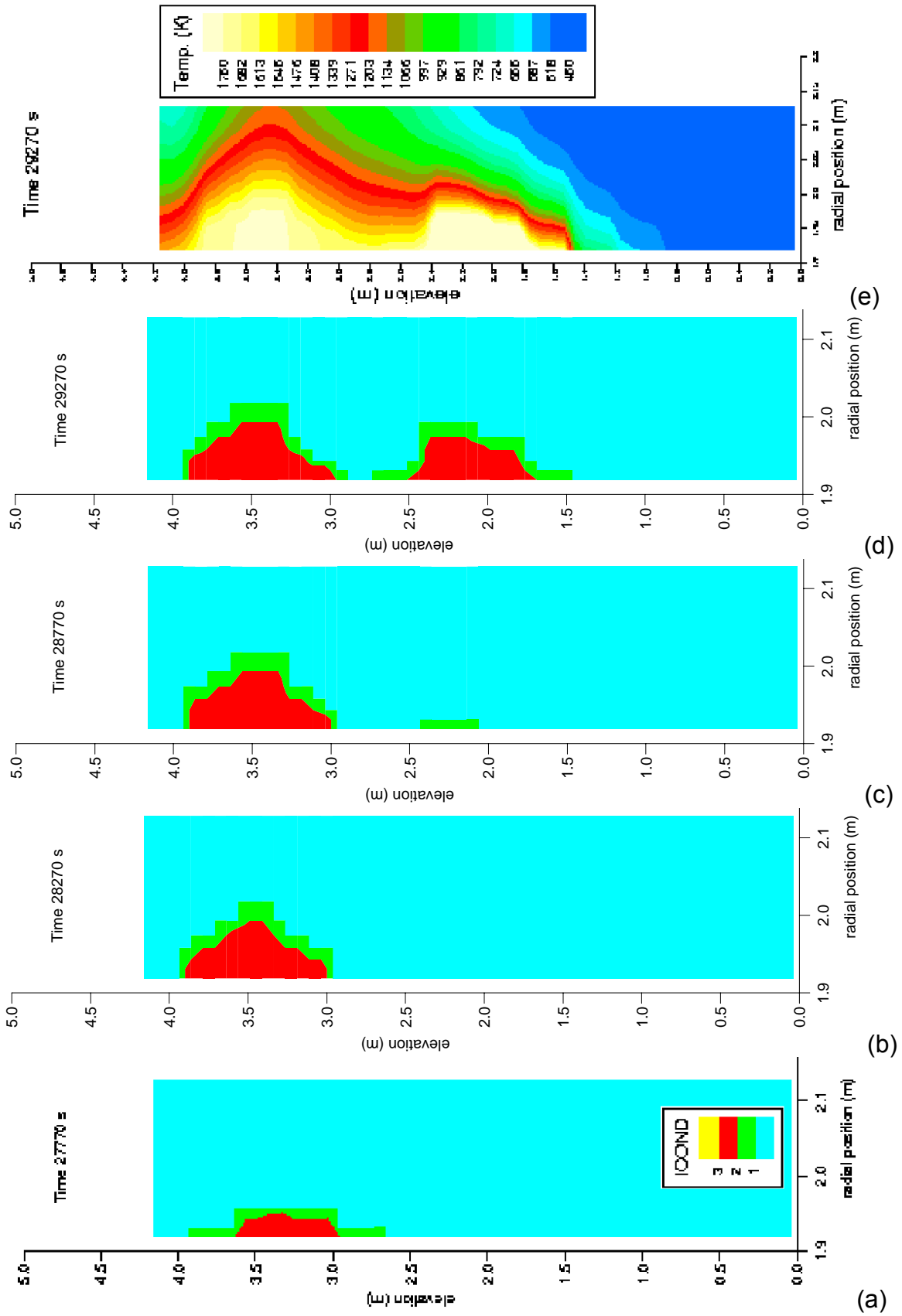
Figure 4.5 Sequence of damage propagation (a-d) and 2-d temperature profile (e) in the heavy reflector and core barrel under inner thermal loads as calculated with S/R5 for the SBLOCA 3" break. ICOND: =1: $T<T_{solidus}$; =2: $T_{solidus} \leq T < T_{liquidus}$; =3: $T=T_{liquidus}$
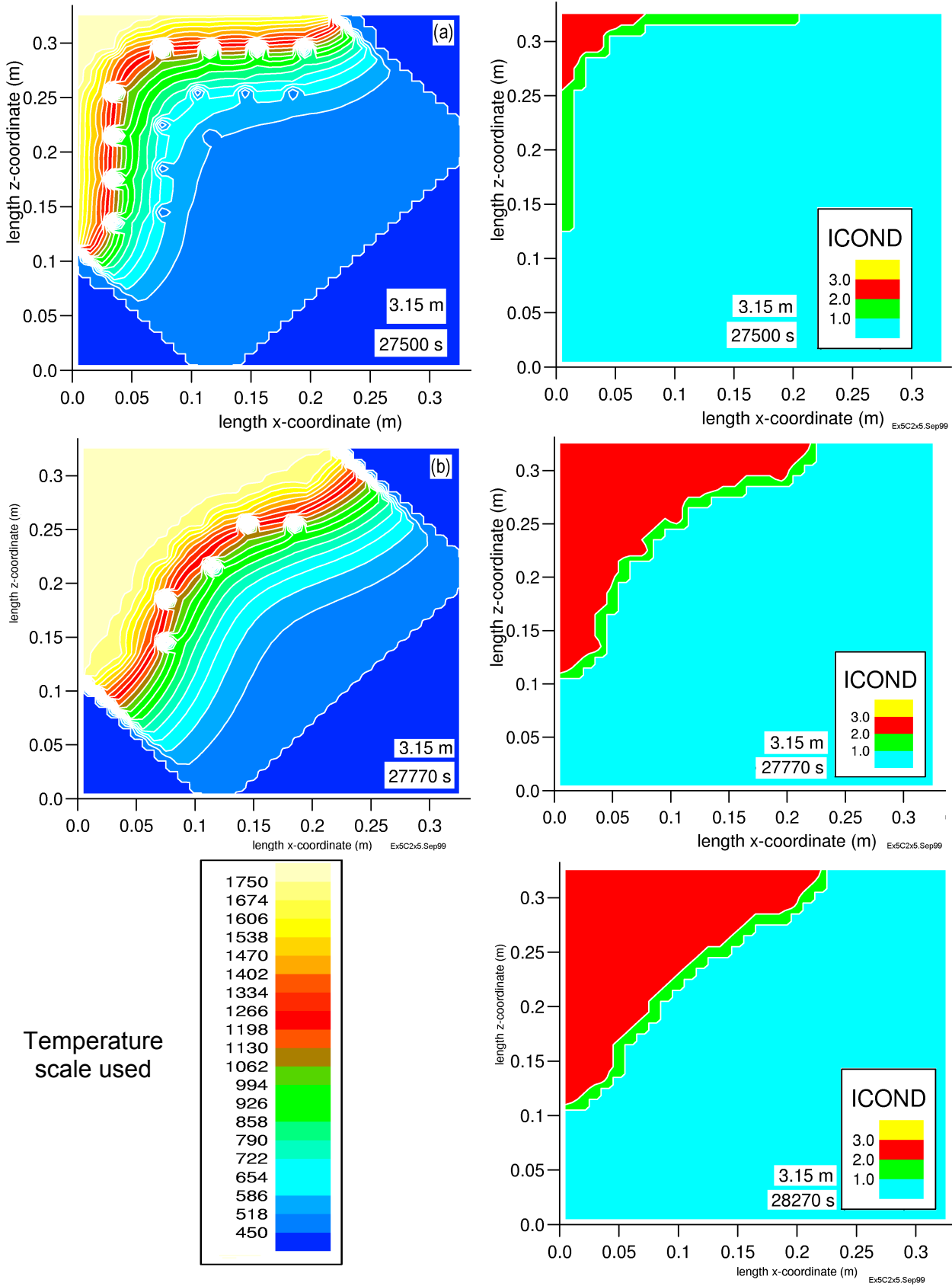
Figure 4.6   Sequence of temperature evolution and damage propagation in a repre-
sentative cross-sectional element at the elevation of 3.15 m for the
SBLOCA scenario evaluated with S/R5m32b boundary conditions
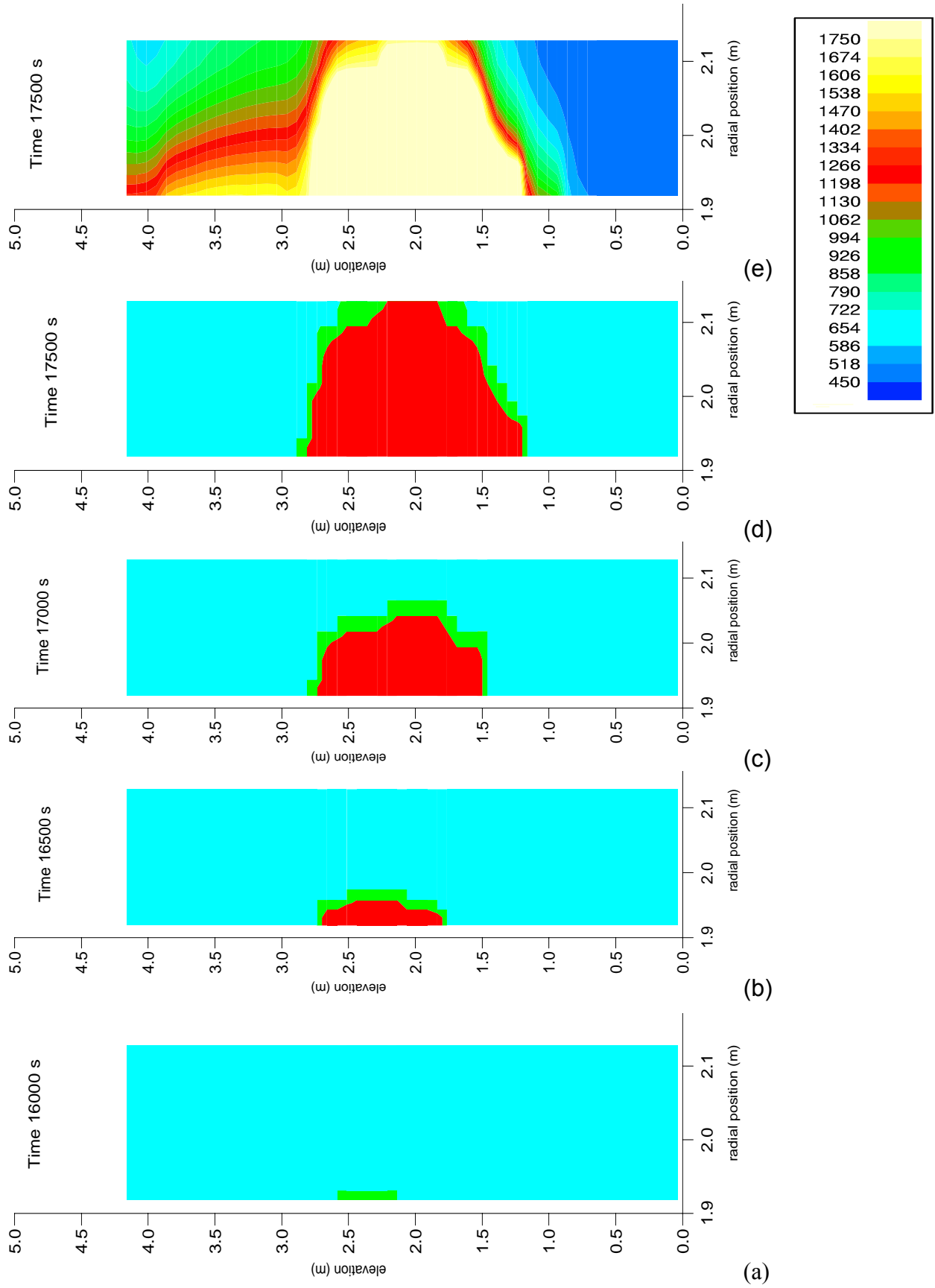
Figure 4.7   Sequence of damage propagation (a-d) and temperature distribution (e) in the HR and CB under inner thermal loads as calculated with S/R5m32 for the LOOP scenario.
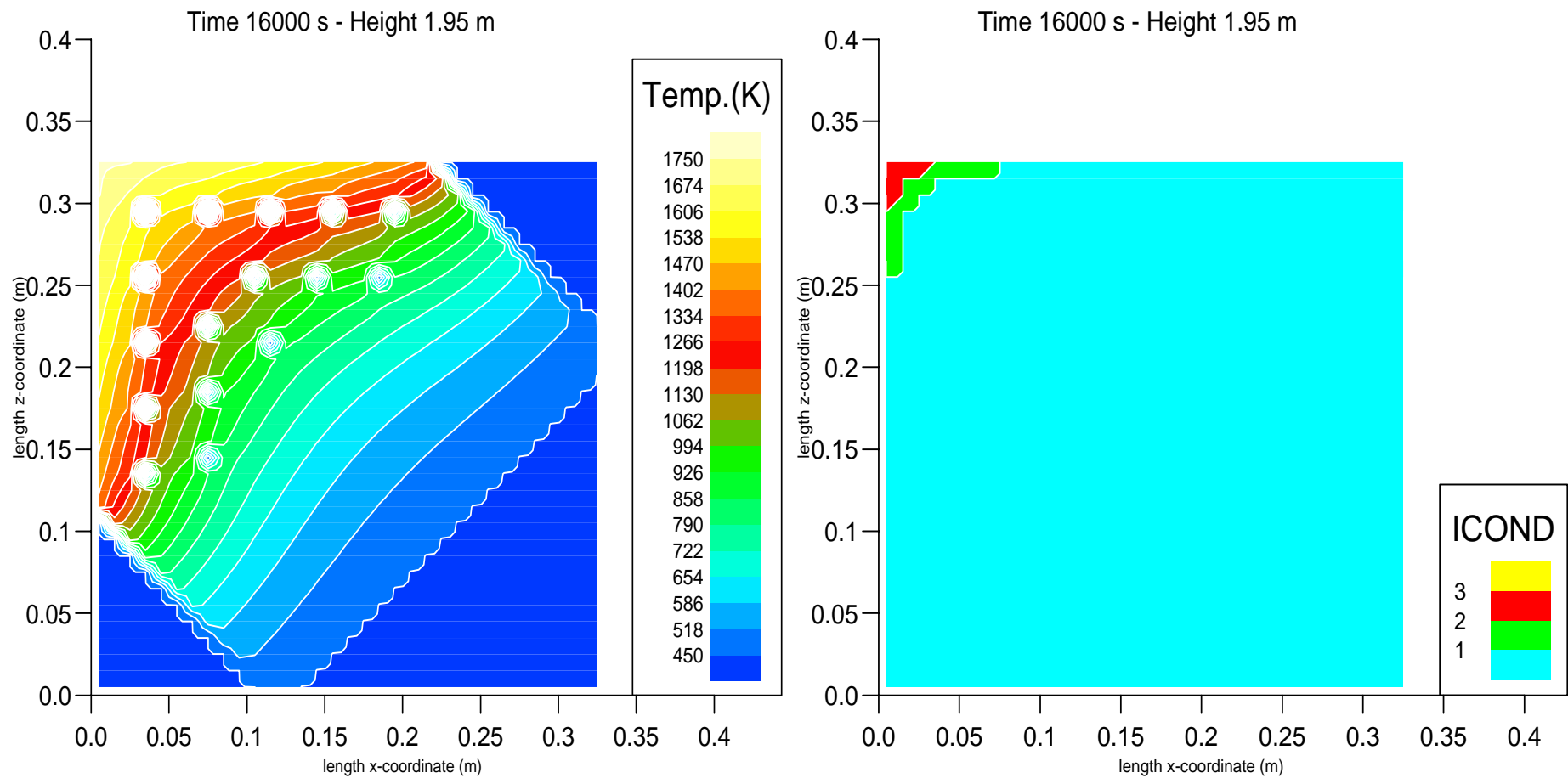
Figure 4.8   Temperature distribution calculated in cartesian geometry at onset of damage propagation (16000s) for a represen-
tative cross-sectional element of HR and CB at 1.95 m core elevation using S/R5 LOOP boundary conditions.
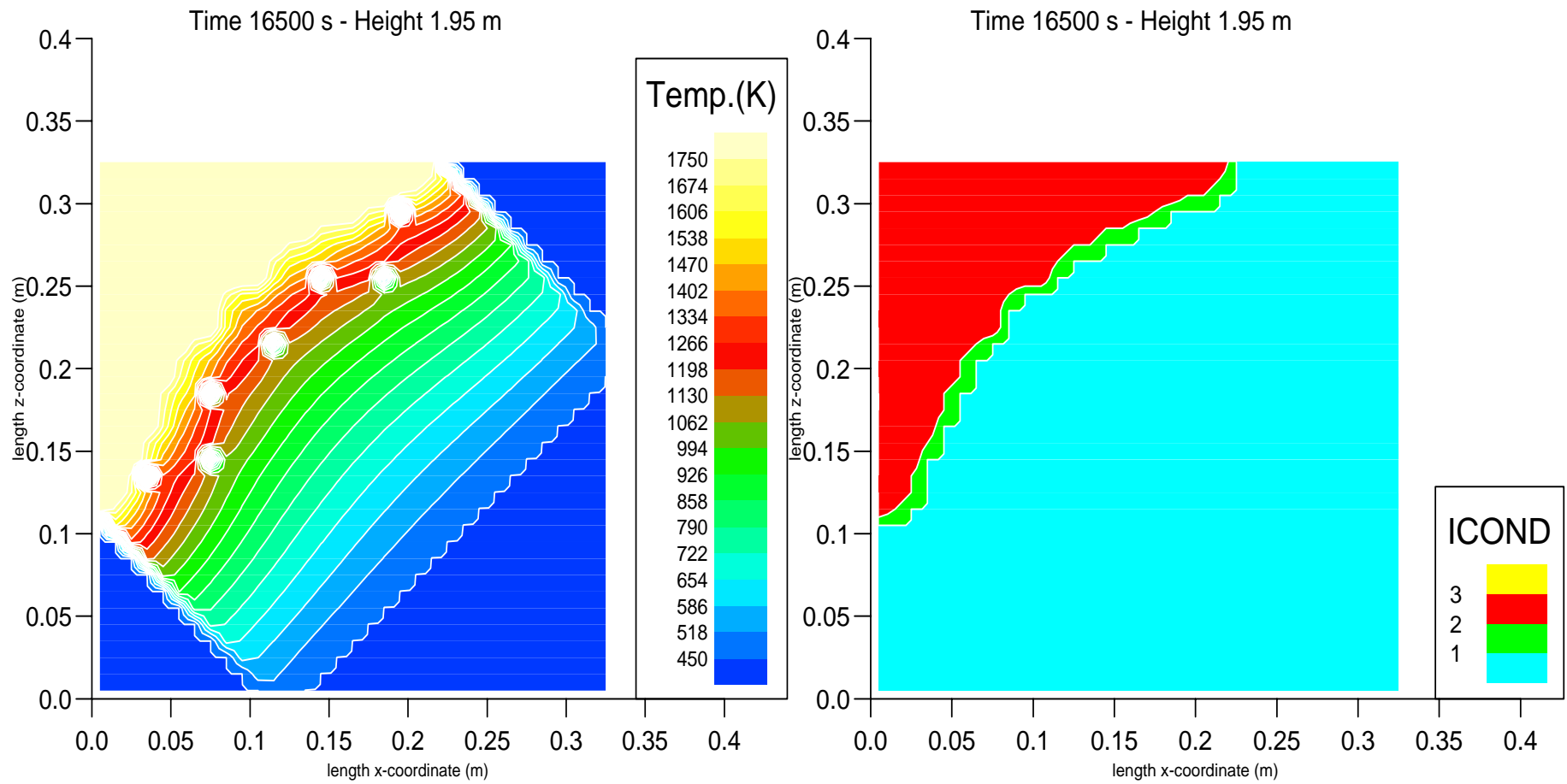
Figure 4.9   Temperature distribution calculated in cartesian geometry at 16500s for a representative cross-sectional element of HR and CB at 1.95 m core elevation using S/R5 LOOP boundary conditions.
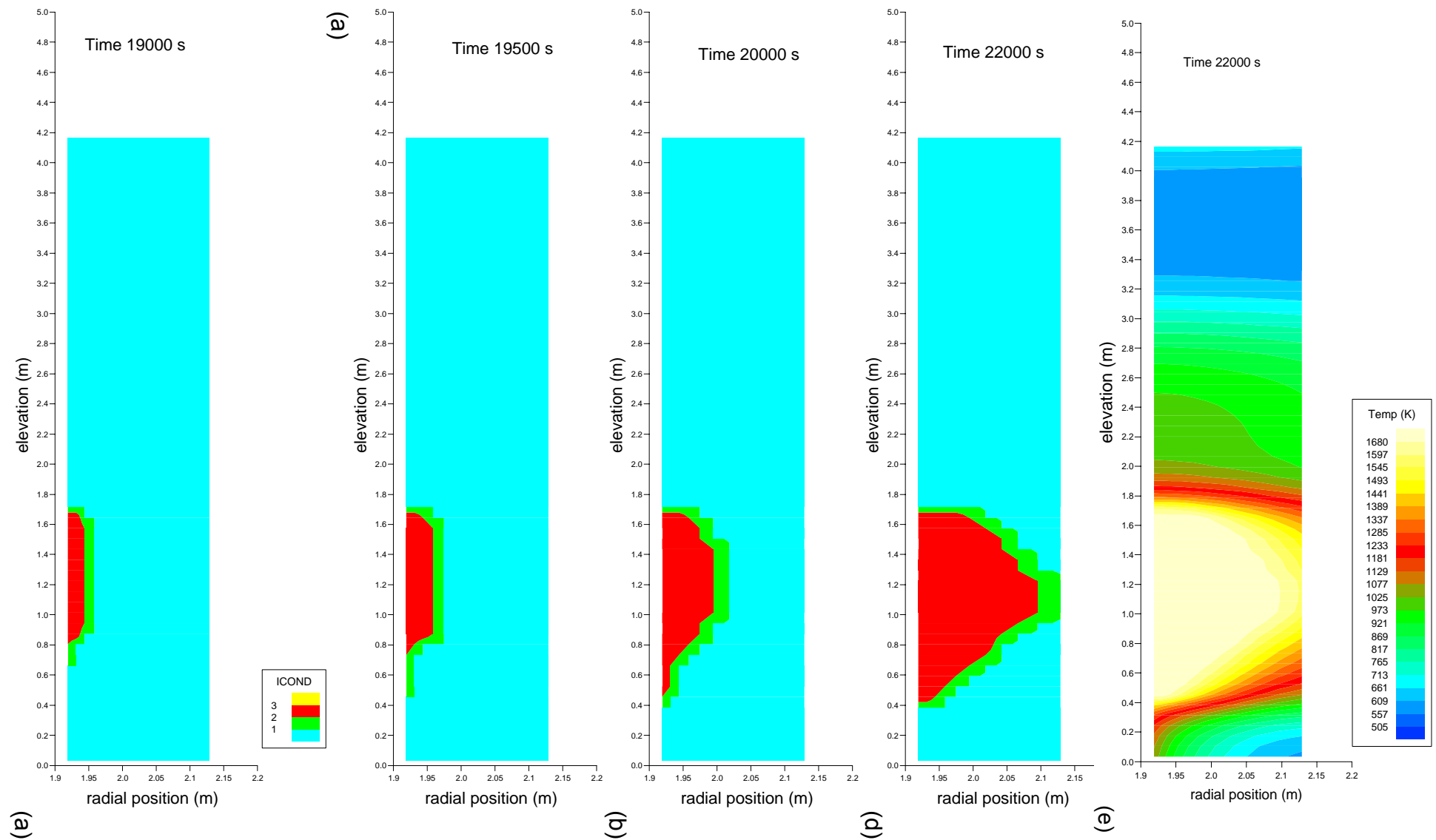
Figure 4.10 Sequence of damage propagation (a-d) and temperature distribution (e) in the HR and CB from 19000s to 22000 s corresponding under inner thermal loads caluclated by MELCOR for SBLOCA scenario.
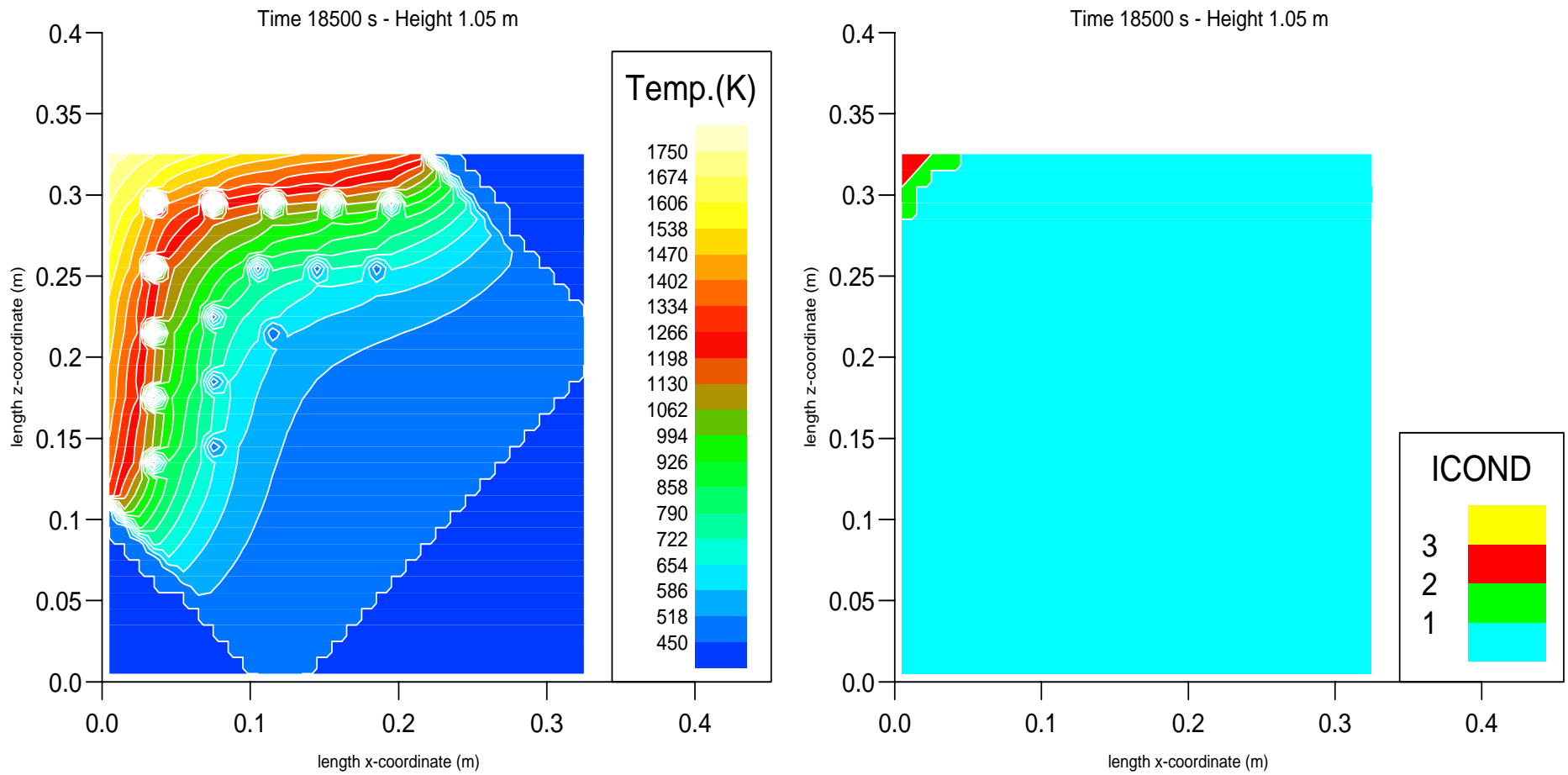
Figure 4.11 Temperature distribution calculated in cartesian geometry at onset of damage propagation (18500s) for a representative cross-sectional element of HR and CB at 1.05 m core elevation using MELCOR SBLOCA boundary conditions.
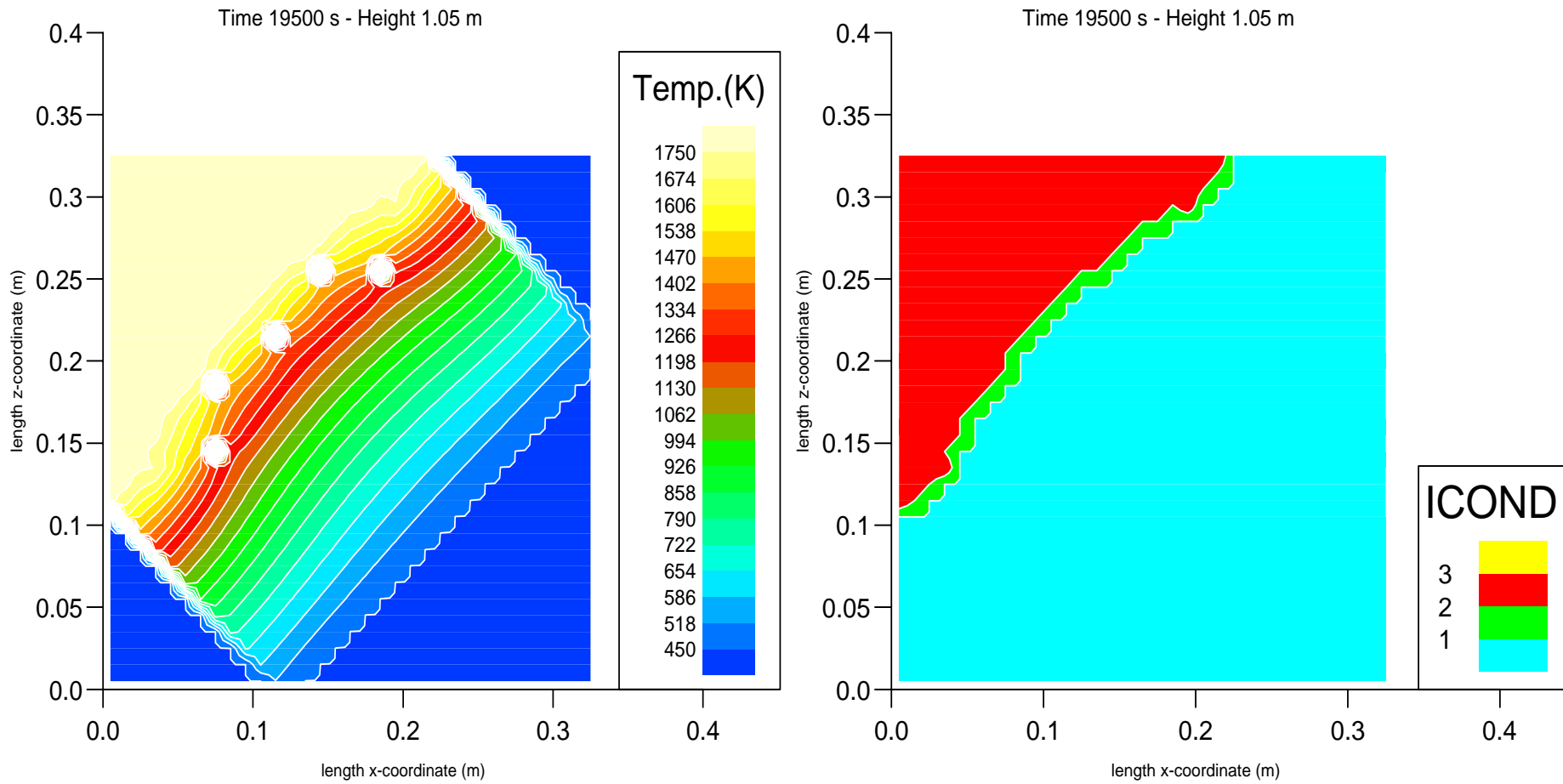
Figure 4.12 Temperature distribution calculated in cartesian geometry at 16500s for a representative cross-sectional element of HR and CB at 1.05 m core elevation using MELCOR SBLOCA boundary conditions.

4.4 Melt source term

One main advantage of LOWCOR2 is that the melt is simulated to relocate so that a melt source term for the severe core damage codes can be calculated. In case of a coupled version the melt mass and properties can be added to the debris simulation of e. g. S/R5 mod 3.3.

For the three scenarios investigated with LOWCOR2 the steel mass source rates are indicated in Figure 4.13a and below the total mass of steel released from HR is given (Figure 4.13b). For comparison, the HR mass is app. 86 Mg, composed of 11 slabs each 0.44 m thick with a typical weight of 7.6 Mg steel. The CB mass amounts to app. 49 Mg.
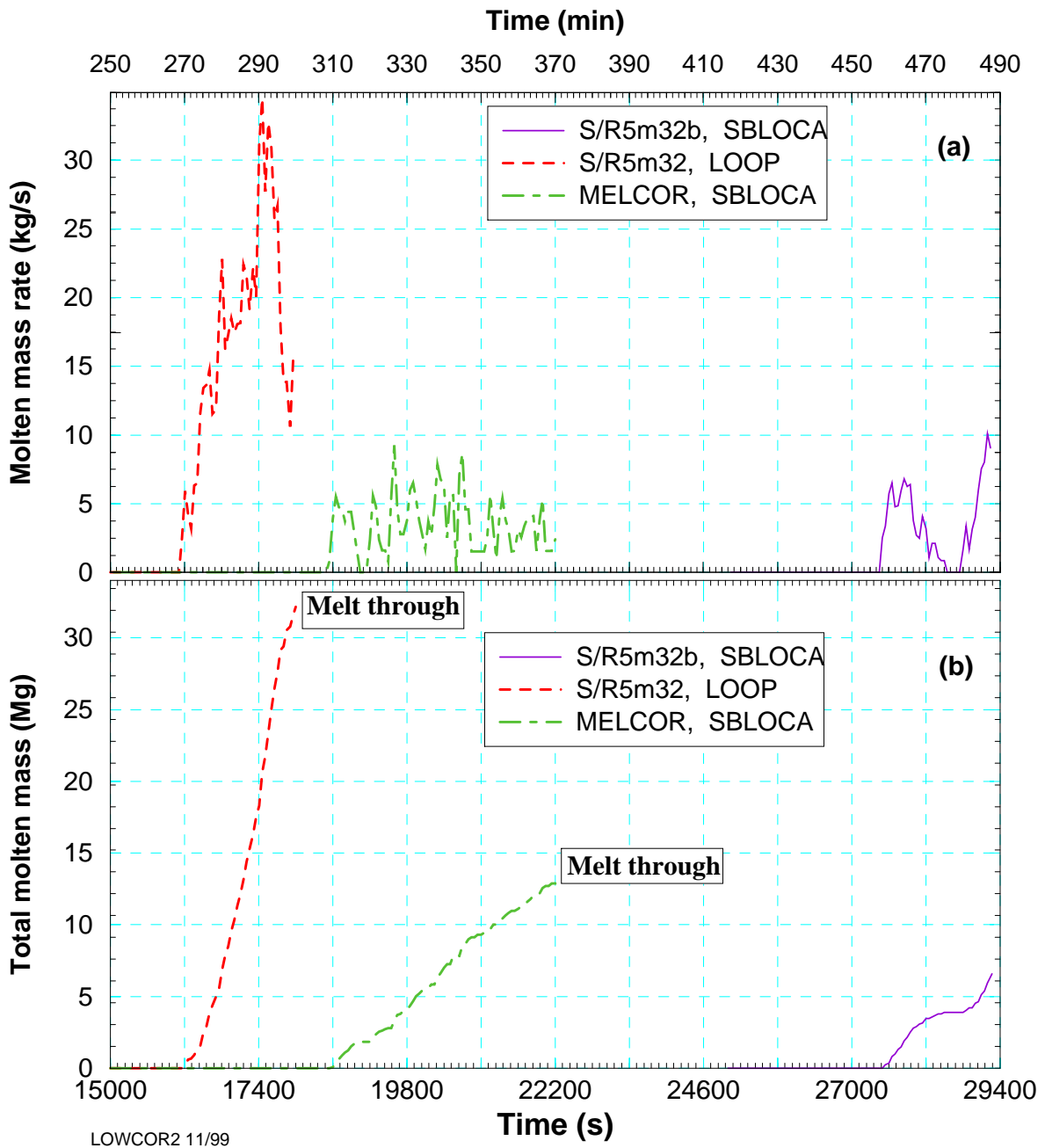
Figure 4.13   Calculated molten mass source term relocation along inner HR surface (a) and total molten mass from HR and CB melting (b) for the scenarios investigated.

The maximum mass source term varies between 8 kg/s and 35 kg/s with an average values of app. 1.7 kg/s and 5 kg/s, respectively. These values originate from the whole inner HR perimeter whose length amounts to app. 12 m. The S/R5m32, LOOP values reflect the high surface temperature (2900 K) for a time period > 40 min (Figure 4.3), so this case can be considered as an upper limit for HR melt through velocity. In the two cases of S/R5m32-LOOP (Figure 4.7 d), and MELCOR-SBLOCA (Figure 4.10 d) a complete penetration was calculated, whereas in the S/R5m32b, SBLOCA case (Figure 4.5) only 50 % of HR and CB thickness was liquefied.

4.5 Discussion

In all scenarios investigated here the hot spot is situated axially between 1.2 and 2.0 m core elevation, except for the S/R5 mod 3.2b SBLOCA scenario. This deviation can be explained, by two effects: (1) a code error which overpredicts the thermal radiation absorption in the fluid, and (2) the radial radiative heat transfer across the five rings to the HR may be over-predicted. This becomes obvious when core wide radiation heat transfer was deactivated completely, but this solution is only applicable when convective heat transfer is dominant, e.g. in high pressure scenarios.

The LOWCOR2 calculations generally show that within 10 – 15 min the inner shape of the HR has faded away, even if no direct contact of debris or molten pool is supposed. As a consequence, the inner shape of the HR has no direct influence on the melt through of the HR and CB, and hence no reliable information can be derived for the hole size to the downcomer.

Another issue is the melt source term. The LOWCOR2 relocated the melt along the inner surface of the HR accumulating it if temperature is below T_{sol} . The calculated stainless steel melt masses are summarised in Table 4.1 for the different scenarios.

Table 4.1   Essential results of LOWCOR2 analyses

Scenario	Time after onset of oxidation (min)	Time to round off (min)	Time to melt through (min)	Axial Position of melt-trough (m)	Maximum steel mass source (kg/s)	Total molten mass (Mg)
SBLOCA, S/R5m32β	*32*	*10 - 15*	*20 - 25*	*3.15*	*10*	*7 (#)*
SBLOCA, *MELCOR*	68	17	50	1.05	13	9
LOOP, *S/R5m32*	88	10	25	1.95	35	32

Remark: (#) no complete melt through calculated due to end of S/R5m32b calculation.

However, this study cannot answer whether or not molten steel contributes to a lower liquidus temperature of the corium in the molten pool, because only relocation along the HR inner surface is assumed.

For the behaviour of the lower core support plate (LCSP) LOWCOR2 analyses are scheduled using MELCOR and S/R5 results in which some molten corium is already present in the lower plenum. In this scenario the heat sink at the lower surface of the LCSP is absent, so that a nearly adiabatic behaviour has to be assumed at bottom surface of the LCSP.

5 ANALYSES WITH ICARE2

In parallel to the work concerning the development and application of the LOWCOR2 model, available tools such as ICARE2 and FIDAP have been intensively checked in order to assess and demonstrate their applicability for HR and CB melt down analyses. Basis for the analyses with ICARE2 described in the following are LBLOCA studies for the EPR performed with S/R5m31f (section 2.2.1).

5.1 Selection of initial conditions

Initial conditions are taken from S/R5m31 results at a time in the accident course late enough so that steam mass flow rates through the core are low. At the selected time (2100 s into the accident) S/R5 mod 3.1 calculates a loss of geometry (formation of debris bed) for the inner three of the five radial core channels as shown in Figure 3.2. The fuel rods in the outer channels 4 and 5 are still in cylindrical configuration, because the fuel rod temperatures are rather low as can be seen in Figure 5.1. A radial temperature profile across the core is outlined in Table 5.1.

Table 5.1   Initial conditions for ICARE2 calculations derived from S/R5 LBLOCA analyses at app. 50 min.

Maximum temperature channel 1	K	2860
Maximum temperature channel 2	K	2860
Maximum temperature channel 3	K	2800
Maximum temperature channel 4	K	2600
Maximum temperature channel 5	K	2200
Power variation (P_{total} / $P_{nominal}$)	%	1.638

5.2 ICARE2 V2 reactor core models

The core model used in this study (Figure 5.3) is based on a previous analysis /19/ so that the conditions required by ICARE2 V2 for reactor calculations are fulfilled. Actually two modified reactor in-vessel models ("cases") are used to describe correctly different core states. In both cases the same initial conditions are used, but due to different domains and physical models applied, results differ. In the following sections the input and model specifications for ICARE 2 will be given.

The scoping case

- fuel is in rod configuration (relocation modelled but no debris bed configuration)
- radial extension of control volume: two outermost core channels up to RPV wall,
- axial extension of control volume: whole core except for lowest zone with water (0.3 m)
- radiative heat exchange between fuel rods and HR
- conductive and radiative heat exchange between CB outer surface and the RPV wall (downcomer filled with steam)
- outer RPV temperatures extracted from S/R5m31 calculation /20/,
- thermal influence of the internal core channels 1 to 3 which are not represented in this scoping case is accounted for indirectly by impressing fuel rod and fluid temperatures on the outer channels 4 and 5 (Figure 5.2) as given by the S/R5m31 calculation.
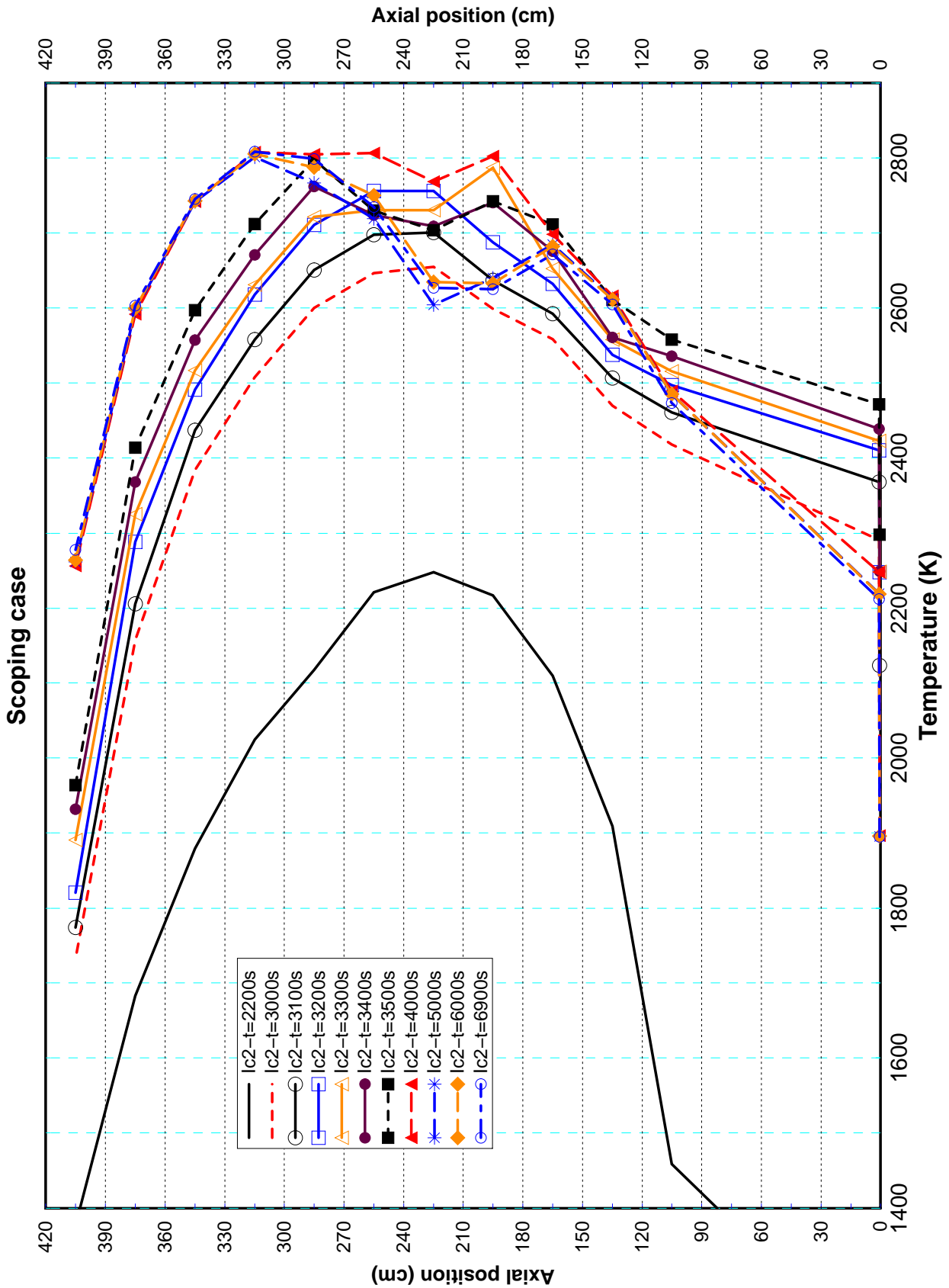
Figure 5.1   Fuel rod temperatures of the outermost fuel rod at indicated core elevations calculated by ICARE2 for the "scoping case" analysis.

In other words the *"scoping case"* reproduces - starting from a given initial state with a reduced core section - the conditions of a previous S/R5 mod 3.1 calculation. It makes use of the capability of ICARE2 to compute the heavy reflector and core barrel temperature evolution including melting and melt relocation which cannot be obtained from S/R5m31 analyses and ends up with difficulties applying S/R5m32.

The detailed geometry is shown in Figure 5.2: between the core and the RPV the HR and the CB are located. The HR itself is subdivided into two partitions: HR1 (0.041 m) and HR2 (0.157 m), where HR2 takes into account the cooling channels (Figure 5.2) approximately by a lower steel density and conductivity. The core barrel is indicated by HR3 (0.063 m).

HR1= HR1II (0.1cm), HR1I (1.5cm), HR1E (1.5cm), HR1EE (1cm)
HR2= HR2II (1.0cm), HR2I (5.9cm), HR2E (4.5cm), HR2EE (4.3cm)
HR3 : 6.3 cm
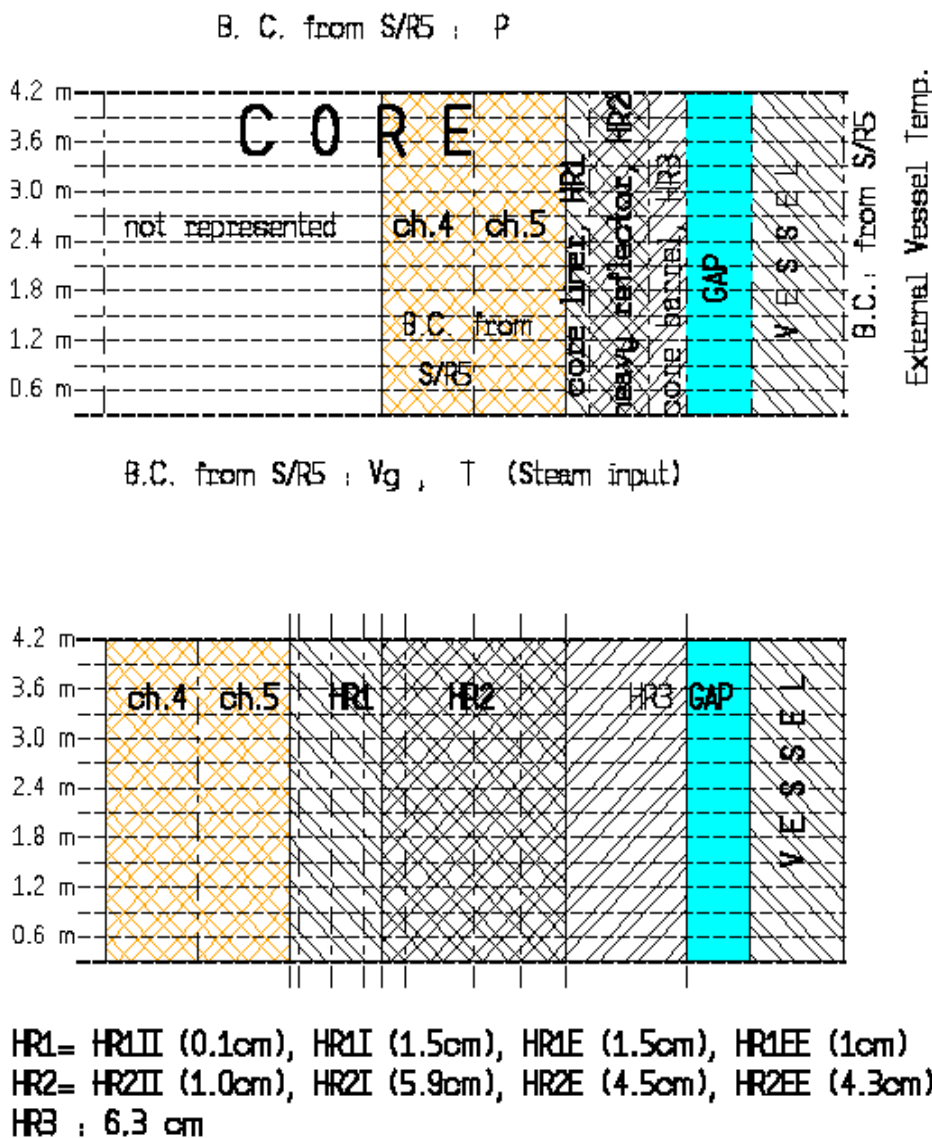
Figure 5.2   Restricted core and shroud geometry for the "scoping case"

Furthermore, to have a better radial resolution for the temperature calculations, the shrouds HR1 and HR2 are subdivided into 4 shroud layers each, named HR1II, HR1I, HR1E, HR1EE (and HR2II, ... HR2EE) from the most internal to the most external one. The vessel wall is also radially subdivided into 4 layers. The downcomer is represented through a steam filled gap between the core barrel and the vessel. In total 13 axial meshes each 0.30 m high account for the repre-

sented core height between 0.30m and 4.20 m. The whole model is composed of a domain of 39 ICARE meshes composed of 3 radial meshes and 13 axial ones, each mesh with different internal layers.

The debris case

uses the capability of ICARE2 to define debris beds. The computed domain extends axially from the LCSP to the upper core plate (UCP) and covers radially all 5 core channels of the original core model (Figure 5.3). In total this domain is represented by 144 meshes (6 radial and 24 axial meshes) with 14 axial meshes of 0.3 m length along the active core height.

The physical models involved in the *"debris case"* are as follows:

- fuel is modelled as debris bed in all channels (also in the outermost ones) and steel structures are defined as shrouds
- material repartition in the initial debris bed fits the initial mass fractions (i.e. 78% UO_2 and 22% Zr). Zr in turn is redistributed in form of ZrO_2 (50%), ZrO (30%), and Zr (20%)
- convective heat transfer between debris bed as well as shroud and molten pool;
- heat transfer across the molten pool external boundaries described by correlation;
- conductive and radiative heat transfer in debris bed, while radiation is taken into account through an increased effective conductivity;
- conductive and radiative heat exchange between debris bed and heavy reflector;
- conduction in the steam filled DC inside steel structures representing the CB and RPV.
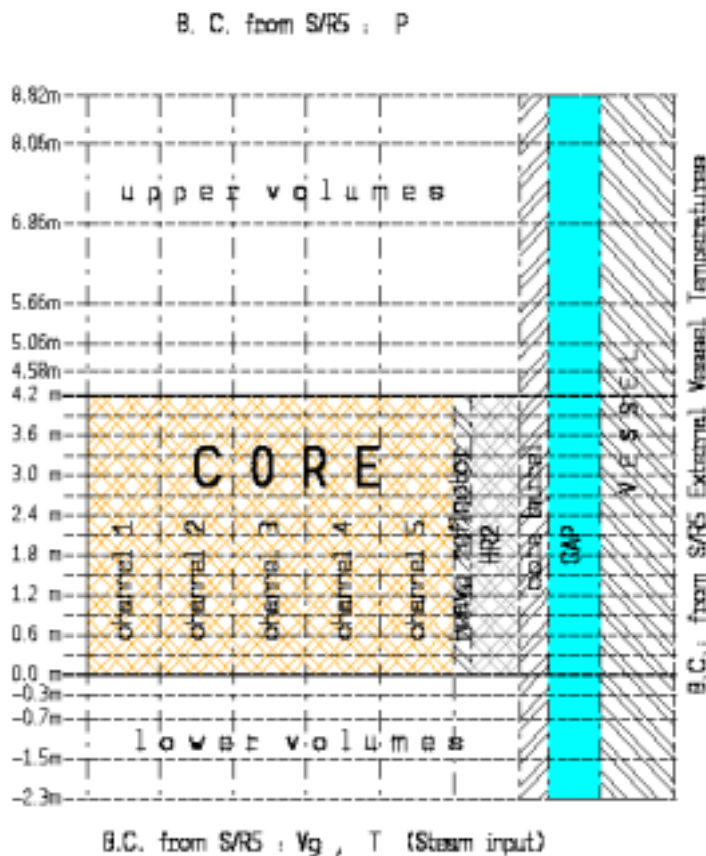
Figure 5.3   Core model for ICARE2 reactor accident analyses ("debris case") as outlined in detail in /19/.
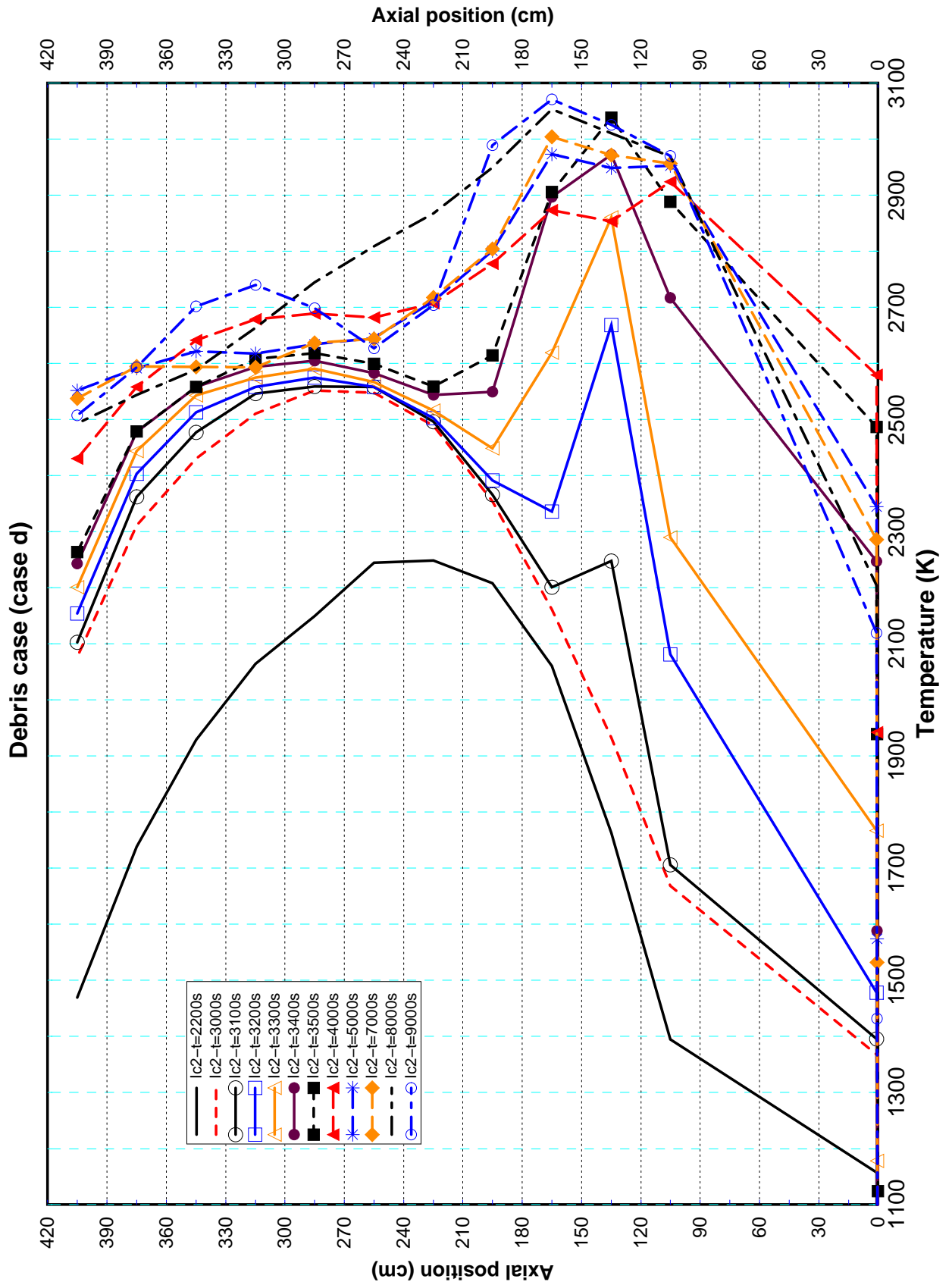
Figure 5.4   Evolution of the axial temperature profile between 2100 s and 9000s for the "debris case" in the core.

The detailed geometry is shown in Figure 5.6. HR, CB and RPV wall are simulated by shroud components which are defined in the same way as discussed for the *"scoping case"*. Just their axial extension is different as shown in Figure 5.3 compared to Figure 5.2. In the ICARE2 version used, the calculation of Zircaloy and steel oxidation caused convergence difficulties due to the low steam concentration in the fluid. Therefore, no steel oxidation could be considered.

In contrary to the *"scoping case"*, in the *"debris case"* fuel and coolant temperatures calculated by S/R5 are not imposed to core structures but the decay power released in the debris bed is used. The ICARE2 calculations (*"scoping case"* as well as *"debris case"*) start at ~2100 s when the core enters the debris bed formation. At this time the HR is heating up to the solidous temperature. ICARE2 computations ran well after 3800 s, and they were stopped at about 8000 s (*"scoping case"*) and between 8000 and 16000 s (*"debris case"*), respectively.

This means that for the *"scoping case"*, the period between 3800 s and 8000 s is calculated under the assumption that the core status obtained with S/R5 at 3800 s will remain unchanged so that the *"scoping case"* reflects a sequence of HR and CB degradation with fuel and coolant thermal conditions as obtained from S/R5 at 3800 s. Consequently, from 3800 s on the *"scoping case"* model provides the thermal behaviour of the heavy reflector in terms of melting and relocating with steady-state heating source.

For the *"debris case"* the temperature evolution of the fuel in the debris bed is calculated by ICARE2 from the initial condition obtained from S/R5 (Figure 5.1) and from the power evolution (decay power), so that the condition of a steady-state heating source does not hold.

5.3 Results

"Scoping case" results are presented in detail in /20/ and are briefly discussed here (Figure 5.7). They were actually obtained with ICARE2 V2mod2.2 instead of mod2.3 used for the *"debris case"* calculation, however, there exists no relevant difference with respect to this problem. The two cases (*"scoping case"*, *"debris case"*) result in two significantly different sequences of HR and CB melting due to the different modelling of boundary conditions at the inner HR surface. With ICARE2 V2 the progressive evolution of fuel rod degradation from cylindrical geometry to a debris bed is not feasible. So the two models act as bounding cases for the heat loads on the HR. The *"scoping case"* results in a hot spot in the HR facing the peak temperature in a rod-like fuel geometry (above axial mid-line). The *"debris case"* on the other side results in a downward moving hot spot which is first settled slightly above the axial mid-line, and then penetrates below it when the debris bed in the outermost channel begins to collapse into a molten pool.

5.3.1 Scoping case with fuel rod geometry and low steam mass flow

In that model the steam mass flow rates in channels 4, 5, and 6 (DC) use values calculated by S/R5. Beyond 3800 s these values are taken constant, i.e. the last values delivered by the S/R5 calculation with 300 g/s, 850 g/s and 23 g/s, respectively. The convective heat transfer between steam and clad surface as well as steam and HR inner side is modelled.

Under *"scoping case"* assumptions, about 3300 s after accident begin, temperatures above 1000 K are calculated to appear beyond the heavy reflector radial mid-line. Steel is found to be

locally molten through the whole structure of HR and CB at an elevation of about 3.0 m , about 6200 s after accident begin. At the end of the calculation ($\approx$ 7000 s) the core barrel reaches temperatures around 1630 K at the hottest spot and about 7500 kg steel have relocated (azimuthal symmetry). Radial melt progression was estimated to be 0.3 cm per minute which would lead (under the steady-state heat source conditions as described) to the core barrel local melting-through within $\approx$ 2 hours.

5.3.2 Debris case with debris-bed geometry and distributed steam mass flows

In that model only the initial conditions are adopted from the core state as calculated by S/R5, 3100 s after accident begin. Concerning the conditions of convective heat transfer, calculations have been performed under several hypotheses:

- no convective heat transfer with steam at all,
- convective heat transfer involving steam is considered: between steam and debris bed as well as between steam and HR. Several ranges of steam mass flow rates are assumed.

All calculations assume convective heat transfer between molten pool and debris-bed, and include other heat transfer mechanisms like conduction and radiation in the debris-bed and between debris-bed and the steel structures. Assuming no convective heat transfer with steam, the calculation stopped at 8300 s because of convergence problems before achieving the core barrel melting through. At 8200 s, locally 78 %[1] of the HR thickness is found to be molten through. With increasing steam mass flow rates the time to local melting through is decreased, corresponding to a more efficient heat transfer from core to steel structures. But further increasing the steam mass flow rate in the core leads to an increase of the delay to local melting through because the external core channel is better cooled down. In Table 5.2 and Figure 5.5 the calculational results of ICARE2 are resumed:

Table 5.2   "Debris case": Boundary conditions assumed for ICARE2 analyses and results concerning local melting of the HR and the CB

Steam flow rate in the outermost channel (g/s)	Remark	Delay to 78% HR local melting through (s) (#)	Delay to CB local melting through (s)	Melting through Axial elevation (m)
0	(a)	8200	Not calculated	1.20-1.50
260	(b)	7900	10400	1.20-1.50
1000	(c)	5450	7400	1.20-1.50
1000	(d)	5470	7600	1.20-1.50
1560	(e)	11700	14200	2.70-3.00

(a)   steam mass flow rate 0 g/s in all core channels
(b)   steam mass flow rate 1000. g/s distributed to each channel according to free channel area
(c)   steam mass flow rate 0 g/s in all other core channels
(d)   steam mass flow rate 1000 g/s in all other core channels
(e)   steam mass flow rate 6000 g/s distributed to each channel according to free channel area.
(#)   at indicated times, the HR is locally molten through up to 78% of its thickness. This value is chosen for comparison because the case with no steam mass flow (first row) failed.

---

[1] the inner surface of the HR is locally at melting temperature

Figure 5.5 summarises these results. There is a region for the steam mass flow rates in the core where they act by increasing the heat transfer towards the HR without any significant cooling down of the debris bed. They correspond to the minimum of the curve. Beyond both sides of this region the HR heating up is slowed down which corresponds to a greater time delay for the HR and CB melt through.

Figure 5.5   "Debris case": HR and CB melt trough depending on the steam mass flow rates in the outermost core channel

The "debris case" scenario studied with ICARE2 V2mod2.3 shows a period of about 2 hours for the local melting through of the HR and CB structure, starting from late phase initial conditions evaluated with S/R5 for a SBLOCA scenario without any core cooling by the emergency cooling system. In such a case when the debris bed cooling is insufficient, the axial position of HR and CB melt through is at about 1.0 to 1.5 m core elevation. This is caused by the fusion of the debris bed and an early extension of the molten pool into the outermost core channel. In the last case, the debris bed remains solid for a longer time period because of improved convective cooling, so that the axial position of melt through is at app. 3 m, similar to the result of the rod-like geometry case ("scoping case").

Figure 5.8 shows the temperature evolution in the core and the steel structures. The three rows of graphs correspond to three different cases according to the convective heat transfer hypothesis taken into account:

- The upper graphs refer to the case with no convective exchange between steam and debris-bed (first row, remark (a) in Table 5.2). Time of local melting of 78% HR thickness is 8200 s. Time of CB melting through could not be reached.
- The graphs of the middle row assume convective heat transfer to steam having a forced mass flow rate of 1 kg/s in all 5 core channels and the downcomer (fourth row, remark (d) in Table 5.2). Time of local melting of 78% HR thickness is 5470 s. Time of CB melt through is 7600 s.
- This case is not very different from the one where the same steam massflow rate of 1 kg/s is applied in the outermost core channel (channel 5) but there is no convective exchange with steam in the other core channels,(third row, remark (c) in Table 5.2). This is because the heavy reflector melt behaviour mainly depends on the heat transfer mechanisms prevailing in the outermost core channel.

- The lower graphs also assume convective heat transfer with steam (fifth row, remark (e) in the Table 5.2). Although the total mass flow rate in the core is the same as in the case of the central graphs (6 kg/s), its repartition follows the channels initial free flow areas which gives the following values for steam mass flow rates in channels 1 to 6: 210 g/s, 660 g/s, 1500 g/s, 1800 g/s, 1560 g/s, 270 g/s. These values are to be compared to uniformly 0 g/s and 1000 g/s for the upper and middle graphs, respectively. Time of local melting of 78% HR thickness is 11700 s. Time of CB melting through is 14200 s.

The two columns in Figure 5.8 correspond to two different times in the accident calculation:

- the left column represents the temperature evolution at 2200 s, i.e. 100 s after start from identical initial conditions. In spite of differences in debris bed temperatures due to different convective heat transfer hypotheses, the temperatures in the core outermost channel (channel 5) and in the steel structures don't show any remarkable differences..
- the right column represents the temperature evolution at 7600 s which is the time at which the core barrel is locally molten through in the case of the middle graph.

The differences in the HR melting process are related to the power possibly extracted and transported by the steam as shown in Figure 5.9. In these graphs the curves (-A-) reflect the convective power extracted from or received by the debris beds in channel 5 at the core height between 1.2m and 1.5m. In this heat exchange processes with the debris bed, steam and magma (liquefied corium) are involved, and the power received by the steam is indicated by the (-C-) curves, whereas the one exchanged with magma (mainly extracted) is represented by the (-B-) curves. The (-D-) curves show the convective and the(-E-) curves the radiative and conductive power received by the HR. It can be seen that when steam extracts power from the debris bed the radiative and conductive power received by the HR is lower than without steam. But on the other hand the convective power received by the steel structure to some extent compensates the difference.

The status of the HR and CB damage by melting is summarised in Figure 5.10. For accident scenarios with higher mass flow rates the outermost core channel is cold enough to prevent the molten pool from spreading in this channel. As a result the CB melt through area is in the core upper part according to the axial power distribution in the fuel. In all other cases the molten pool reaches the outermost channel and the CB melt through area is located in the core lower part at about 1.2m.

5.4 Discussion

In the frame of the investigation of the consequences of a surge line break reactor accident without emergency cooling a model for estimating the HR and CB melting behaviour has been established on the base of the application of the ICARE2 code. The initial phase of the accident, as long as heat transport by water or two-phase steam-water mixture is prevailing, has been calculated by S/R5. The beginning of the debris bed formation is characterised by a moderate convective heat transfer to steam. With progressive core degradation and molten pool formation, heat transport by conduction and radiation may dominate, and at this stage of core damage the radial core enclosing structures will undergo severe thermal loads.

Here, ICARE2 with its advanced models of heat transport in solid structures including phase-change phenomena is an appropriate tool for detailed studies of such HR and CB damage proc-

esses. However, the initial and time-dependent boundary conditions including total steam mass flow rates through the degraded core region have been provided by SCDAP/RELAP5.

The approach used for this study to estimate the melting behaviour of HR and CB seems to be feasible as long as the main contributions to heat transfer processes between core material and steel structures can be described by conductive and radiative heat transfer.

However, the parametric variation of the contribution of the convective heat transfer to the HR and CB heat-up shows a quite non-linear behaviour with a minimum time delay for CB local melt through. This indicates that for a more detailed analyses the steam flow rates calculated by the code itself have to be used, which is to a certain extend possible with ICARE2V3.
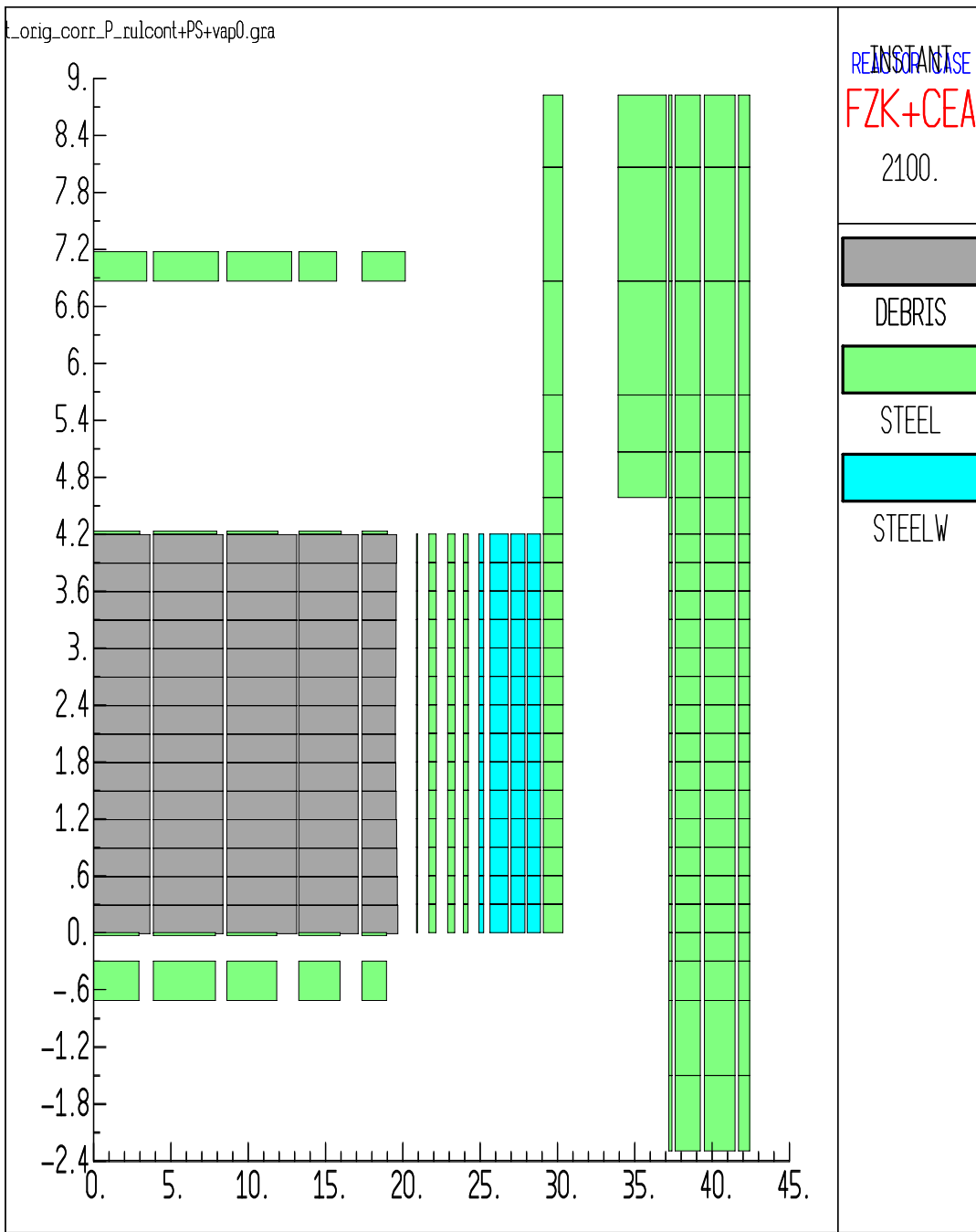
Figure 5.6   Computed domain for "debris case"
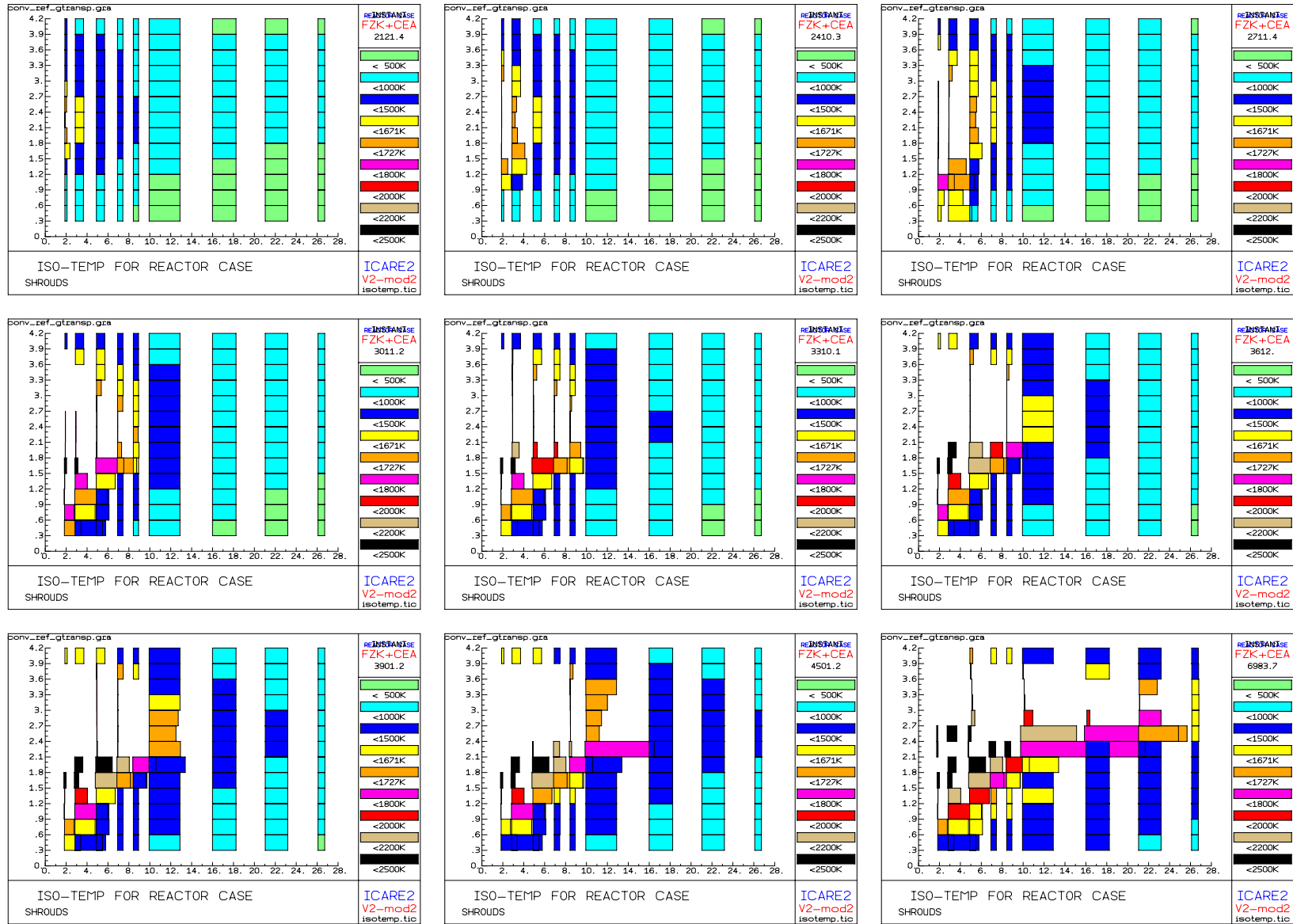
Figure 5.7   Steel iso-temperatures, transparent gas case. The nine structures are: the 4 radial meshes of heavy reflector HR1 (thickness: 0.1 cm, 1.5 cm, 1.5 cm, 1.0 cm), the 4 radial meshes of heavy reflector HR2 (thickness: 1.0 cm, 5.9 cm, 4.5 cm, 4.3 cm) and one mesh for the core barrel (thickness: 6.3 cm). Time: from 2100 s to 3900 s, 4500 s, and 6980 s
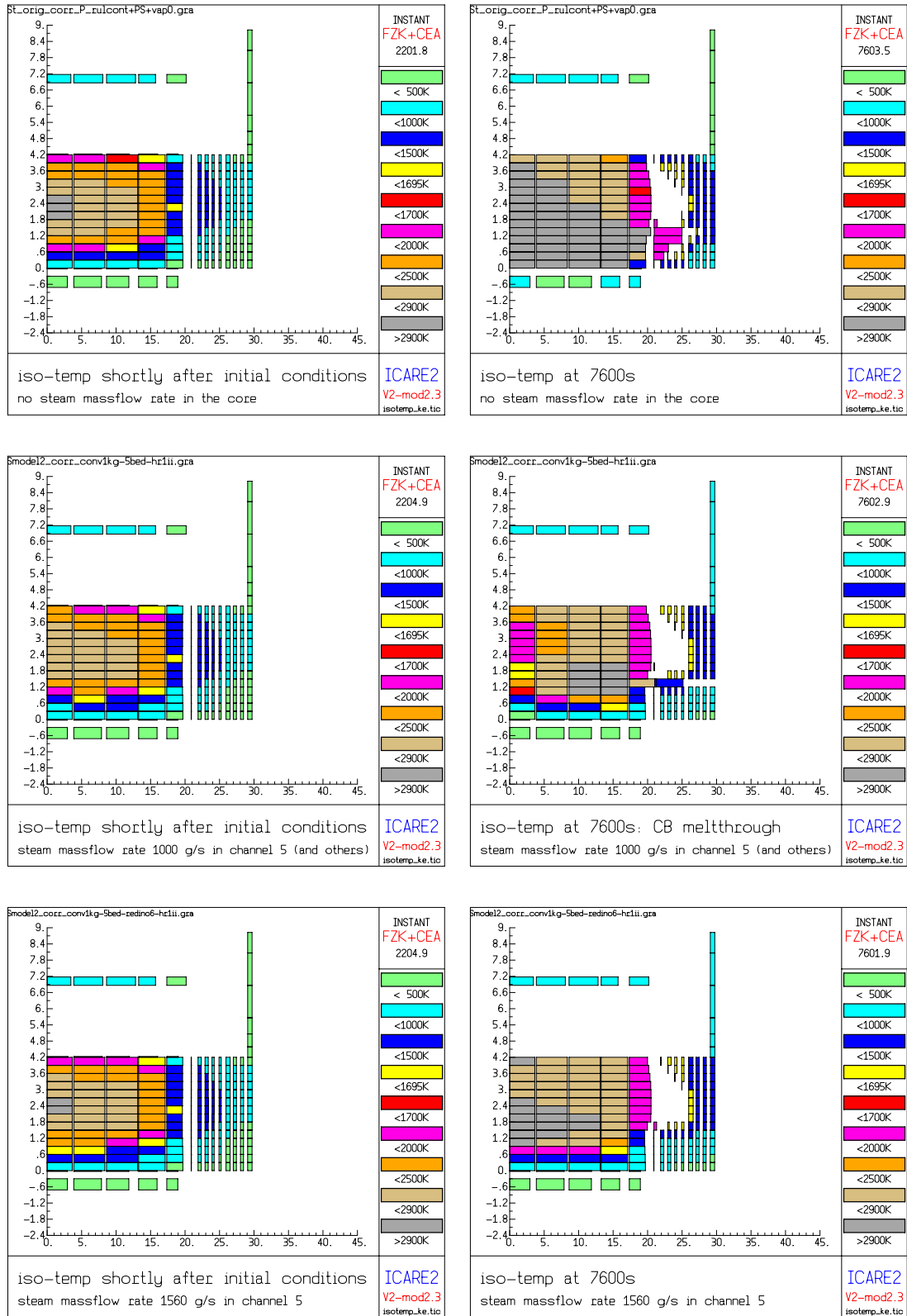
Figure 5.8   Temperature evolution depending on steam convective heat transfer in the outermost core channel at 7600s. The first five bars between 0 and 4.2 m represent the 5 core channels filled with debris-bed or molten corium. The following thinner nine bars are for HR1, HR2 and core barrel as indicated in Figure 5.7.
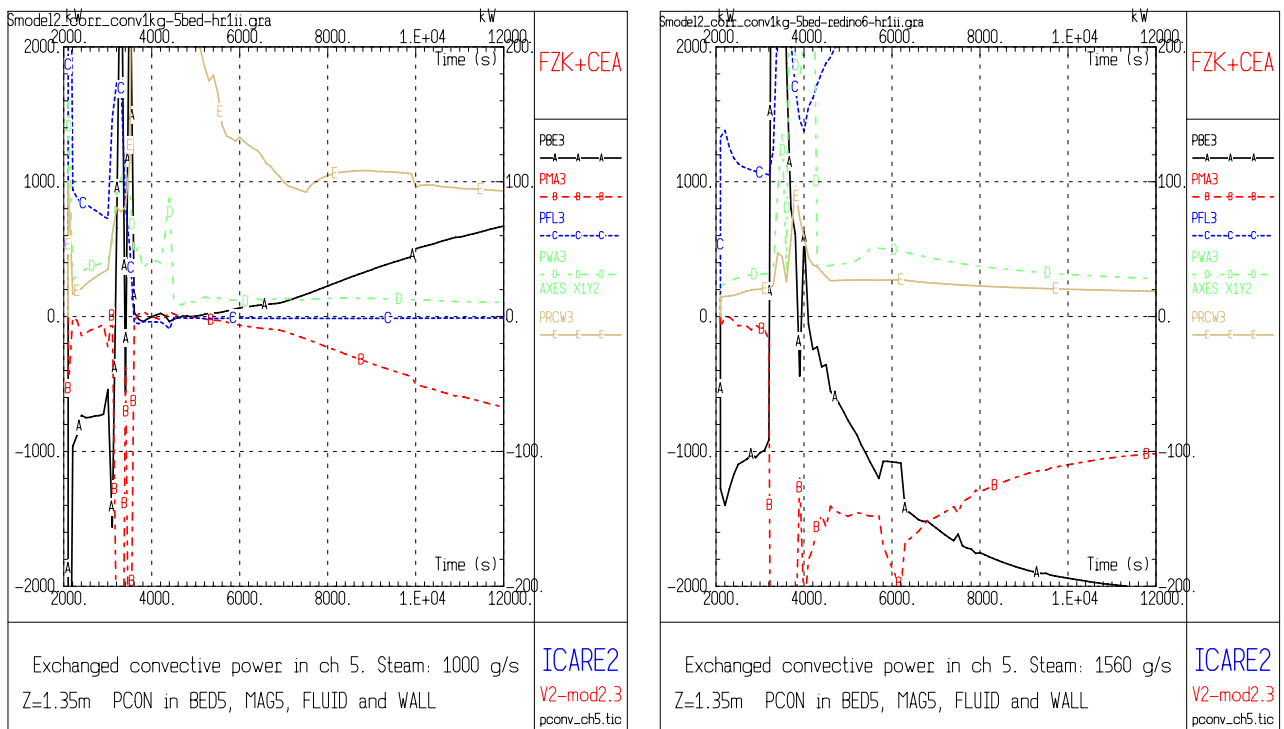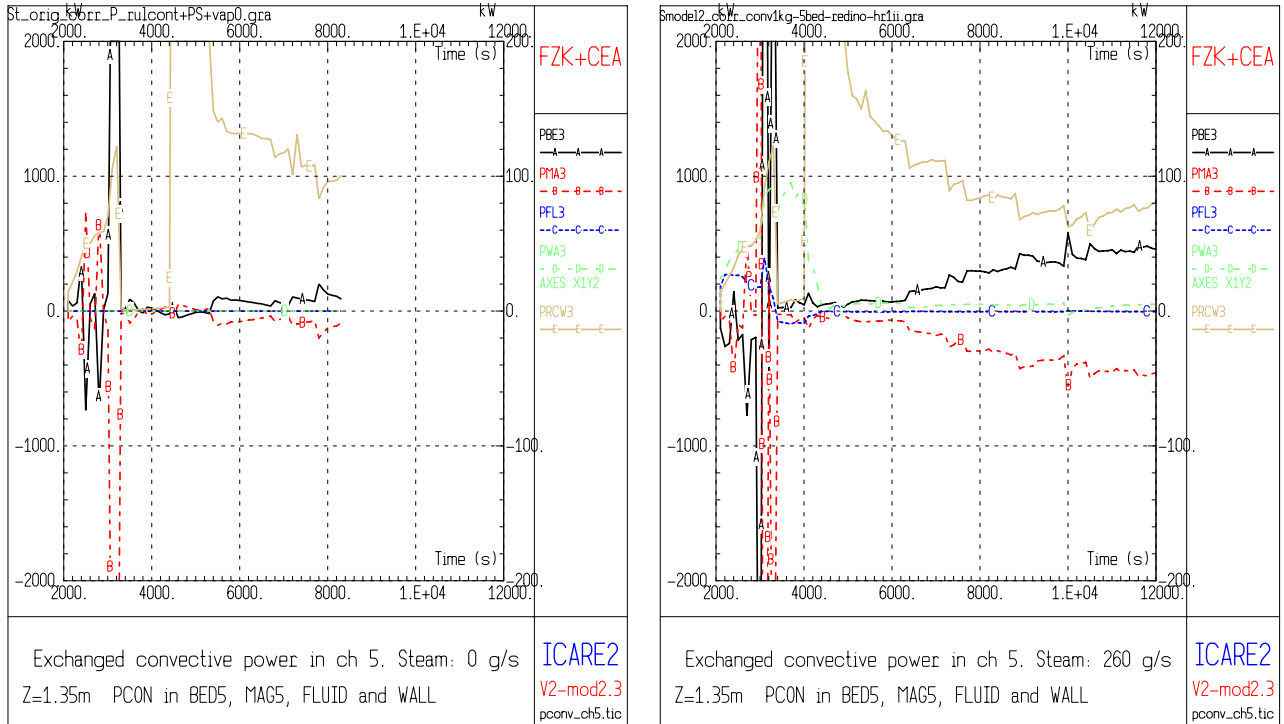
Figure 5.9   Power balance in debris bed (-A-), in magma (-B-), in steam (-C-), in HR (-D-) for outer channel steam flow rates of 0g/s, 260g/s, 1000g/s, and 1560g/s. Comparison with the radiative (-E-) and conductive power received in the HR. Curve (-D-) refers to the right Y-axis. All powers taken between 1.2 and 1.5 m core height.
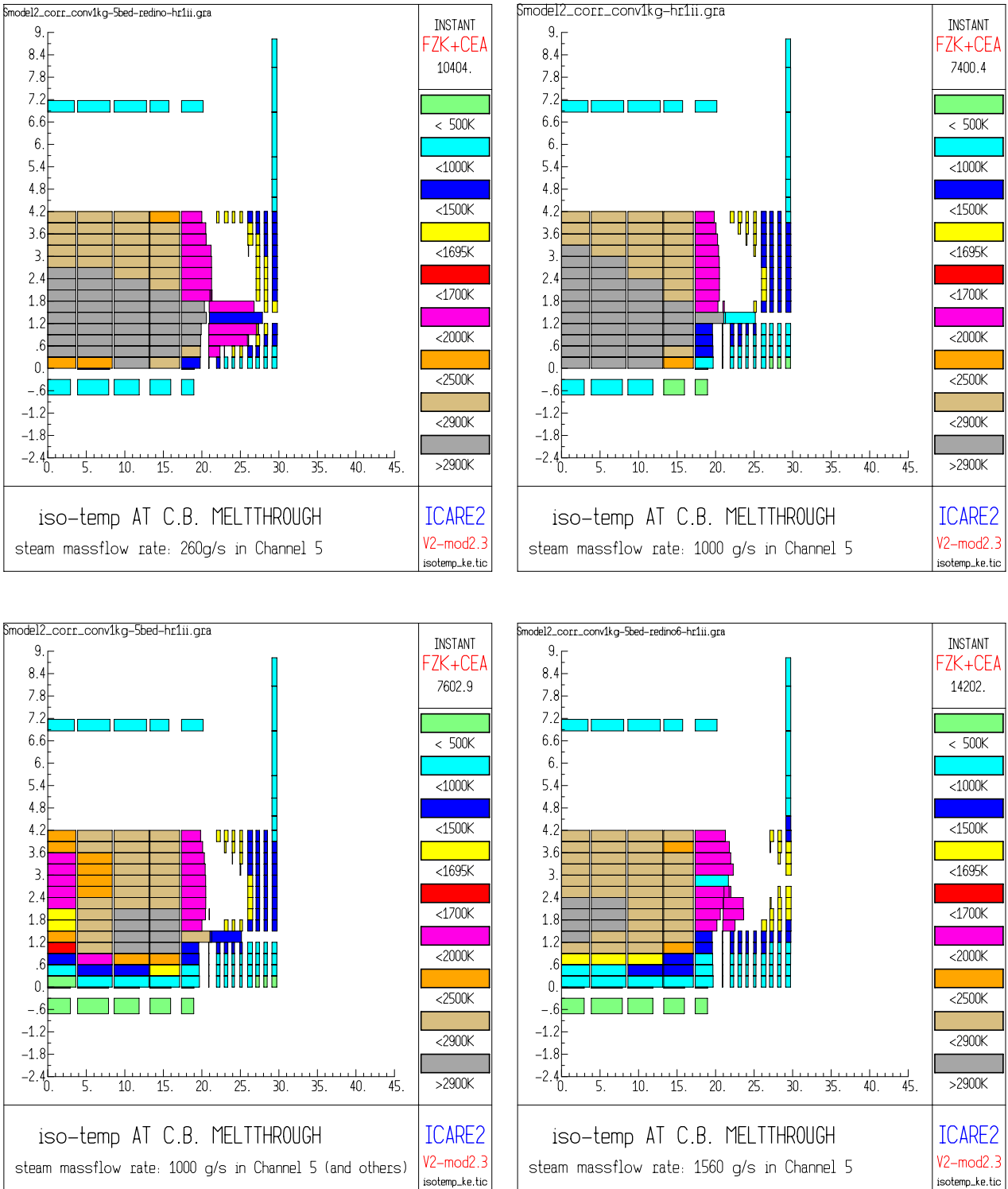
Figure 5.10   Core and steel structure temperature distribution with material repartition at time of CB melt through for steam mass flow rates of 260g/s, 1000 g/s, and 1560 g/s.

6 ANALYSES WITH FIDAP

The course of the melting process of HR and CB originating from the inner side of the HR and thus the possible extent of local severely damaged areas may be influenced by the real HR geometry characterised by inner edges implied by the adjacent positions of fuel elements. In order to understand the details of such local degradation processes with formation of possible hot spots, the application of a special tool such as the FIDAP /23/ package may be helpful. In the following, the first experiences with such simulations using FIDAP are discussed.

6.1 FIDAP models

The process to be studied is the HR melting in presence of debris bed and possibly molten pool materials at its inner side. The outer side is bordered by the core barrel. The latter exchanges heat with the downcomer steam flow (convection) and the vessel (radiation).

In the debris bed the nuclear decay heating is taken into account as a space and time dependant source. Heat is exchanged in the debris bed by conduction and radiation, the combined effects of which are taken into account by an effective heat conduction coefficient. Also heat transfer from debris bed to the HR is modelled through conduction and radiation. No convective heat transfer has been considered because of the uncertainties to model it within a single horizontal plane.

The geometry of the model was selected as outlined in Figure 6.1 in order to:

- minimise the size of the problem,
- cover the maximum thickness variation (thinnest and thickest position) of HR,
- define correctly the boundary conditions.

In Figure 6.1 the initial shape is indicated for the simulated horizontal 45º section of the core including the debris/molten pool region with a debris bed temperature (TB) and the steel structures of HR and CB at an initial temperature (TSi). The layer of the liquefied steel is indicated by "e".

Furthermore, the innermost fuel assemblies (or debris bed areas) have no influence on the HR heating so that they have not been considered. Concerning the boundary conditions, zero heat flux is defined on the inner boundary as well as on the boundaries in azimuthal direction because of the symmetry condition. On the outer surface of the core barrel convective heat transfer has been assumed with a convective heat transfer coefficient of 10 $W.m^{-2}.K^{-1}$ and a sink temperature of 453 K.

6.1.1 FIDAP 2D model

In a finite element program like FIDAP the meshing is crucial because it heavily influences both the accuracy of the results and the computation time. The best way to optimize it is to solve a problem whose analytic solution is known. In the case of the HR melting considered here, the problem has first to be simplified into a pure conduction problem for purpose of comparison with an analytical solution. The meshing of this simplified problem has been updated until FIDAP7.6 calculated the analytical solution within a predetermined error band.

e= molten steel thickness
at t= X s

(TSi , t=0)

STEEL

CORIUM

(TB, t>0)

HR
+
CB

> e <
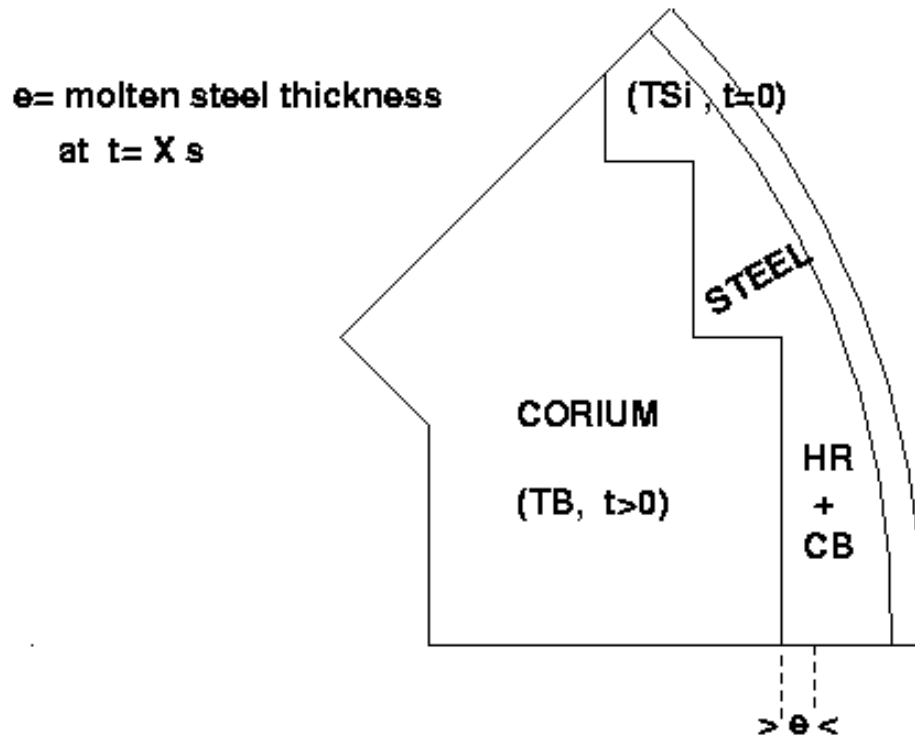
Figure 6.1   Pure heat conduction study with corium (at T_B) and steel material (T_{Si}) , as well as 1/8 core geometry for 2D meshing optimisation. At a given time X, the calculated "e" thickness must equal the analytical one of the sample problem. The largest meshing meeting this condition is selected.

EPR- Heavy reflector + Core barrel -Keqc2G3-

ELEMENT
MESH PLOT

TIME   .100E-01
SCREEN LIMITS
XMIN   .589E+00
XMAX   .231E+01
YMIN -.381E-02
YMAX   .152E+01
FIDAP 7.62
8 Dec 98
13:29:47
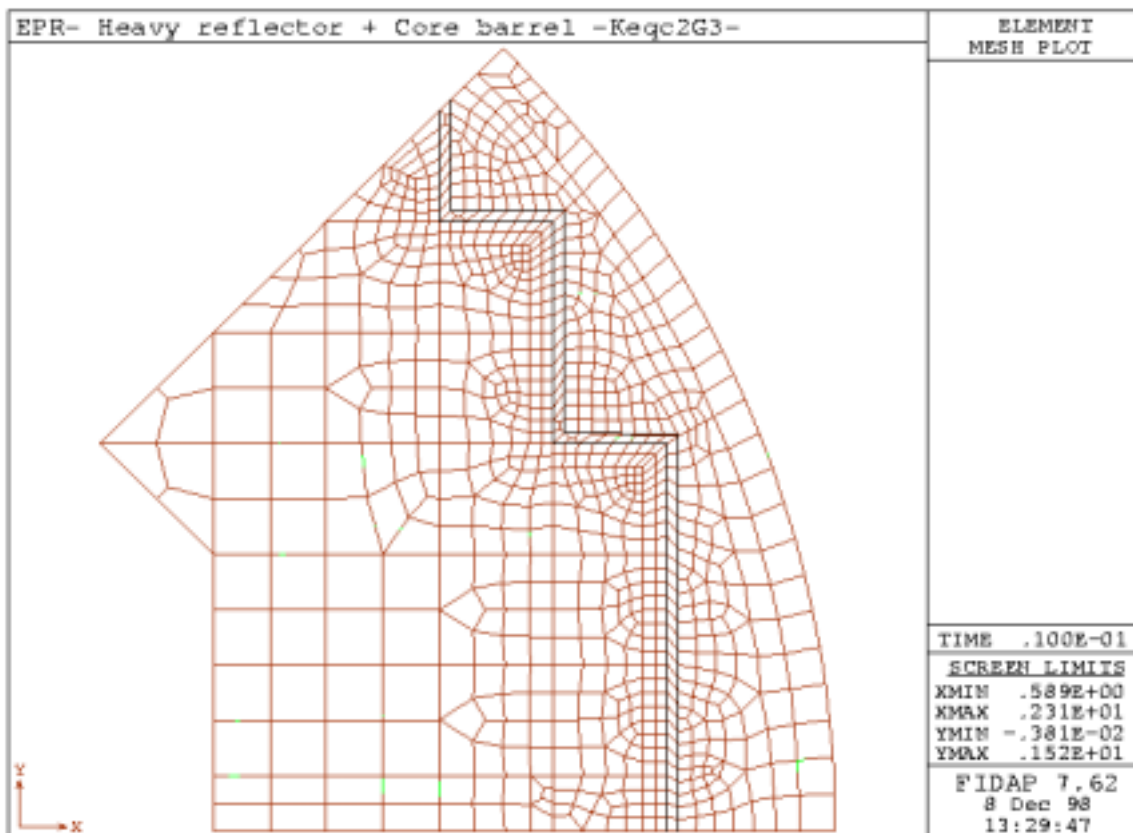
Figure 6.2   Optimised 2D-meshing for FIDAP heat conduction analysis with HR and CB melting caused by a corium heat source

The problem considered represents the geometry of the HR with some simplifications as outlined in Figure 6.1: pure conduction problem with corium and steel material, as well as 1/8 core geometry for 2D-meshing optimisation. At a given time X, the calculated "e" thickness must equal the analytical one. The larger meshing respecting this condition is selected. The debris bed material is homogenous and has a constant temperature TB. The steel is given a melting temperature TS_m, and an initial temperature TS_i. The solution of the problem adapted from /27/ is a transcendental equation relating the time and the melt area thickness.

With the material data used in this test and the debris bed temperature assumed, 14.4 cm steel thickness should be molten within 3600 s. The satisfactory meshing corresponding to the initial phase of the melting process is reported in Figure 6.2. With the progress of the melting, area refinement of the meshing in the concerned areas is possible.

6.1.2 FIDAP7.6 3D-model

A 3D model has been constructed with a refined meshing around the melting areas and the boundaries. Such a 3D model allows to take into account the debris bed cooling down due to axial heat losses at the upper and lower core boundaries. The meshing would be updated to follow the evolution of the melting zone interface. Due to high computer time consumption the use of such a model is only of interest for a well defined scenario problem. A part of the 3D model is shown in Figure 6.3
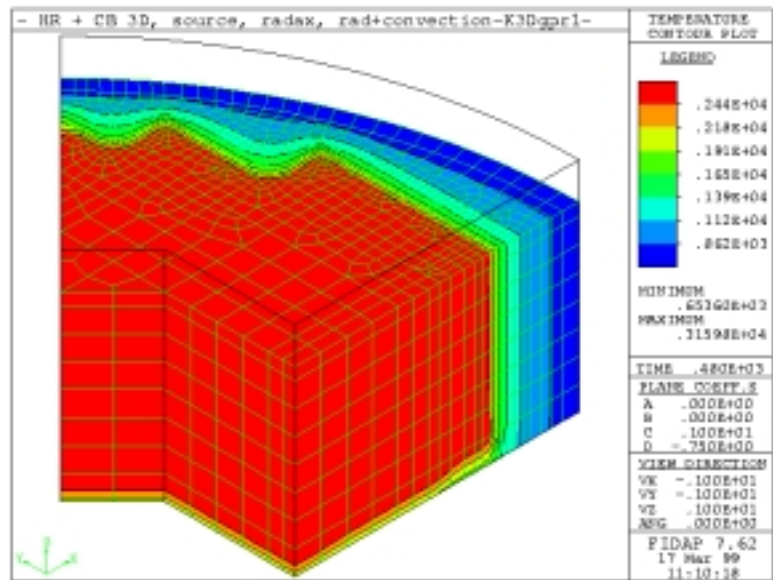
Figure 6.3   Example of a detailed 3D model for a restricted core height

6.2 Results

With that model we can follow the erosion of the HR corners and it is possible to estimate a time delay prior to HR cylindrisation (Figure 6.4). In the scenario analysed here this process lasts app. 60 min, and at app. 135 min a local thinning at the position of the lowest initial HR thickness is still visible (Figure 6.4 bottom). This time scale is somewhat larger caused by the simplification of FIDAP which is not able to remove molten masses. So this can be interpreted as the longest time interval required to melt down HR inner edges.

From this calculation a rough estimation of the azimuthal melt through position can be deduced around the 45° position. However, this result could not be verified by the other tools used. If this tendency can be proved by more precise analyses with an advanced ICARE version, a complete 3D- calculation may be fruitful.
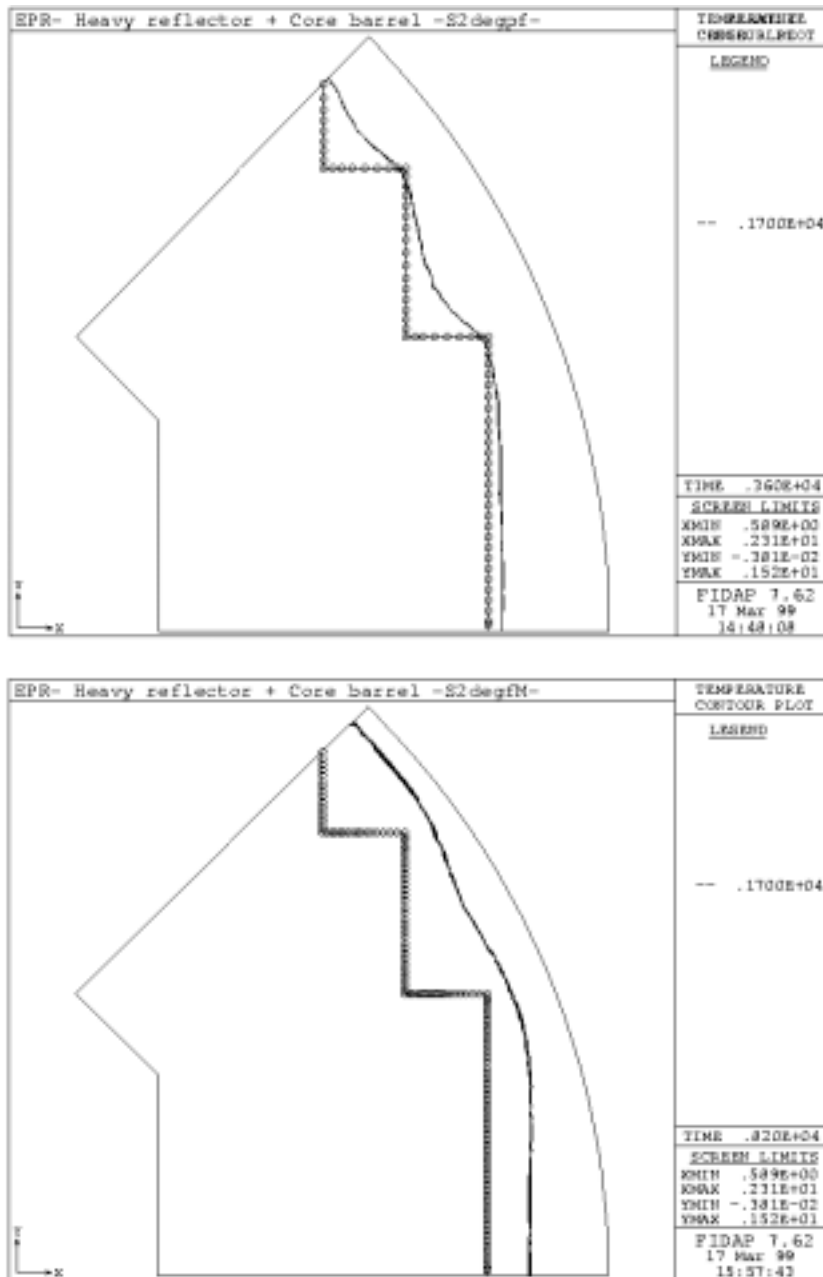
Figure 6.4   Results of FIDAP analyses of local melting of HR inner edges at 60 min (top) and at 136 min (bottom).

7 SUMMARY AND CONCLUSIONS

The basic question of primary failure of core enclosures has been investigated. Based on several scenarios calculated with S/R5 and MELCOR the in-vessel core degradation process has been analysed for various scenarios (SBLOCA, LOOP; LBLOCA) up to S/R5 code failure at contact of the in-core molten pool with the heavy reflector (HR).

With the axial temperature profile derived from S/R5 and MELCOR detailed analyses were performed using ICARE2, LOWCOR2, and FIDAP. The main result is that a lateral melt through occurs much earlier than an attack of the lower core support plate. Another important result is that despite of different axial positions, resulting from different core degradation and melt relocation models in S/R5, ICARE2, and MELCOR, the time scale starting from onset of melting up to potential release of molten corium into the downcomer is approximately the same. The melting of the HR inner edges lasts between 10 min and 17 min. The complete melt through of HR and CB varies between 25-50 min after onset of melting. Up to melt through up to 32 Mg of molten steel can be released relocating down at the inner side of the HR.

Estimation of CB breach location

From FIDAP analyses the thinnest position of the HR (at 45° degree) has largest possibility to be penetrated first. However, these analyses were only 2-D in a horizontal plane, and did not include material relocation due to melting. With the other tools, a direct influence of the rectangular non-cylindrical inner shape of the HR (Figure 2.1) on the final melt through size of the CB could not be found, especially if a large axial relocation of the hot spot (debris / molten pool) is taken into account. The main reason is that the inner edges vanish before HR cylindrical part starts to melt.

Axial position of the CB penetration is dependant on the scenario and severe fuel damage codes used to simulate the course of the scenario. It varies between 1.0 m and 2.5 m elevation of the core. However, the shape of the breach inside HR and CB seems to be impartial of the axial position, so that the mass of molten corium pouring initially through the breach may not be influenced by the total mass of molten corium in the pool.

For a more realistic HR and CB melt through analysis real 3D calculations have to be performed and a non-cylindrical arrangement of the pool in the core has to be supposed to define a local hot spot. As found in other studies /28/, /29/ a small increase of surface temperature may be sufficient to start inhomogeneous HR heat-up which would create a local hot-spot.

Estimation of HR Erosion rates

The erosion or melt through rates extracted from the various calculations met rather well with experimental studies performed in solid metal – liquid metal systems /30/. The result indicate an erosion rate of app. 1 mm/s whereas in this study a value of 0.9 mm/s was found.

8 ACKNOWLEDGEMENT

9 REFERENCES

/1/ Summers at al.: MELCOR Computer Code Manuals, Vol. 1 - 2 (Vers: 1.8.3), NUREG/CR-6119, SAND93-2185, March 1995. On-line: http://melcor.sandia.gov/.

/2/ MAAP4 - Modular Accident Analysis Program for LWR Power Plant - Computer Code Manual", 1-4, principal investigators, R. E. Henry, C. Y. Paik, and M. G. Plys, EPRI Research Project 3131-02, Fauske & Associates, Inc., Burr Ridge, IL (May, 1994)

/3/ Allison et al.: SCDAP/RELAP5 mod3.1 Code Manual, Vol. I - IV. NUREG/CR-6150, EGG-2720, Oct. 1993.

/4/ The SCDAP/RELAP5 Development Team: SCDAP/RELAP5/MOD 3.2 Code Manual, NUREG/CR-6150, INEL-96/0422, Idaho Fall, Idaho, USA,1997

/5/ A. Porracchia, R. Gonzales, P. Chatelard: "ICARE: A Computer Code for Severe Fuel Damage Analysis - Models and Validation", CSARP Meeting, Bethesda (MD), USA, May 1991.

/6/ R. Gonzales, P. Chatelard, F. Jacq. ICARE2 - a computer program for severe core damage analysis in LWRs. Note technique SEMAR 93/33. ICARE2.

/7/ van der Hardt, A. V. Jones, C. Lecomte: The Phebus FP Severe Accident Experimental Program, Nuc. Safety 35(2), 1994, pp. 187 - 205.

/8/ Hering, W.; Homann, Ch.; Sanchez, V.H.; Sengpiel, W.; Smit, S.O.; Hofmann, P.; Steinbrück, M.; Piel, D.; Schmidt, L.; Current FZK-investigation on core degradation. The European Pressurized Water Reactor EPR : KTG/SFEN Conf., Köln, October 19-21, 1997 Proc. pp. 157-160.

/9/ E. Elias, V. Sanchez, W. Hering; Development and validation of a transition boiling model for RELAP5/MOD3 reflood simulations, NEDEA 183 177-332 (1998).

/10/ Hering W., Reflood Calculations for the Projected European Pressurized Water Reactor Using SCDAP/RELAP5 mod 3.1, FZKA-6299, December 1999. http://bibliothek.fzk.de/zb/berichte/FZKA6299.pdf

/11/ Hering, W.; Homann, Ch.; Sanchez, V.H.; Sengpiel, W.; Smit, S.O.; Struwe, D.; Messainguiral, Chr.; Elias, E.; In-Vessel Unfallabläufe. Projekt Nukleare Sicherheitsforschung. Jahresbericht 1996. Wissenschaftliche Berichte, FZKA-5963 (September 97) pp. 343-368

/12/ Hering, W. Hofmann, P.: Material Interactions during Severe LWR Accidents; Summary of Separate-effects Results, KfK 5125, February 1994.

/13/ C. Messainguiral: Calculation of CORA-13 with ICARE2 and SC- DAP/RELAP5. N.T. CEA-DER/SERA/LEPS 96/2048

/14/ R.D. Gasser et al, Late-Phase Melt Progression Experiment: MP-2, Results and Analysis, NUREG/CR-6167, SAND93-3931, May 1997.

/15/ Petti, D. A. et al, Fission Product Behavior During The PBF Severe Fuel Damage Test 1-1, NUREG/CR-4925, May 1987

/16/ B. Berthet, J. Bonnin, S. Bayle, N. Hanniet, F. Jeury, S. Gaillot, Y. Garnier, C. Martin, M. Laurie, B. Siri: "Phebus PF -- FPT1 Preliminary Report", Document Phebus PF IP/97/334, Cadarache, 30. Oct. 1997.

/17/ Haste et al.: In-Vessel Core Degradation in LWR Severe Accidents, Final Report, Nuc. Sci. and Techn., report EUR 16695 en.

/18/ S. Smit, W. Hering, W. Sengpiel: Analysis of Fuel Bundle Behavior in Phebus FPT0 with SCDAP/RELAP5, FZKA 5882, 1998.

/19/ C. Messainguiral, W. Hering: Computing reactor core severe degradation with ICARE2-V2-mod2, Icare2 2nd International users seminar. Aix-en-Provence 21-22 October 1996.

/20/ C. Messainguiral, W. Hering: Steel annular core structures: temperature evolution during a severe accident. Calculation with Icare2-V2-mod2. N.T. CEA-DER/SERA/LEPS 97/2042.

/21/ W. Sengpiel, Internal Report 4/00, Feb. 2000.

/22/ FIDAP, http://www.fluent.com/software/FIDAP/index.htm

/23/ FIDAP, http://www.uni-karlsruhe.de/~FIDAP/

/24/ W. Hering, Ch. Homann, V.H. Sanchez, W. Sengpiel, S.O. Smit, P. Hofmann, M. Steinbrück, D. Piel, L. Schmidt, C. Messainguiral: Untersuchungen zur Kernzerstörung. Nachrichten – Forschungs-zentrum Karlsruhe, 29(1997) pp. 309-17

/25/ W. Hering, W. Sengpiel, S.O. Smit: Theoretische Interpretation der experimentellen Ergebnisse. Projekt Nukleare Sicherheitsforschung. Jahresbericht 1996. Wissenschaftliche Berichte, FZKA-5963 (September 97) pp. 410.

/26/ W. Hering, Investigation of In-vessel Core Degradation with SCDAP/RELAP5 mod 3.2, FZKA un-der preparation, 2000.

/27/ H.S. Carslaw and J.C. Jaeger: Conduction of heat in solids. 2nd Edition, Oxford, At the Clarendon Press.

/28/ Mühl, B., Investigations for the EPR Concept – KAPOOL and Kats Experiments, Projekt Nukleare Sicherheitsforschung Jahresbericht 1998. Wissenschaftliche Berichte, FZKA-6300 (September 99) pp. 261-280.

/29/ Mühl, B., Projekt Nukleare Sicherheitsforschung Jahresbericht 1999, Wissenschaftliche Berichte, FZKA-6480 (August 2000) pp. 448-471.

/30/ Hohmann H., Magallon D., Benuzzi A., Yerkess A., Results of the FARO programme, Proceedings of the Seminar on the Commission Contribution to Reactor Safety Research, Congress Centre, Villa Ponti, Varese, Italy, November 20-24 1989, p. 837-854.